Investigating the Synthesis of Monosubstituted Keggin Polyoxometalates

Master Thesis in Chemistry

by

Lene Revheim Sandøy

Department of Chemistry

University of Bergen

October 2020

Acknowledgements

I would like to thank some amazing people for their help and guidance during this project!

Dr. Mali Husby Rosnes, Associate Professor, for being my brilliant and patient supervisor, always inspiring me, taking the time to answer my questions and giving me guidance. I have learnt a lot from her.

Egil Nodland, Head Engineer, for teaching me how to use the IR instrument. He also helped me a lot with the MLR analysis, for which I am very grateful.

Inger Johanne Fjellanger, Head Engineer, for answering my questions about EA and providing me with the results used in this thesis.

Dr. Karl Wilhelm Törnroos, Professor, for providing me with the SXRD results and **Dr. Pascal D. C. Dietzel, Professor**, for providing me with the TG results.

And lastly, **my family and friends**, for their support and encouragement during this time.

Table of Contents

Abstract

For any successful catalyst, there needs to be a cheap and reliable route to synthesising the catalytic material. It is therefore desirable to find syntheses that are time efficient, do not require any highly toxic chemicals and give high yields. In this thesis, the syntheses of a range of different polyoxometalates (POMs) with the well-known Keggin structure were investigated. The compounds of interest were the potassium and tetrabutylammonium (TBA) salts of $[SiXW_{11}O_{39}]^{n-}$, where X = Al^{3+}, Co^{2+}, Cr^{3+}, Cu^{2+}, Fe^{3+}, Mn^{2+}, Ni^{2+} and Zn^{2+}, since they had previously shown or were suspected to have interesting catalytic properties, particularly for the cycloaddition and copolymerisation of CO_2 with epoxides.

In the case of the potassium salts, two different syntheses were attempted. It was found that one of the syntheses produced a higher yield and required less time than the other one. However, as opposed to the other synthesis, it produced an unknown precipitate and was not easily compatible with X = Al^{3+}, Cr^{3+} and Fe^{3+}. Regarding the TBA compounds, three different syntheses were attempted. The first synthesis resulted in low yields, was time consuming and required the use of dichloromethane (DCM), the second synthesis removed the need for DCM and was overall more effective, and finally, the third synthesis drastically improved the yield.

Based on results from infrared spectroscopy (IR) and elemental analysis (EA) the desired Keggin-type POM compounds were successfully obtained. The IR data of the different compounds were thoroughly analysed and compared, and the observed differences were viewed in relation to the properties of the transition metals inserted into the structures. In addition to the IR and EA analysis, some of the compounds were also analysed using thermogravimetry (TG) and single crystal X-ray diffraction (SXRD).

The investigations of the syntheses and analyses of the results presented in this work, provide a further understanding of these interesting materials, facilitating future studies of their catalytic properties.

1 Introduction

During the last century, the global use and need for carbon-based polymers (plastics) has grown immensely. From 1950 to 2015 the global production of plastic increased from 2 million to 380 million metric tons, and the plastic and petrochemical industries are planning to expand their production. There is, however, a concern regarding the environmental impact of the polymer industry, both in terms of the production and the disposal of plastics. There is also the issue that most polymers are made from fossil fuels, which are finite resources.[1] If the current production of polymers is to be maintained, or even to grow, there is a dire need to find a way of producing it cheaply from bio-renewable resources.

One promising way of dealing with this problem is chemical fixation of CO_2 through catalysed cycloaddition with bio-renewable epoxides. This reaction produces cyclic carbonates which can be used as precursors for polycarbonates and other polymers.[2, 3] Utilisation of CO_2 is considered interesting as it could contribute to cycling carbon, as well as reduce the usage of chemicals with higher environmental impact.[4] CO_2 is also a nontoxic, cheap and readily available raw material from a completely renewable feedstock.[5] However, finding effective and economically beneficial ways of implementing such reactions for CO_2 can be challenging due to its high thermodynamic stability and chemical inertness.[6]

In the search for catalysts that will make these CO_2 reactions greener and more effective, polyoxometalates (POMs) have proven interesting. POMs have intrigued scientists over the past two centuries and continue to astonish with their diversity in chemical and physical properties. This area of chemistry has consequently become well-researched, resulting in many publications on the subject.[6, 7] Specifically regarding the catalysis, the fact that POMs are low in toxicity, recyclable and stable towards humidity and air, make them desirable for use.[8] Besides, their promising avenues for further tailoring to enhance catalytic activity and recycling encourages further research.

Not only are POMs great catalysts, but they also attract a great deal of attention due to their application in many other fields, such as medicine, coatings and sensors.[6, 7] This interest in POMs accompanied by evolved analytical instrumentation and synthetic procedures has led to the discovery of many new POM structures,[9] which indicates there is still much to be discovered about these compounds.

1.1 Polyoxometalates

Polyoxometalates are metal-oxo cluster anions, which are made from transition metals in their highest oxidation state. The most commonly used transition metals in polyanions are Mo, W and V; however, Nb and Ta are also used, but to a lesser extent.[6, 10] Polyanions are constructed from metal oxide subunits, $[MO_x]$, where M denotes the transition metals and x = 4-7. These subunits have a polyhedral structure with oxygen molecules at the vertices, which allows the units to fuse oxygen atoms and connect by sharing corners, edges and/or faces.[11-13] The number of subunits and how they are connected within a polyanion can vary greatly. Some polyanions contain as few as three metal atoms,[14] while some have been made to include 368 metal atoms in one single cluster molecule.[15] This allows polyanions to display an array of different compositions and sizes ranging from 1 to 5.6 nm.[16]

There are two types of POMs: hetero- and isopolyoxometalates. These types of POMs can be illustrated by the following formulas:

$$[X_xM_mO_y]^{q-}, \text{ where } x \leq m$$

Formula 1: General formula for heteropolyanions.

$$[H_nM_mO_y]^{p-}$$

Formula 2: General formula for isopolyanions.

The addenda atom, M, is the early transition metal. The main difference between hetero- and isopolyoxometalates is that heteropolyoxometalates have at least one internal heteroatom, while isopolyoxometalates do not. Since POMs are almost always anions, the heteroatoms are cations, and they can be considered either primary or secondary. Primary heteroatoms are essential to the POM structure, while the secondary heteroatoms can be removed leaving a still stable structure.[12] The primary heteroatoms are usually main group elements such as Si, P, S, Ge and As, but can also be transition metals such as Co or Fe. Which addenda atoms and heteroatoms the polyanion contains can greatly affect their properties and may allow for the creation of specialised polyanions.[6, 11] Generally, most heteropolyoxometalates are composed of either Mo or W, while many isopolyoxometalates contain V, Nb or Ta.[14] Heteropolyoxometalates are by far the most researched subset of the POMs because of the different combinations of addenda atoms and heteroatoms providing a wide variety of compounds.

1.1.1 The Keggin structure

The ability to vary the number of subunits within a POM, and how they are connected, allows for a great number of different combinations. Since the discovery of POMs, many different structures have therefore been defined, such as the Anderson, Lindqvist and Keggin anions.[17]

The focus of this thesis is the Keggin structure, which was first suggested by L. Pauling in 1929[18] and then defined by J. F. Keggin in 1933.[19, 20] The structure has the general formula $[XM_{12}O_{40}]^{n-}$,[17] where the addenda atom, M, is usually tungsten or molybdenum. This thesis focuses on synthesis, characterisation and analysis of various monosubstituted tungsten-Keggins; where one addenda atom has been replaced by another metal centre.

The Keggin ion is a heteropolyoxometalate which means that it has a heteroatom in its structure. The heteroatom is usually a tetrahedral template anion, such as for example Si or P, located at the centre of the structure. The heteroatom is surrounded by four oxygen atoms, creating a tetrahedron structure, and these oxygen atoms are then connected to 12 metal-oxo clusters. These clusters have an addenda atom surrounded by 8 oxygen atoms, creating an octahedron structure (see Figure 1).[21]

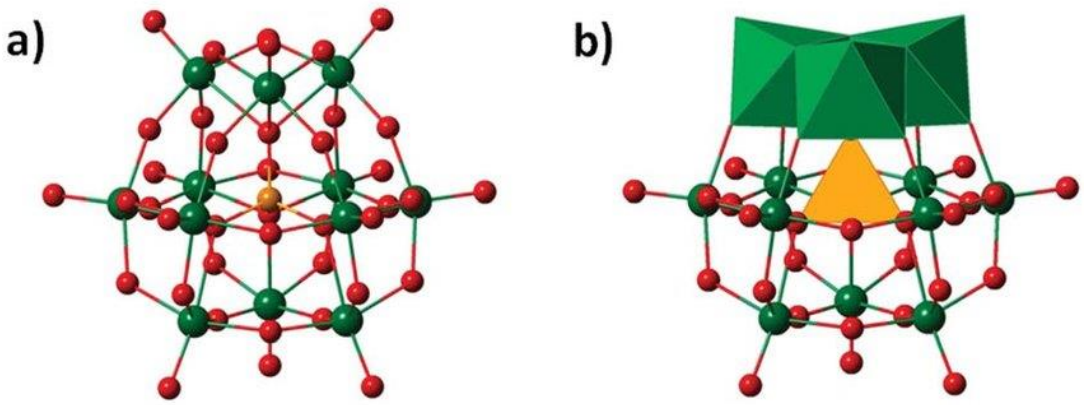

Figure 1: The Keggin structure represented by a) a ball and stick model, and b) a polyhedral model of a M_3O_{13} framework on the ball and stick model.[22] Colour scheme: addenda atom, green; oxygen, red; heteroatom, orange. Reproduced from Ref. 22 with permission from The Royal Society of Chemistry.

1.2 The synthesis of POMs

Part of the appeal of POMs is that they appear to be rather simple to synthesise. Generally, the syntheses of POMs can be considered “one-pot” reactions as they only require a few steps, or even just one step, that can be carried out in one reaction flask.[17] The most common method for

synthesising POMs is through acidification of an aqueous solution containing the necessary oxoanions and heteroatoms. In many cases, the stoichiometry indicated by the formation equation provides a good direction to a design of the synthesis. In these cases, the equilibrium constants and rates of formation are large enough for the polyanions to crystallise from the stoichiometrically acidified solutions at room temperature. However, in other cases, excess of heteroatoms, or careful control of temperature or pH might be necessary.[12]

Though the practical execution of the syntheses can be relatively simple, the pathway of the reaction can be quite complex. This is because POMs are synthesised through self-assembly,[23] where different reagents come together and create an organised structure without external direction. By controlling the reaction parameters, such as the temperature, pressure, pH and which heteroatoms are present,[6, 16] the reaction pathway of the self-assembly can be directed to produce the desired POM structure. By changing the reaction parameters, POMs of different shapes, sizes and chemical properties can be created.[24]

The presence of different cations is also something that can change the final structure and chemical properties of the synthesised POM. Since POMs are almost always polyanions, they cannot exist without a cation to balance the charge. Research has shown that the characteristics of the cations, such as size, charge and symmetry, can affect the product obtained in a POM synthesis.[17] Usually POMs are highly soluble in water and inorganic solvents; however, they can be made organically soluble by substituting the inorganic cations with organic cations.[6] An example of such a cation is tetrabutylammonium (TBA), which was the cation of choice in this thesis to create organically soluble compounds. Even with the simplicity of the syntheses, they can give an enormous structural diversity to the POM clusters, and that is part of what has garnered interest.

1.2.1 The lacunary Keggin structure

Within the different types of structures, such as Keggin and Anderson, there is also the possibility of variation within the composition of the structure. As mentioned previously, the choice of addenda atoms, heteroatoms and cations will affect the properties of the POM; however, there is also the possibility of removing one or more of the addenda atoms from the structure, replacing it with a different metal.

The removal of addenda atoms from a POM structure creates a lacunary or "defect" derivative of the original structure. Since the addenda atoms are connected through sharing oxygen atoms, their removal results in the stoichiometric loss of a MO^{n+} group (see Figure 2). Subsequent removals adjacent to the initial vacancy, would lead to the loss of either MO_2 or MO_3 groups.[12] The mono-, di- and trilacunary Keggin structures can be made in solution by controlled hydrolysis of the parent Keggin structure. This is usually achieved by either careful addition of base to a solution of the parent Keggin or by strict pH control of a solution simply containing the desired addenda metal atoms and heteroanion salts.[16]

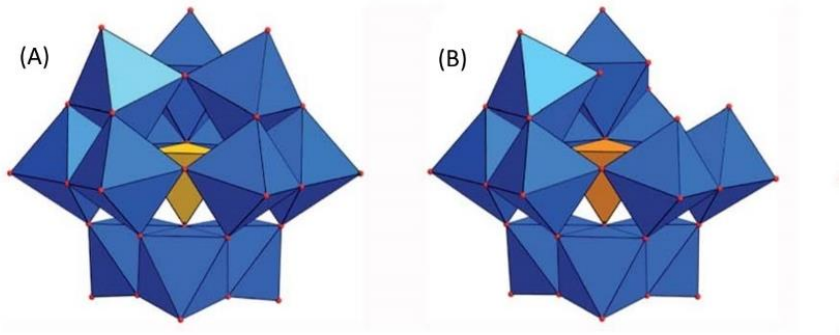

Figure 2: The polyhedral models for (A) a Keggin anion, $[XM_{12}O_{40}]^{n-}$ and (B) a Keggin monolacunary anion, $[XM_{11}O_{39}]^{m-}$.[25] Colour scheme: MO_6, blue; O, red; XO_4, yellow/orange. Adapted from Ref. 25 with permission from The Royal Society of Chemistry.

The removal of an addenda atom creates a monolacunary structure which is quite reactive and often will bind to a new addenda atom, such as Mo, W or V, or another electrophile capable of octahedral coordination, such as Fe, Mn, Co, Ni or Zn.[10, 16] Introducing new metal ions to the POM structure in this manner is the most efficient way to create active metal sites on the POM,[26] and depending on the metal inserted, certain aspects of the POM, such as redox and acid/base properties, can be tuned. Some metal ions can also be used to connect two or more structures together, to create a new, larger structure.[14] Within tungstate chemistry, this was pioneered by Pope and later Kortz who created some large nanostructures by joining lacunary Keggin anions together with large metal cations.[16, 27] The ability to substitute an addenda atom for a different metal ion creates the possibility for a large variety of structures with different properties that can be tailored to the desired use. Their usefulness in a wide range of applications has made them widely researched over the last forty years.[28]

1.3 Polyoxometalates in catalysis

Because of the different properties of POMs, their application as catalysts is one of the most researched areas in the field. Their properties include tuneable acidity, redox properties, resistance to oxidation, thermal stability and sensitivity to light and electricity. This has made them useful in chemical oxidation, photochemical oxidation, electrochemical oxidation, acid catalysis and more. Part of what makes POMs versatile catalysts is that they have many active sites, such as protons, oxygen atoms and metal atoms. Due to available protons acting as Brønsted acids and the oxygen rich POM surface, POMs can function as both acid and base catalysts.[6]

Even though POMs traditionally have been used as Brønsted acid and oxidation catalysts, over the last decade or so there have also been reports of POMs being used as Lewis acid catalysts.[29-31] Unlike their Brønsted acidity, the Lewis acidity of POMs is believed to be caused by the presence of metal ions with unoccupied orbitals that can accept electrons. The POMs used for Lewis catalysed reactions are therefore, generally, substituted by metals with strong Lewis acidity, such as Al, Zn or Cu.[6] One of the earlier studies on this topic was by Kikukawa *et al.*[31] in 2008, which found that an aluminium substituted Keggin structure was an efficient Lewis acid catalyst in the cyclisation of citronellal.[31] This means that POMs can contain up to two different types of acidic sites, either acidic protons and/or metal ions with Lewis acidity. Both of these acidic sites can function as active sites in catalysis, making POMs very interesting in the field of acid catalysis.[6]

POMs can be used in both heterogenous and homogeneous catalysis. In a homogeneous catalysis, the catalyst and the reagent are in the same phase, usually liquid, while in heterogeneous catalysis they are in different phases, usually with the catalyst as a solid and the reactants as either gases or liquids.[32] The highest catalytic activity is usually achieved through homogeneous catalysis, since the catalyst has a larger available active surface area when the catalysis happens in one phase. With everything in one phase, however, the recovery of the catalyst can be difficult, sometimes prompting the switch to a heterogenous catalytic system. Limited recovery is an issue both because it hinders reuse of the catalyst, and because it leaves traces of the catalyst in the product, which can limit its practical application later on, especially since many catalysts contain heavy metals. In an effort to create POM catalysts for homogeneous catalysis, the structure of POMs can be changed to control their solubility in

different solvents.[33] In this thesis, as mentioned previously, this is done by changing the cation bound to the POM.

Among the different types of POMs, the Keggin structure is considered very interesting, because of its stability as a catalyst. Catalyst stability is of concern because it affects the catalyst's activity and recyclability. To what degree, and in what way, they are stable varies depending on the type of POM in question, and can encompass different combinations of thermal, hydrolytic and oxidative stability. Most POM catalysts are thermally stable, and some Keggin-type POMs are so stable that they can even be used in gas-phase reactions at high temperatures.[6] Keggin POMs, in particular those made of tungsten, are also highly acidic which means they can be used in catalytic reactions with strong Brønsted acidity.[14]

1.3.1 POMs in the cycloaddition and copolymerisation of CO_2 with epoxides

The focus of this thesis is on catalysts that can be useful in the cycloaddition and copolymerisation of CO_2 with epoxides. Chemical fixation of CO_2 through catalysed cycloaddition with bio-renewable epoxides, is a noteworthy reaction because it produces cyclic carbonates which can be used as precursors for polycarbonates and other polymers.[2, 3] The use of CO_2 is interesting for several reasons, but finding effective and economically beneficial ways of utilising CO_2 in reactions can be challenging due to its high thermodynamic stability and chemical inertness.[6] CO_2 has the benefit of being a nontoxic, cheap and readily available raw material from a completely renewable feedstock.[5] Furthermore, its use could contribute to cycling carbon, as well as reduce the usage of chemicals with higher environmental impact, such as chlorofluorocarbons (CFCs).[4] Many different catalysts have therefore been attempted used in the cycloaddition of CO_2 with epoxides, but they typically require the reaction to happen under high temperatures (>100 ºC) and pressures (>2 MPa),[34-36] making it less ideal for industrial use. Finding new catalysts is therefore still necessary to make the reaction accessible and advantageous.

Already in 1998, a study by Szczepankiewicz *et al.*[37] demonstrated the activation of CO_2 by different tetraheptylammonium salts of transition metal substituted POMs, including α-$[SiW_{11}O_{39}M]^{n-}$, M = Co^{2+}, Ni^{2+}, Mn^{2+}, in nonpolar solvent. Since then, the interest for the cycloaddition reaction and copolymerisation of CO_2 with epoxides has become greater, and more research has been dedicated to use the activation of CO_2 by POMs to find catalysts that

will make the reaction cheaper and more efficient. Research on the cycloaddition reaction of CO_2 has shown that catalysts with Lewis acid and base centres offer good yield under mild reaction conditions,[3, 38] and as mentioned previously, POMs have been reported to act as Lewis acids when they contain certain metal ions.[29-31, 39] In order to find good catalysts for the reaction, it would therefore be of interest to examine POMs containing different metal ions. Some work has already been done in this field, among others, there was a study published in 2004 by Sankar *et al.*[40] which examined the catalytic effects of a zinc substituted POM, $Na_{12}[WZn_3(H_2O)_2(ZnW_9O_{34})_2]$, in the cycloaddition reaction. There was also a paper published by Chen *et al.*[41] in 2010 that reported the catalytic effects of monosubstituted α-Keggin-type POMs $[(n\text{-}C_7H_{15})_4N]_x[\alpha\text{-}GeW_{11}MO_{39}]$ ($M = Co^{2+}$, Cu^{2+}, Fe^{3+}, Mn^{2+}, Ni^{2+}) in the conversion of CO_2 to cyclic carbonates. Two years later, *i.e.* in 2012, they also proposed a reaction mechanism for the cycloaddition of CO_2 to epoxides.[2] More closely related to this thesis is a study by Yasuda *et al.*[42] from 2005, where transition metal substituted Keggin POMs $[(n\text{-}C_7H_{15})_4N]_6[\alpha\text{-}SiW_{11}MO_{39}]$ ($M = Co^{2+}$, Mn^{2+}) were used to catalyse the formation of cyclic carbonates from CO_2 at 150 °C and 3.5 MPa. To further investigate the catalytic effect of these monosubstituted POMs, it would be interesting to build upon this previous research and expand the range of substitution metals used to include other metals known to have strong Lewis acidity, such as Al, Zn and Cu.

Herein, the focus is to improve the syntheses of mono-substituted Keggin materials in preparation for future catalytic projects investigating their catalytic activity for cycloaddition and copolymerisation of CO_2 with epoxides. Both organic and inorganic cations are used to allow for both homogeneous and heterogeneous catalysis in the future.

1.4 Experimental theory

The methods used to analyse and characterise the POMs synthesised in this project were elemental analysis, infrared spectroscopy, multiple linear regression, single crystal X-ray diffraction and thermogravimetry. The following sections will give a brief description of each of these methods.

1.4.1 Elemental analysis (EA)

Elemental analysis (EA) is an analytical method that provides information about the elemental composition of a sample.[43] There are multiple ways of obtaining this information, and this thesis covers CHN analysis by combustion because it was the method used in this project.

CHN analysis, specifically, detects the amount of carbon, hydrogen and nitrogen in a sample. To start a CHN analysis the system is firstly flushed with helium gas to remove all traces of O_2, H_2O and CO_2, before a measured amount of oxygen is added to the helium stream.[44] Then the sample, packed in a tin, aluminium or silver capsule, and accurately weighed, is dropped into a preheated ceramic crucible. Here the capsule melts and the sample is oxidised:

$$\mathrm{C, H, N} \xrightarrow{1050°\mathrm{C},\ \mathrm{O_2}} \mathrm{CO_2(g) + H_2O(g) + N_2(g)}$$

Formula 3: Oxidation reaction for C, H and N.

The products are then passed through a WO_3 oxidation catalyst to complete the combustion of carbon to CO_2. After that it flows through a chamber with heated metallic copper where the nitrogen oxides are reduced to N_2, and the excess of O_2 is removed. CO_2, H_2O and N_2 are then separated using gas chromatography and measured using a thermal conductivity detector.[43, 44] In the context of this project, EA was mainly used to determine how many water molecules were coordinated to the different compounds, and how many potassium atoms were successfully substituted with tetrabutylammonium when synthesising organically soluble POMs.

1.4.2 Infrared spectroscopy (IR)

Infrared (IR) spectroscopy is a commonly used analytical technique in chemistry. This technique utilises molecular vibrations to identify covalent bonds between different atomic nuclei. The covalent bonds only absorb radiation with specific energies, and this absorption causes them to vibrate. The specific energies that get absorbed must have the same frequency (ν) as the molecular vibrations, which are expressed as:

$$E = h\nu_0\left(\nu + \frac{1}{2}\right) \text{ for } \nu = 0, 1, 2, 3 \ldots$$

Formula 4: Energy levels available to molecular vibrations.

where h = Planck's constant and v_0 = the zero-point vibrational level of the bond. The energy of the radiation that is absorbed can be determined by using either:

$$\Delta E = hc\left(\frac{1}{\lambda}\right) \text{ or } \Delta E = hc(\bar{\nu})$$

Formula 5: The energy of the absorbed radiation.

where c = the speed of light in vacuum, λ = wavelength and $\bar{\nu}$ = wavenumber. By sending IR radiation through the compound, the IR spectrometer can measure the amount of the radiation that gets absorbed, and thereby create a spectrum.[45] The absorption of radiation is plotted as transmittance against wavenumber in an IR spectrum, and their position on the x-axis is therefore determined by the vibrational frequency of the bond. The vibrational frequency varies as a function of the bond strength divided by the reduced mass of the vibration system.[46]

$$m_r = \frac{m_1 m_2}{m_1 + m_2}$$

Formula 6: The reduced mass of a two-body system.

where m = mass. The force required to stretch a bond is determined by Hooke's law:

$$F_x = -k_f x$$

Formula 7: Hooke's law.

where F_x = restoring force, k_f = force constant of the bond and x = displacement. Together, these expressions combine into the formula for vibrational frequency and wavenumber:

$$\nu = \left(\frac{1}{2\pi}\right)\left(\frac{k_f}{m_r}\right)^{\frac{1}{2}} \text{ or } \bar{\nu} = \left(\frac{1}{2c\pi}\right)\left(\frac{k_f}{m_r}\right)^{\frac{1}{2}}$$

Formula 8: Vibrational frequency and wavenumber.

IR spectroscopy gives information that can help identifying compounds, and it is useful for quantitative analysis of mixtures and to determine the structure of compounds. The IR spectrum for a compound is exclusive to that compound; consequently, it can be used as a fingerprint for the compound.[47] One of the main reasons IR spectroscopy is interesting when analysing POMs,

is that the majority of the early researchers that characterised these compounds had access to IR, which has provided a vast library of IR spectra.[48]

1.4.3 Multiple Linear Regression (MLR)

In statistics, simple linear regression is a method for modelling the linear correlation between one dependent (response) variable and one independent (explanatory) variable.[49] Multiple linear regression (MLR) is an expansion of simple linear regression, which uses multiple independent variables, rather than just one.[49, 50] One of the advantages of MLR is that it can provide a more accurate understanding of the impacts of each variable on the outcome, as it allows for the effects of multiple independent variables on one dependent variable to be studied at the same time. This information can then be used to predict dependent variables or see how well a set of independent variables can explain a dependent variable, among other things.[50]

In this project MLR was used to look for correlations between observed peak positions in the recorded IR spectra and the chemical properties of the metals inserted into the silicon tungsten Keggin structures.

1.4.4 Single Crystal X-ray diffraction (SXRD)

Single crystal X-ray diffraction (SXRD) is another analytical tool utilised in this project to characterise the synthesised POMs. The technique uses the diffraction of X-rays, which is the phenomenon where interference is created due to an object obstructing the path of the X-ray waves. The interference can be both constructive and destructive, depending on whether their displacements add or subtract.[46] Due to the arrangement of the atoms in a crystal, X-rays that hit the crystal at certain well-defined angles produce scattering of X-rays that give constructive interference. These angles can be calculated using Bragg's law which describes the diffraction and interference of X-rays as reflections at the atomic plane of the crystal lattice.[51] To calculate the angle, Bragg's law uses the optical path length difference, *2s*, between two reflected rays at neighbouring interplanar spacings.

$$s = d \sin \theta$$

Formula 9: Half of the optical path length difference.

where d = the interplanar spacing and θ = Braggs-angle θ_B.

If the optical path length difference is an integer multiple of the wavelength of the X-rays, λ, the reflected radiation will be in phase creating constructive interference.

$$n\lambda = 2d \sin\theta$$

Formula 10: Bragg's law.

where 2θ = angle between the incident and the reflected beam and n = "order" of the interference n = 1, 2, 3…[51, 52]

The diffraction is caused by the fact that the wavelength of X-rays is comparable to the bond lengths of molecules and the distance between atoms in crystals, and therefore get scattered by the electrons of the atoms in a crystal. The "scattering power" is dependent on the number of electrons, and for this reason it is possible to distinguish between different types of atoms. It may, however, be impossible to locate hydrogen atoms in the presence of heavy atoms.[43, 46]

In single crystal X-ray diffraction, the X-rays are diffracted by one single crystal that is rotated around various axis to achieve many different reflections. The crystal structure may then be determined by the angular position and the intensity of these reflections, and the diffraction data is recorded as frames in a data set. Hundreds or thousands of such frames are required to create a complete data set, which can then be used to determine the crystal structure.[43, 51]

1.4.5 Thermogravimetry (TG)

The last analytical method utilised in this project was thermogravimetry (TG). Thermogravimetry is a form of gravimetric analysis, which is defined as quantitative analysis by weight.[53] In TG analysis, a sample is gradually heated while its weight is being monitored against either time or temperature.

TG analysis is very useful when trying to determine the amount of solvent in the lattice structure of a crystal and how strongly the solvent is bound to the lattice. It can also be used to determine the amount of organic material in a sample or the thermal degradation of inorganic compounds or polymers.[43, 53] In this project TG has therefore been used, in combination with EA, to determine the amount of solvent coordinated to a POM compound and to evaluate how many TBA ligands are bound to a compound.

2 Aims

For any successful catalyst, there needs to be a cheap and reliable route to synthesising the catalytic material. In other words, it is not only important to synthesise the best catalyst, it also has to be cost-effective and easily available.

The potassium and TBA salts of $[SiXW_{11}O_{39}]^{n-}$ have shown potential as catalysts for the cycloaddition and copolymerisation of CO_2 with epoxides. Even though these POMs are well known, there is still a need for more reliable and efficient syntheses. Because of this, an aim of this thesis was to find syntheses for a range of POM compounds, that are time efficient, do not use highly toxic reagents and give high yields. This project focused on both potassium and TBA salts of $[SiXW_{11}O_{39}]^{n-}$, since they have promising potential for heterogeneous and homogeneous catalysis, respectively. The TBA salts were especially interesting, both because they had more potential for improvement, and also because they can be used in homogeneous catalysis, which is known to typically be the most beneficial.

Another aim of this project was to provide further IR characterisation of the synthesised compounds. This was of interest as many sources give varying IR data for the same POM, while little or no IR data is reported in the literature for other POMs. Comparison of the IR data was also of interest due to observed shifts in the spectra depending on the metal inserted into the structure. To get comparable data across the compounds, all the compounds were analysed using the same instrument and parameters. The goal was then to compare the IR data with respect to the chemical properties of the inserted metals to find potential correlations between the IR shifts.

3 Experimental

3.1 Materials

All the chemicals and solvents used in the syntheses presented were acquired from Sigma–Aldrich, Inc.

3.2 Instruments

All the samples in this thesis were analysed using infrared spectroscopy (IR) and elemental analysis (EA). Some samples were also analysed by thermogravimetry (TG) and some by single crystal X-ray diffraction (SXRD).

3.2.1 Elemental Analysis (EA)

The carbon, nitrogen and hydrogen content of the samples were measured using a Vario EL III from Elementar. Though the Vario EL III is capable of measuring sulphur, it was not calibrated for sulphur as it did not pertain to the samples.

3.2.2 Infrared spectroscopy (IR)

The IR spectra were recorded using a Nicolet iS50 FTIR Spectrometer (iS50 ATR). The spectra were recorded from 4000 to 400 cm^{-1} and the intensities have been denoted as w = weak, m = medium, s = strong, sh = sharp, br = broad. The analysis software OMNIC 9.8 by Thermo Fisher Scientific (Waltham, MA, US) was used to derivate the spectra, giving an insight into the composition of peaks and to provide more accurate values for comparison of the measured data. The software Sirius 8.1 by Pattern Recognition Systems (Bergen, Norway) was used to perform MLR analysis of the IR data.

3.2.3 Single Crystal X-ray diffraction (SXRD)

The single crystal X-ray diffraction was done on a Bruker AXS TXS rotating anode system with an APEXII Pt^{135} CCD detector using graphite monochromated Mo K_α radiation (λ = 0.71073 Å).

3.2.4 Thermogravimetry (TG)

The thermogravimetry analysis was done using a Netzsch Jupiter STA 449 F1. The temperature program went from 30 to 600 ºC, increasing by 2 ºC per minute, and the gas flow was at 50 mL

per minute using an 80/20 mixture of Ar and O_2. To view the TG data Proteus 6.1.0 from NETZSCH (Selb, Germany) was used.

3.3 Synthesis of α-$K_8SiW_{11}O_{39}\cdot xH_2O$ (SiW_{11})

The synthesis of α-$K_8SiW_{11}O_{39}\cdot xH_2O$ was based on literature procedures.[48]

Na_2WO_4 (45.50 g, 137.94 mmol) was dissolved in boiling distilled water (75 mL). HCl (41 mL, 4 M) was then added dropwise for 30 min. In a different beaker Na_2O_3Si (2.75 g, 22.53 mmol) was dissolved in distilled water (25 mL), and the solution was filtered if it was not completely clear. After that, this solution was added to the acidified Na_2WO_4 solution, and quickly, more HCl (13 mL, 4 M) was also added. The solution was kept boiling for 1 hour, before it was cooled to room temperature and filtered if it was not completely clear. While the solution was being stirred magnetically KCl (37.50 g, 503.02 mmol) was added, which produced a white precipitate. The solution was then filtered, and the product washed with about 100 mL cold distilled water. Finally, the product was air dried and kept in a desiccator for two days. This synthesis produced 32.518 g (7.373 mmol) of crude product in the form of a white powder.

Yield: 58.80 %
EA: Calculated for $K_8SiW_{11}O_{39}\cdot 79H_2O$ (4410.29 g mol^{-1}): N, 0.00; C, 0.00; H, 3.61; Found: N, 0.08; C, 0.33; H, 3.63
IR: 3395.06 (w, br), 1623.97 (w, sh), 994.61 (w, sh), 959.09 (w, sh), 880.81 (s, sh), 862.27 (s, sh), 785.49 (s, sh), 702.91 (s, sh), 499.57 (s, sh), 463.33 (m, sh)

3.4 Synthesis of $K_nSiXW_{11}(H_2O)O_{39}\cdot xH_2O$ (K-$SiXW_{11}$), where X = Al^{3+}, Co^{2+}, Cr^{3+}, Cu^{2+}, Fe^{3+}, Mn^{2+}, Ni^{2+}, Zn^{2+}

Two different syntheses were attempted to synthesise the potassium POM compounds. The first one, ^{I}K, was based on publications by Ma *et al.*[54, 55] and was used to synthesise the X^{3+} compounds (X = Al^{3+}, Cr^{3+}, Fe^{3+}). The other synthesis, ^{II}K, was based on a publication by Weakley *et al.*[56] and was used to synthesise the X^{2+} compounds (X = Co^{2+}, Cu^{2+}, Mn^{2+}, Ni^{2+}, Zn^{2+}). For all the potassium POM syntheses, three parallels were carried out.

3.4.1 ^{I}K: Synthesis of $K_5SiXW_{11}(H_2O)O_{39}\cdot xH_2O$ (^{I}K-$SiXW_{11}$), where X = Al^{3+}, Cr^{3+}, Fe^{3+}

The synthesis of $K_5SiXW_{11}(H_2O)O_{39}\cdot xH_2O$, where X = Al^{3+}, Cr^{3+}, Fe^{3+}, was based on publications by Ma *et al.*[54, 55] In this synthesis SiW_{11} from Section 3.3 was used.

SiW_{11} (3.226 g) was added to distilled water (10 mL). A solution of $X(NO_3)_3\cdot 9H_2O$ (0.994 mmol) dissolved in distilled water (5 mL), was then added dropwise. The pH of the solution was adjusted to between 5 and 6 using a diluted sodium bicarbonate solution (0.32 M). Thereafter, the solution was heated to 35-40 ºC, and kept at this temperature for 15 min. The solution was then removed from the heat and cooled down to room temperature. The volume of the solution was doubled using ethanol. This produced a precipitate, which was removed using gravity filtration. The filtrate was cooled to 5 °C to aid crystallisation, and the product created was long needlelike crystals. Once the crystallisation was done, the crystals were removed from the solution, air dried, and kept in a desiccator for at least two days.

$K_5SiAlW_{11}(H_2O)O_{39}\cdot xH_2O$ (^{I}K-$SiAlW_{11}$): The synthesis produced 0.284 g (0.078 mmol) of white needlelike crystals.
Yield: 10.67 %
EA: Calculated for $K_5SiAlW_{11}(H_2O)O_{39}\cdot 41H_2O$ (3653.41 g mol^{-1}): N, 0.00; C, 0.00; H, 2.32; Found: N, 0.07; C, 0.18; H, 2.31
IR: 3407.26 (w, br), 2971.09 (w, br), 1614.31 (w, br), 1401.45 (w, sh), 1009.44 (w, sh), 964.63 (m, sh), 909.01 (s, sh), 876.89 (m, sh), 771.68 (s, sh), 733.83 (s, sh), 672.36 (s, sh), 666.54 (s, sh), 499.80 (s, sh)

$K_5SiCrW_{11}(H_2O)O_{39}\cdot xH_2O$ (^{I}K-$SiCrW_{11}$): The synthesis produced 0.302 g (0.084 mmol) of green needlelike crystals.
Yield: 11.48 %
EA: Calculated for $K_5SiCrW_{11}(H_2O)O_{39}\cdot 36H_2O$ (3588.35 g mol^{-1}): N, 0.00; C, 0.00; H, 2.08; Found: N, 0.06; C, 0.20; H, 2.10
IR: 3431.53 (w, br), 2974.68 (w, br), 1613.35 (w, sh), 1008.84 (w, sh), 962.31 (m, sh), 908.16 (s, sh), 872.59 (m, sh), 758.89 (s, sh), 646.22 (s, sh), 496.69 (s, sh)

$K_5SiFeW_{11}(H_2O)O_{39}\cdot xH_2O$ (^{I}K-$SiFeW_{11}$): The synthesis produced 0.681 g (0.175 mmol) of yellow needlelike crystals.

Yield: 23.93 %

EA: Calculated for $K_5SiFeW_{11}(H_2O)O_{39}\cdot 53H_2O$ (3898.46 g mol^{-1}): N, 0.00; C, 0.00; H, 2.79; Found: N, 0.07; C, 0.67; H, 2.80

IR: 3451.22 (w, br), 2975.00 (w, br), 1614.97 (w, sh), 1005.97 (w, sh), 961.82 (m, sh), 902.34 (s, sh), 745.68 (s, sh), 694.11 (s, sh), 641.93 (s, sh), 520.87 (s, sh), 502.92 (s, sh)

3.4.2 ^{II}K: Synthesis of $K_6SiXW_{11}(H_2O)O_{39}\cdot xH_2O$ (^{II}K-$SiXW_{11}$), where X = Co^{2+}, Cu^{2+}, Mn^{2+}, Ni^{2+}, Zn^{2+}

The synthesis of $K_6SiXW_{11}(H_2O)O_{39}\cdot xH_2O$, where X = Co^{2+}, Cu^{2+}, Mn^{2+}, Ni^{2+}, Zn^{2+}, was based on a publication by Weakley *et al.*[56]

$H_4SiW_{12}O_{40}\cdot xH_2O$ (2.800 g, 0.973 mmol) was dissolved in distilled water (10 mL) at 95 ºC, and the metal compound (1.217 mmol) was dissolved in distilled water (1 mL) at 85 ºC. A solution of CH_3COOK (3.000 g, 30.569 mmol) dissolved in distilled water (3 mL) at 85 ºC was then prepared, and the pH adjusted to 7 using acetic acid. The solution of the metal compound was then added dropwise to the $H_4SiW_{12}O_{40}$ solution, followed by the CH_3COOK solution which was also added dropwise. The solution was kept stirring at 95 ºC for 1 minute before it was quickly filtered. After the crystals were formed, they were removed from the solution by filtration. The product was then air dried, before being stored in a desiccator for at least two days.

$K_6SiCoW_{11}(H_2O)O_{39}\cdot xH_2O$ (^{II}K-$SiCoW_{11}$): The synthesis produced 2.375 g (0.532 mmol) of wine-red crystals. The metal compound used in this synthesis was cobalt(II) acetate tetrahydrate ($Co(CH_3COO)_2\cdot 4H_2O$).

Yield: 54.69 %

EA: Calculated for $K_6SiCoW_{11}(H_2O)O_{39}\cdot 82H_2O$ (4463.09 g mol^{-1}): N, 0.00; C, 0.00; H, 3.75; Found: N, 0.00; C, 0.59; H, 3.77

IR: 3414.72 (w, br), 1614.34 (w, sh), 1398.78 (w, sh), 1340.64 (w, sh), 997.94 (w, sh), 953.25 (m, sh), 886.93 (s, sh), 775.93 (s, sh), 742.72 (s, sh), 681.22 (s, sh), 505.22 (s, sh), 479.12 (s, sh)

$K_6SiCuW_{11}(H_2O)O_{39}\cdot xH_2O$ (^{II}K-$SiCuW_{11}$): The synthesis produced 2.168 g (0.540 mmol) of pale blue crystals. The metal compound used in this synthesis was copper(II) acetate monohydrate ($Cu(CH_3COO)_2\cdot H_2O$).

Yield: 55.46 %

EA: Calculated for $K_6SiCuW_{11}(H_2O)O_{39}\cdot 57H_2O$ (4017.32 g mol^{-1}): N, 0.00; C, 0.00; H, 2.91; Found: N, 0.00; C, 0.39; H, 2.92

IR: 3577.07 (w, br), 3459.95 (w, br), 1613.51 (w, sh), 1010.09 (w, sh), 979.25 (w, sh), 950.25 (m, sh), 921.39 (m, sh), 888.85 (s, sh), 730.31 (s, sh), 685.90 (s, sh), 506.21 (s, sh), 476.46 (s, sh)

$K_6SiMnW_{11}(H_2O)O_{39}\cdot xH_2O$ (^{II}K-$SiMnW_{11}$): The synthesis produced 2.019 g (0.582 mmol) of orange crystals. The metal compound used in this synthesis was manganese(II) acetate tetrahydrate ($Mn(CH_3COO)_2\cdot 4H2O$).

Yield: 59.83 %

EA: Calculated for $K_6SiMnW_{11}(H_2O)O_{39}\cdot 27H_2O$ (3468.26 g mol^{-1}): N, 0.00; C, 0.00; H, 1.63; Found: N, 0.00; C, 0.65; H, 1.62

IR: 3399.65 (w, br), 1617.28 (w, sh), 1568.18 (w, sh), 1396.85 (w, sh), 1342.52 (w, sh), 998.01 (w, sh), 950.18 (m, sh), 880.72 (s, sh), 781.93 (s, sh), 754.22 (s, sh), 687.27 (s, sh), 503.65 (s, sh)

$K_6SiNiW_{11}(H_2O)O_{39}\cdot xH_2O$ (^{II}K-$SiNiW_{11}$): The synthesis produced 2.285 g (0.648 mmol) of bright yellow-green crystals. The metal compound used in this synthesis was nickel(II) sulphate hexahydrate ($Ni(SO_4)\cdot 6H_2O$).

Yield: 66.60 %

EA: Calculated for $K_6SiNiW_{11}(H_2O)O_{39}\cdot 30H_2O$ (3526.06 g mol^{-1}): N, 0.00; C, 0.00; H, 1.77; Found: N, 0.00; C, 0.15; H, 1.79

IR: 3409.39 (w, br), 1616.64 (w, sh), 998.55 (w, sh), 952.78 (m, sh), 890.52 (s, sh), 756.47 (s, sh), 680.55 (s, sh), 515.11 (s, sh)

$K_6SiZnW_{11}(H_2O)O_{39}\cdot xH_2O$ (^{II}K-$SiZnW_{11}$): The synthesis produced 2.207 g (0.628 mmol) of small white crystals. The metal compound used in this synthesis was zinc acetate dihydrate ($Zn(CH_3COO)_2\cdot 2H_2O$).

Yield: 64.54 %

EA: Calculated for $K_6SiZnW_{11}(H_2O)O_{39}\cdot 29H_2O$ (3514.74 g mol^{-1}): N, 0.00; C, 0.00; H, 1.72; Found: N, 0.00; C, 0.35; H, 1.74

IR: 3417.11 (w, br), 1615.75 (m, sh), 1399.04 (w, sh), 1341.67 (w, sh), 1000.64 (w, sh), 951.17 (m, sh), 882.28 (s, sh), 777.56 (s, sh), 746.82 (s, sh), 680.09 (s, sh), 507.00 (s, sh)

3.5 Synthesis of $TBA_{n-x}K_xSiXW_{11}(H_2O)O_{39}$ (TBA-$SiXW_{11}$), where X = Al^{3+}, Co^{2+}, Cr^{3+}, Cu^{2+}, Fe^{3+}, Mn^{2+}, Ni^{2+}, Zn^{2+}

Three different syntheses were attempted to synthesise POMs with TBA cations. The first synthesis, ^{I}TBA, was based on a publication by Balula *et al.*,[28] and was attempted with most of the X^{2+} metal compounds (X = Cu^{2+}, Mn^{2+}, Ni^{2+}, Zn^{2+}). As this synthesis required the use of dichloromethane (DCM), the TBA POMs were also attempted synthesised by modifying a $TBA_4(Mo_8O_{26})$ synthesis from Ginsberg,[48] ^{II}TBA, but this synthesis was only tried with one of the X^{2+} metal compounds (X = Co^{2+}). Finally, the TBA POMs were synthesised using a synthesis from Kato *et al.*,[26] ^{III}TBA. This synthesis was used both for the X^{2+} metals compounds (X = Co^{2+}, Cu^{2+}, Mn^{2+}, Ni^{2+}, Zn^{2+}), as well as the X^{3+} metal compounds (X = Al^{3+}, Cr^{3+}, Fe^{3+}).

3.5.1 ^{I}TBA: Synthesis of $TBA_{6-x}K_xSiXW_{11}(H_2O)O_{39}$ (^{I}TBA-$SiXW_{11}$), where X = Cu^{2+}, Mn^{2+}, Ni^{2+}, Zn^{2+}

As mentioned previously, the first attempt to synthesise the TBA POMs was based on a publication by Balula *et al.*,[28] and was attempted for X = Cu^{2+}, Mn^{2+}, Ni^{2+}, Zn^{2+}. No parallels were performed for the ^{I}TBA synthesis.

Firstly, the respective potassium compound synthesised in Section 3.4.2 (0.500 mmol) was dissolved in distilled water (30 mL) and vigorously mixed with a solution of tetrabutylammonium bromide (TBABr) (1.290 g, 4.000 mmol) in DCM (45 mL). After stirring, the water and DCM layers separated, and the DCM layer was collected. The DCM was then removed by evaporation leaving behind an oil. The oil was dissolved in acetonitrile and the TBA compound was precipitated by adding a minimum amount of water. The product was then isolated by filtration, air dried and kept in a desiccator for at least two days. In the cases where the product was recrystallised, it was done through vapor diffusion from methanol.

$TBA_{6-x}K_xSiCuW_{11}(H_2O)O_{39}$ (^{I}TBA-$SiCuW_{11}$): The synthesis produced 0.548 g (0.144 mmol) of pale blue powder. The EA data for this sample is from a recrystallised sample.

Yield: 28.81 %

EA: Calculated for $(N(C_4H_9)_4)_4K_2SiCuW_{11}(H_2O)O_{39}$ (3803.91 g mol^{-1}): N, 1.47; C, 20.21; H, 3.87; Found: N, 1.51; C, 20.99; H, 3.96

IR: 2958.40 (w, sh), 2933.80 (w, sh), 2871.85 (w, sh), 1483.82 (w, sh), 1380.73 (w, sh), 1001.81 (w, sh), 959.33 (m, sh), 908.27 (s, sh), 874.67 (m, sh), 796.29 (s, sh), 735.40 (m, sh), 694.84 (m, sh), 610.07 (w, sh), 591.54 (w, sh), 541.12 (m, sh), 490.53 (w, sh), 468.69 (w, sh)

$TBA_{6-x}K_xSiMnW_{11}(H_2O)O_{39}$ (^{I}TBA-$SiMnW_{11}$): The synthesis produced 0.056 g (0.015 mmol) of pale orange powder.

Yield: 2.95 %

EA: Calculated for $(N(C_4H_9)_4)_4K_2SiMnW_{11}(H_2O)O_{39}$ (3795.30 g mol^{-1}): N, 1.48; C, 20.25; H, 3.88; Found: N, 1.56; C, 21.34; H, 3.92

IR: 2960.26 (w, sh), 2873.06 (w, sh), 1484.02 (w, sh), 1381.04 (w, sh), 1032.10 (w, sh), 1005.64 (w, sh), 960.56 (m, sh), 918.50 (s, sh), 876.81 (m, sh), 787.54 (s, sh), 531.61 (m, sh)

$TBA_{6-x}K_xSiNiW_{11}(H_2O)O_{39}$ (^{I}TBA-$SiNiW_{11}$): The synthesis produced 0.209 g (0.055 mmol) of pale green powder. The EA data for this sample is from a recrystallised sample.

Yield: 11.00 %

EA: Calculated for $(N(C_4H_9)_4)_4K_2SiNiW_{11}(H_2O)O_{39}$ (3799.06 g mol^{-1}): N, 1.47; C, 20.23; H, 3.87; Found: N, 1.52; C, 20.71; H, 4.35

IR: 2960.67 (w, sh), 2934.96 (w, sh), 2873.01 (w, sh), 1627.01 (w, sh), 1484.37 (w, sh), 1462.57 (w, sh), 1380.60 (w, sh), 1151.91 (w, sh), 1106.55 (w, sh), 1057.50 (w, sh), 999.56 (w, sh), 956.98 (m, sh), 901.73 (s, sh), 793.77 (s, sh), 770.21 (s, sh), 539.41 (m, sh)

$TBA_{6-x}K_xSiZnW_{11}(H_2O)O_{39}$ (^{I}TBA-$SiZnW_{11}$): The synthesis produced 0.059 g (0.016 mmol) of white powder.

Yield: 3.10 %

EA: Calculated for $(N(C_4H_9)_4)_4K_2SiZnW_{11}(H_2O)O_{39}$ (3805.75 g mol^{-1}): N, 1.47; C, 20.20; H, 3.87; Found: N, 1.51; C, 20.73; H, 3.96

IR: 2960.12 (w, sh), 2934.79 (w, sh), 2872.88 (w, sh), 1484.90 (w, sh), 1380.75 (w, sh), 1151.46 (w, sh), 1058.49 (w, sh), 1000.26 (w, sh), 958.72 (m, sh), 902.05 (s, sh), 799.45 (s, sh), 540.51 (m, sh)

3.5.2 ^{II}TBA: Synthesis of $TBA_{6-x}K_xSiXW_{11}(H_2O)O_{39}$ (^{II}TBA-$SiXW_{11}$), where X = Co^{2+}

The next attempt to synthesise TBA-$SiXW_{11}$ was based on a synthesis by Ginsberg.[48] It was attempted with X = Co^{2+}, and again, it utilised the potassium compound synthesised in Section 3.4.2. Three parallels were carried out for the ^{II}TBA synthesis.

The potassium compound (0.578 mmol) was dissolved in a minimum amount of distilled water at 70 ºC. The solution was kept at 70 ºC and vigorously stirred while a solution of TBABr (1.680 g, 5.200 mmol) dissolved in distilled water (5 mL) was added dropwise, producing a precipitate. The solution was cooled to room temperature and stirred for 30 min. The product was collected by filtration and washed successively with water, ethanol, acetone and diethyl ether. Finally, the product was air dried and kept in a desiccator for two days, before it was recrystallised through vapor diffusion from methanol.

$TBA_{6-x}K_xSiCoW_{11}(H_2O)O_{39}$ (^{II}TBA-$SiCoW_{11}$): The synthesis produced 0.543 g (0.143 mmol) of pale pink powder. The EA data for this sample is from a recrystallised sample.
Yield: 24.73 %
EA: Calculated for $(N(C_4H_9)_4)_4K_2SiCoW_{11}(H_2O)O_{39}$ (3799.30 g mol^{-1}): N, 1.47; C, 20.23; H, 3.87; Found: N, 1.48; C, 20.71; H, 4.32
IR: 2959.25 (w, sh), 2932.76 (w, sh), 2872.03 (w, sh), 1628.26 (w, sh), 1482.54 (w, sh), 1379.92 (w, sh), 1151.54 (w, sh), 1000.06 (w, sh), 956.58 (m, sh), 901.86 (s, sh), 790.44 (s, sh), 737.12 (s, sh), 536.33 (m, sh), 473.99 (w, sh)

3.5.3 ^{III}TBA: Synthesis of $TBA_{n-x}K_xSiXW_{11}(H_2O)O_{39}$ (^{III}TBA-$SiXW_{11}$), where X = Al^{3+}, Co^{2+}, Cr^{3+}, Cu^{2+}, Fe^{3+}, Mn^{2+}, Ni^{2+}, Zn^{2+}

The last synthesis that was attempted to synthesise the TBA POMs was based on a publication by Kato *et al.*[26] This synthesis was used to synthesise $TBA_{6-x}K_xSiXW_{11}(H_2O)O_{39}$, where X = Co^{2+}, Cu^{2+}, Mn^{2+}, Ni^{2+} and Zn^{2+}, as well as to synthesise $TBA_{5-x}K_xSiXW_{11}(H_2O)O_{39}$, where X = Al^{3+}, Cr^{3+} and Fe^{3+}. Three parallels were carried out for all the compounds synthesised using the ^{III}TBA synthesis.

In this synthesis SiW_{11} from Section 3.3 was used. SiW_{11} (1.281 g, 0.400 mmol) was dissolved in distilled water (40 mL) at 60 ºC. The metal compound (0.400 mmol) was then dissolved in a

minimum amount of distilled water at 60 ºC and added dropwise to the SiW_{11} solution. The pH of the solution was adjusted to 3.7 - 4.2 using acetic acid. The solution was then cooled to room temperature and left to stir for three hours. Solid TBABr (3.868 g, 12.000 mmol) was then added, creating a precipitate, followed by stirring at room temperature for three days. The solution was then filtered to isolate the product. Finally, the product was air dried and then kept in a desiccator for at least two days.

$TBA_{5-x}K_xSiAlW_{11}(H_2O)O_{39}$ (^{III}TBA-$SiAlW_{11}$): The synthesis produced 1.239 g (0.332 mmol) of white powder. The metal compound used in this synthesis was aluminium nitrate nonahydrate ($Al(NO_3)_3 \cdot 9H_2O$).

Yield: 83.08 %

EA: Calculated for $(N(C_4H_9)_4)_4KSiAlW_{11}(H_2O)O_{39}$ (3728.25 g mol^{-1}): N, 1.50; C, 20.62; H, 3.95; Found: N, 1.41; C, 19.17; H, 3.89

IR: 2959.59 (w, sh), 2933.98 (w, sh), 2872.12 (w, sh), 1630.09 (w, sh), 1482.99 (w, sh), 1379.69 (w, sh), 1151.79 (w, sh), 1003.41 (w, sh), 954.43 (m, sh), 910.10 (s, sh), 874.21 (m, sh), 773.41 (s, sh), 738.52 (s, sh), 525.81 (m, sh), 506.19 (m, sh)

$TBA_{6-x}K_xSiCoW_{11}(H_2O)O_{39}$ (^{III}TBA-$SiCoW_{11}$): The synthesis produced 1.323 g (0.348 mmol) of pale pink powder. The metal compound used in this synthesis was cobalt(II) acetate tetrahydrate ($Co(CH_3COO)_2 \cdot 4H_2O$).

Yield: 87.06 %

EA: Calculated for $(N(C_4H_9)_4)_4K_2SiCoW_{11}(H_2O)O_{39}$ (3799.30 g mol^{-1}): N, 1.47; C, 20.23; H, 3.87; Found: N, 1.66; C, 22.81; H, 3.80

IR: 2959.35 (w, sh), 2872.46 (w, sh), 1484.32 (w, sh), 1380.14 (w, sh), 998.89 (w, sh), 956.70 (m, sh), 899.88 (s, sh), 791.43 (s, sh), 776.69 (s, sh), 539.36 (m, sh), 474.51 (w, sh)

$TBA_{5-x}K_xSiCrW_{11}(H_2O)O_{39}$ (^{III}TBA-$SiCrW_{11}$): The synthesis produced 1.283 g (0.323 mmol) of pale green powder. The metal compound used in this synthesis was chromium(III) nitrate nonahydrate ($Cr(NO_3)_3 \cdot 9H_2O$).

Yield: 81.07 %

EA: Calculated for $(N(C_4H_9)_4)_5SiCrW_{11}(H_2O)O_{39}$ (3956.62 g mol^{-1}): N, 1.77; C, 24.28; H, 4.64; Found: N, 1.78; C, 23.93; H, 4.18

IR: 2960.00 (w, sh), 2936.02 (w, sh), 2873.15 (w, sh), 1483.64 (w, sh), 1380.79 (w, sh), 1020.16 (w, sh), 1003.89 (w, sh), 955.71 (m, sh), 909.26 (s, sh), 788.36 (s, sh), 680.84 (m, sh), 526.04 (m, sh)

$TBA_{6-x}K_xSiCuW_{11}(H_2O)O_{39}$ (^{III}TBA-$SiCuW_{11}$): The synthesis produced 1.393 g (0.348 mmol) of pale blue powder. The metal compound used in this synthesis was copper(II) acetate monohydrate ($Cu(CH_3COO)_2 \cdot H_2O$).

Yield: 86.90 %

EA: Calculated for $(N(C_4H_9)_4)_5KSiCuW_{11}(H_2O)O_{39}$ (4007.27 g mol^{-1}): N, 1.75; C, 23.98; H, 4.58; Found: N, 1.67; C, 23.02; H, 4.25

IR: 2959.40 (w, sh), 2873.17 (w, sh), 1484.06 (w, sh), 1380.83 (w, sh), 1000.65 (w, sh), 958.59 (m, sh), 949.69 (m, sh), 905.62 (s, sh), 874.76 (m, sh), 792.47 (s, sh), 735.84 (s, sh), 693.56 (m, sh), 607.79 (w, sh), 540.68 (m, sh), 490.64 (w, sh)

$TBA_{5-x}K_xSiFeW_{11}(H_2O)O_{39}$ (^{III}TBA-$SiFeW_{11}$): The synthesis produced 1.464 g (0.370 mmol) of pale yellow powder. The metal compound used in this synthesis was iron(III) nitrate nonahydrate ($Fe(NO_3)_3 \cdot 9H_2O$).

Yield: 92.41 %

EA: Calculated for $(N(C_4H_9)_4)_5SiFeW_{11}(H_2O)O_{39}$ (3960.47 g mol^{-1}): N, 1.77; C, 24.26; H, 4.63; Found: N, 1.84; C, 24.46; H, 4.42

IR: 3485.43 (w, br), 2958.93 (w, sh), 2934.69 (w, sh), 2872.50 (w, sh), 1632.57 (w, sh), 1482.38 (w, sh), 1380.31 (w, sh), 1345.68 (w, sh), 1021.64 (w, sh), 998.44 (w, sh), 952.90 (m, sh), 901.74 (s, sh), 871.94 (m, sh), 779.52 (s, sh), 766.85 (s, sh), 661.78 (m, sh), 527.08 (m, sh)

$TBA_{6-x}K_xSiMnW_{11}(H_2O)O_{39}$ (^{III}TBA-$SiMnW_{11}$): The synthesis produced 1.373 g (0.343 mmol) of pale orange powder. The metal compound used in this synthesis was manganese(II) acetate tetrahydrate ($Mn(CH_3COO)_2 \cdot 4H_2O$).

Yield: 85.84 %

EA: Calculated for $(N(C_4H_9)_4)_5KSiMnW_{11}(H_2O)O_{39}$ (3998.67 g mol^{-1}): N, 1.75; C, 24.03; H, 4.59; Found: N, 1.73; C, 23.63; H, 4.15

IR: 2960.37 (w, sh), 2872.78 (w, sh), 1483.64 (w, sh), 1380.69 (w, sh), 1152.65 (w, sh), 999.47 (w, sh), 955.07 (m, sh), 895.44 (s, sh), 794.82 (s, sh), 720.36 (s, sh), 529.05 (m, sh)

$TBA_{6-x}K_xSiNiW_{11}(H_2O)O_{39}$ (^{III}TBA-$SiNiW_{11}$): The synthesis produced 1.143 g (0.286 mmol) of pale green powder. The metal compound used in this synthesis was nickel(II) sulphate hexahydrate ($Ni(SO_4)\cdot 6H_2O$).

Yield: 71.39 %

EA: Calculated for $(N(C_4H_9)_4)_5KSiNiW_{11}(H_2O)O_{39}$ (4002.42 g mol^{-1}): N, 1.75; C, 24.01; H, 4.58; Found: N, 1.77; C, 24.36; H, 4.39

IR: 2959.40 (w, sh), 2934.59 (w, sh), 2872.86 (w, sh), 1484.28 (w, sh), 1380.11 (w, sh), 999.68 (w, sh), 957.08 (m, sh), 901.32 (s, sh), 794.84 (s, sh), 770.73 (s, sh), 539.68 (m, sh)

$TBA_{6-x}K_xSiZnW_{11}(H_2O)O_{39}$ (^{III}TBA-$SiZnW_{11}$): The synthesis produced 1.191 g (0.297 mmol) of white powder. The metal compound used in this synthesis was zinc acetate dihydrate ($Zn(CH_3COO)_2\cdot 2H_2O$).

Yield: 74.27 %

EA: Calculated for $(N(C_4H_9)_4)_5KSiZnW_{11}(H_2O)O_{39}$ (4009.12 g mol^{-1}): N, 1.75; C, 23.97; H, 4.58; Found: N, 1.72; C, 23.49; H, 4.56

IR: 2959.74 (w, sh), 2933.87 (w, sh), 2872.25 (w, sh), 1484.23 (w, sh), 1380.23 (w, sh), 999.00 (w, sh), 957.12 (m, sh), 899.76 (s, sh), 794.84 (s, sh), 540.05 (m, sh)

4 Results and Discussion

In this project the potassium and TBA salts of $[SiXW_{11}O_{39}]^{n-}$, where X = Al^{3+}, Co^{2+}, Cr^{3+}, Cu^{2+}, Fe^{3+}, Mn^{2+}, Ni^{2+} and Zn^{2+}, were synthesised because they show interesting catalytic properties. The focus of this project has been on improving the syntheses used to make these compounds and provide more analytical data, particularly within IR, as these were areas with opportunities for improvement. During this project two different syntheses were used to synthesise the potassium compounds: ^{I}K and ^{II}K, and three different syntheses were used to synthesise the TBA compounds: ^{I}TBA, ^{II}TBA and ^{III}TBA. In sections 4.1 to 4.3 we will go through the EA and IR results for the different synthesised compounds, and comment on their syntheses; their yield, efficiency and occasional issues. For some of the TBA compounds we will also look at TG results. In the following section, 4.4, we will look briefly at SXRD results recorded for some of the potassium and TBA compounds, and finally, in Section 4.5, we will be comparing the IR results for all synthesised compounds to see if there is any correlation between them.

When analysing the IR results for the synthesised compounds, different peaks will be assigned to bond stretches known to be in the structures, based on previous analyses and assignments from the literature. These assignments can be found in Table 1 and Table 2. The IR results presented will also include the second derivative of the spectra to provide further insight into the composition of the observed peaks and give more accurate values for the peaks of interest.

Table 1: Theoretical absorption peaks for Keggin-type silicotungstates.

Wavenumber range [cm^{-1}]	**Assignment**
3615	O-H asymmetric stretching
3450	O-H symmetric stretching
1640	O-H scissoring
1000 – 960	W=O stretch
970 – 950	Si-O stretch
890 – 850	W-Ob-W stretch
800 – 760	W-Oc-W stretch

The O-H absorption frequencies in Table 1 are from a book by Nakamoto.[57] These values represent the expected absorption frequencies for symmetric and asymmetric stretching, as well as scissoring in liquid H_2O, and are based on research by Walrafen.[58] The different wavenumber ranges assigned to the W=O, W-Ob-W (inter bridges between corner-sharing octahedra) and

W-Oc-W ("intra" bridges between edge-sharing octahedra) stretches, are from a publication by Bamoharram.[59] Finally, the wavenumber range assigned to the Si-O stretch is based on reported and assigned IR data from Duan *et al*.[60] who characterised some of the same compounds as this thesis.

The TBA salts will also have some additional peaks since they contain organic cations. The values presented in Table 2 are from a book by Mohrig *et al*.,[45] and they are the expected absorption ranges for the C-H bend and stretch for alkanes and the C-N stretch in amines.

Table 2: Additional theoretical absorption peaks for Keggin-type TBA silicotungstates.

Wavenumber range [cm^{-1}]	**Assignment**
2990-2850	C-H stretch
1480-1430	C-H bend for CH_3
1395-1340	C-H bend for CH_2
1250-1025	C-N stretch

The elemental analysis measurements presented in this thesis had an uncertainty of %N: ± 0.01 wt%, %C: ± 0.07 wt% and %H: ± 0.05 wt% and all the theoretical calculations were performed using the Lenntech Molecular Weight Calculator https://www.lenntech.com/calculators/molecular/molecular-weight-calculator.htm..

4.1 EA and IR results and discussion for SiW_{11}

Table 3: EA results for SiW_{11}.

	N [%]	**C [%]**	**H [%]**
Found	0.08	0.33	3.63
Calculated for $K_8SiW_{11}O_{39}\cdot 79H_2O$	0.00	0.00	3.61

The EA results (see Table 3) show that the analysed SiW_{11} sample has a hydrogen value of 3.63 %, which correlates to the hydrogen value of $K_8SiW_{11}O_{39}\cdot 79H_2O$. 79 water molecules per POM molecule is a surprising amount of water, especially considering the synthesis by Ginsberg[48] which reports that SiW_{11} should only coordinate 13 water molecules. It is likely that the high water content is a result of insufficient drying methods used in this project; however, it could also be caused by the fact that the synthesis and analysis for SiW_{11} was carried out during a time of high humidity, making the compound coordinate more water than expected. With 79

water molecules the molar mass of SiW_{11} is 4410.29 g mol^{-1}. This means that the 32.518 g of product, in the form of a white powder, equals 7.373 mmol, making the yield of the synthesis 58.80 %. If the yield had been calculated using the molar mass for $K_8SiW_{11}O_{39}{\cdot}13H_2O$ (M_w = 3221.29 g mol^{-1}), it would have been 78.14 %, which is still lower than the reported yield of 90 % by Ginsberg.[48] Since the SiW_{11} sample was used as a start material in many of the following syntheses, it is useful to know its molar weight to accurately calculate the yield of the syntheses following. The yield calculations for the syntheses that utilises SiW_{11} will therefore be made on the basis that the SiW_{11} sample contains 79 water molecules.

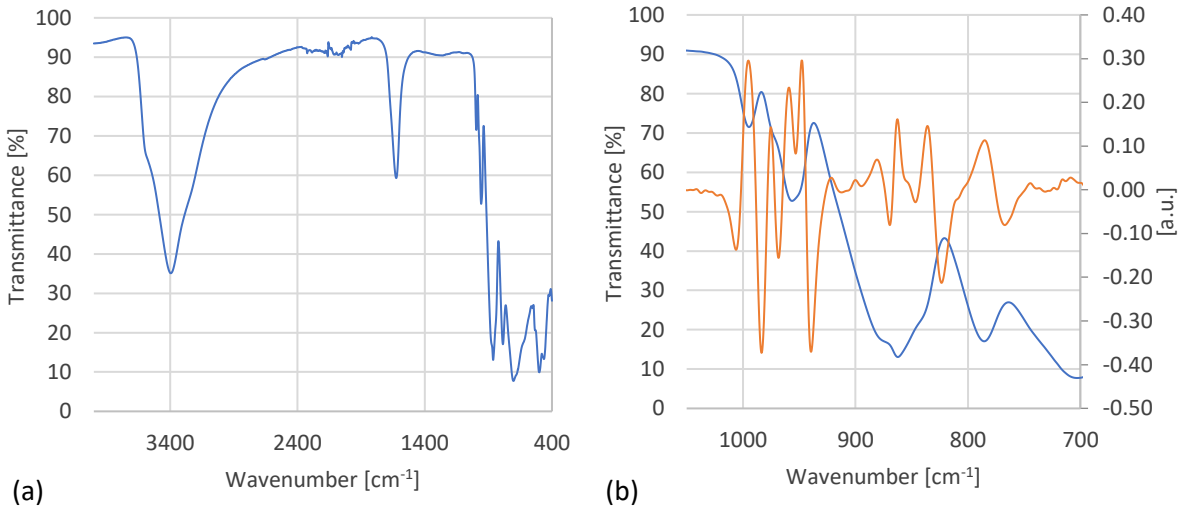

Figure 3: (a) The complete IR spectrum for SiW_{11}, (b) the IR (blue) and second derivative (orange) spectra from 1050 – 700 cm^{-1} for SiW_{11}.

Table 4: Overview of IR data for SiW_{11}.

Wavenumber [cm^{-1}]			**Assignment**
Experimental	**Second derivative***	**Literature[48]**	
994.61	995.18	1000	W=O stretch
959.09	947.61, 959.09, 975.16	952	Si-O stretch
880.81	862.67, 835.93, 880.81, 899.97, 921.43	885	W-Ob-W stretch
785.49	785.07, 744.51, 736.73, 727.95, 723.53	797, 725	W-Oc-W stretch

*Sorted by intensity.

As can be seen from Figure 3, the IR spectrum for SiW_{11} has four peaks in the range 1050-700 cm^{-1} which correlate to the peaks characteristic for the Keggin POMs described in Table 1. As the compound was synthesised from chemicals that do not have the Keggin structure, the IR spectrum shows that the synthesis has changed the structure of the compound.

If we compare the peaks observed in the IR spectrum for SiW_{11} (Figure 3) with the theoretical values presented in Table 1, it can be assumed that the peaks seen at 3395.06 cm^{-1} and 1623.97 cm^{-1} are due to the presence of water in the sample. The signal for water is very strong, which reinforces the EA results presented earlier. When comparing the experimental IR spectrum in Figure 3 to the IR data provided by Ginsberg[48] (see Table 4), the values seem to agree well. Though the peaks assigned to the W=O and W-Ob-W stretches are a bit lower than expected, and the peak for the Si-O stretch is a bit higher, their deviation is not large enough to cause concern. For the peaks assigned to the W-Oc-W stretch, there is a bit more deviation, but as will be seen in following IR results, this is the peak that tends to show the most deviation, both when comparing experimental values with the literature as well as when comparing literature sources with each other.

4.2 Synthesis and analysis of the potassium compounds

4.2.1 EA results and yields for the potassium compounds

K-$SiAlW_{11}$

Table 5: EA results for ^{I}K-$SiAlW_{11}$.

	N [%]	C [%]	H [%]
Found	0.07	0.18	2.31
Calculated for $K_5SiAlW_{11}(H_2O)O_{39}\cdot 41H_2O$	0.00	0.00	2.32

According to the EA results presented in Table 5, the ^{I}K-$SiAlW_{11}$ compound had a hydrogen value of 2.31 %. This hydrogen value is similar to that of $K_5SiAlW_{11}(H_2O)O_{39}\cdot 41H_2O$, which has a molar mass of 3653.41 g mol^{-1}. As the synthesis produced 0.284 g (0.078 mmol) of white needlelike crystals from 0.731 mmol of SiW_{11}, the yield of the synthesis was 10.67 %. Normally, $Al(NO_3)_3$ would have been the limiting reagent in this synthesis; however, due to the surprisingly high water content of SiW_{11} (see Section 4.1), less SiW_{11} than intended was used, thereby making it the limiting reagent in the ^{I}K synthesis.

According to the original synthesis by Ma *et al.*,[54] the water content of the product should be 24 H_2O molecules per POM molecule. If our product had contained 24 water molecules, the molar mass would be 3347.16 g mol^{-1} and the yield would have been 11.61 %. Table 5 also shows that there is nitrogen and carbon in the ^{I}K-$SiAlW_{11}$ sample. A possible explanation for this might be that the synthesis uses a nitrate start material and ethanol to precipitate the product.

K-SiCoW$_{11}$

Table 6: EA results for ^{II}K-SiCoW$_{11}$.

	N [%]	C [%]	H [%]
Found	0.00	0.59	3.77
Calculated for $K_6SiCoW_{11}(H_2O)O_{39}\cdot 82H_2O$	0.00	0.00	3.75

The EA results presented in Table 6 show that the analysed compound has a hydrogen value of 3.77 %, which is similar to the hydrogen value expected for $K_6SiCoW_{11}(H_2O)O_{39}\cdot 82H_2O$. Compared to Wang *et al.*,[61] who report $K_6SiCoW_{11}(H_2O)O_{39}$ with 14 H_2O molecules, 82 H_2O molecules is surprisingly high. Most likely the reason for the high water content is insufficient drying methods and the elemental analysis being performed during a time of very high humidity, causing the sample to hold more water than expected.

The product of the synthesis was wine-red crystals; however, about five min after their crystallisation, a white precipitate was formed on top of the product. The white precipitate was also analysed using EA and the results will be discussed on page 33. The EA results in Table 6 show that there is carbon in the sample, which could be from this white precipitate, or it might be because the synthesis uses CH_3COOK.

With 83 water molecules, the molar mass of ^{II}K-SiCoW$_{11}$ is 4463.09 g mol^{-1}. As the synthesis produced 2.375 g (0.532 mmol) of the product, the yield of the synthesis is 54.69 %. If there had only been 15 water molecules, which according to Wang *et al.*[61] there should have been, the yield would have been 75.38 %.

K-SiCrW$_{11}$

Table 7: EA results for ^{I}K-SiCrW$_{11}$.

	N [%]	C [%]	H [%]
Found	0.06	0.20	2.10
Calculated for $K_5SiCrW_{11}(H_2O)O_{39}\cdot 36H_2O$	0.00	0.00	2.08

According to the EA results presented in Table 7, the hydrogen value for ^{I}K-SiCrW$_{11}$ was 2.10 %, which correlates to the hydrogen value expected for $K_5SiCrW_{11}(H_2O)O_{39}\cdot 36H_2O$. With 36 water molecules, the molar mass of the compound is 3588.35 g mol^{-1}. The synthesis produced 0.302 g (0.084 mmol) of green needlelike crystals and its yield was 11.48 %. Same as with ^{I}K-

$SiAlW_{11}$, SiW_{11} was used as a start material in this synthesis. This means that the high water content of SiW_{11} (see Section 4.1) has been taken into account when calculating the yield for the synthesis of ^{I}K-$SiCrW_{11}$. When compared to the literature for other potassium compounds, it can be assumed that the ^{I}K-$SiCrW_{11}$ sample coordinated more water molecules than expected. If K-$SiCrW_{11}$ coordinated for example 24 water molecules per POM molecule, which is what is expected of K-$SiAlW_{11}$, the molar mass of the compound would be 3372.17 g mol^{-1} and the yield would be 12.24 %. The EA results in Table 7 also show that there is nitrogen and carbon in the analysed sample. This might be because the synthesis uses a nitrate start material and ethanol.

K-$SiCuW_{11}$

Table 8: EA results for ^{II}K-$SiCuW_{11}$.

	N [%]	C [%]	H [%]
Found	0.00	0.39	2.92
Calculated for $K_6SiCuW_{11}(H_2O)O_{39}\cdot 57H_2O$	0.00	0.00	2.91

The EA results presented in Table 8 show that the hydrogen value for the ^{II}K-$SiCuW_{11}$ sample is 2.92 %, which is close to what is expected for $K_6SiCuW_{11}(H_2O)O_{39}\cdot 57H_2O$. 57 water molecules is very high compared to what has been reported by Wang *et al.*,[61] who found there to be 15 water molecules coordinated to the compound. Like with the ^{II}K-$SiCoW_{11}$ sample, this deviation is probably due to the elemental analysis of this sample being done at a time of high humidity, combined with insufficient drying methods. Table 8 also shows that the sample contains carbon, which should not be the case. Again, this could be due to the fact that the ^{II}K synthesis requires CH_3COOK, which could leave traces of carbon.

$K_6SiCuW_{11}(H_2O)O_{39}\cdot 57H_2O$ has a molar mass of 4017.32 g mol^{-1}. As the synthesis produced 2.168 g of pale blue crystals, the yield of the synthesis would be 55.46 %. If there had been 15 water molecules the molar mass would have been 3260.68 g mol^{-1} and the yield 68.33 %.

K-$SiFeW_{11}$

Table 9: EA results for ^{I}K-$SiFeW_{11}$.

	N [%]	C [%]	H [%]
Found	0.07	0.67	2.80
Calculated for $K_5SiFeW_{11}(H_2O)O_{39}\cdot 53H_2O$	0.00	0.00	2.79

According to the EA results presented in Table 9, the hydrogen value for ^{I}K-SiFeW$_{11}$ is 2.80 %, which indicates that the compound coordinates 53 water molecules per POM molecule, making the molar mass of the compound 3898.46 g mol^{-1}. This in turn, means that the yield of the synthesis, which produced 0.681 g of yellow needlelike crystals, is 23.93 %. Similar to ^{I}K-SiAlW$_{11}$ and ^{I}K-SiCrW$_{11}$, this yield is calculated using SiW$_{11}$ as the limiting reagent. Normally, Fe(NO$_3$)$_3$ would be the limiting reagent; however, due to the amount of water found in SiW$_{11}$ (see Section 4.1), less SiW$_{11}$ than intended was used. Neither the original synthesis[54, 55] nor Dual *et al.*[60] provide any elemental analysis results for K-SiFeW$_{11}$. However, if K-SiFeW$_{11}$ coordinated the same amount of water as K-SiAlW$_{11}$ does according to the literature, the formula would be K$_5$SiFeW$_{11}$(H$_2$O)O$_{39}$·24H$_2$O. This would make the molar mass of the compound 3376.02 g mol^{-1} and the yield of the synthesis 27.58 %. The results in Table 9 also show nitrogen and carbon in the analysed sample, which might be caused by the synthesis using a nitrate start material and ethanol to precipitate the product.

K-SiMnW$_{11}$

Table 10: EA results for ^{II}K-SiMnW$_{11}$.

	N [%]	**C [%]**	**H [%]**
Found	0.00	0.65	1.62
Calculated for K$_6$SiMnW$_{11}$(H$_2$O)O$_{39}$·27H$_2$O	0.00	0.00	1.63

The synthesis of ^{II}K-SiMnW$_{11}$ produced 2.019 g (0.582 mmol) of orange crystals, and after about three days, similar to the ^{II}K-SiCoW$_{11}$ sample, a white precipitate was formed on top of the product. The EA results of the white precipitate will be discussed on page 33. According to the EA results presented in Table 10, there are 27 water molecules coordinated to the ^{II}K-SiMnW$_{11}$ compound. This gives a molar mass of 3468.26 g mol^{-1} and a yield of 59.83 %. The data is compared to the values reported from Zonoz *et al.*[62] who found K-SiMnW$_{11}$ to have the chemical formula K$_6$SiMnW$_{11}$(H$_2$O)O$_{39}$·21H$_2$O. With 21 water molecules the molar mass would be 3360.16 g mol^{-1}, making the yield 61.75 %. The EA results in Table 10 also show the presence of carbon in the sample. This could be caused by the fact that CH$_3$COOK is used in the synthesis, or it could be a result of the white precipitate.

K-SiNiW$_{11}$

Table 11: EA results for ^{II}K-SiNiW$_{11}$.

	N [%]	C [%]	H [%]
Found	0.00	0.15	1.79
Calculated for $K_6SiNiW_{11}(H_2O)O_{39}\cdot 30H_2O$	0.00	0.00	1.77

From the EA results in Table 11, it can be seen that the hydrogen value for the ^{II}K-SiNiW$_{11}$ compound is 1.79 %, which correlates to the hydrogen value expected for $K_6SiNiW_{11}(H_2O)O_{39}\cdot 30H_2O$. 30 water molecules per POM molecule would give a molar mass of 3526.06 g mol^{-1} and a yield of 66.62 %. According to the synthesis by Weakley *et al.*[56] there should only be 14 water molecules coordinated to the POM, meaning the molar mass would be 3237.81 g mol^{-1}. If the compound had coordinated 14 water molecules the yield of this synthesis would have been 72.53 %. The synthesis of ^{II}K-SiNiW$_{11}$ produced 2.285 g (0.648 mmol) of bright yellow-green crystals, and after about 15 minutes a white precipitate was formed on top of the product. The EA results of the white precipitate will be discussed on page 33. The EA results in Table 11 also shows some carbon present in the sample. This could be because of the observed white precipitate, or it might be caused by the fact that the synthesis uses CH_3COOK.

K-SiZnW$_{11}$

Table 12: EA results for ^{II}K-SiZnW$_{11}$.

	N [%]	C [%]	H [%]
Found	0.00	0.35	1.74
Calculated for $K_6SiZnW_{11}(H_2O)O_{39}\cdot 29H_2O$	0.00	0.00	1.72

According to the EA results presented in Table 12, the hydrogen value for the ^{II}K-SiZnW$_{11}$ sample corresponds to that of $K_6SiZnW_{11}(H_2O)O_{39}\cdot 29H_2O$. If the compound coordinates 29 water molecules, the molar mass of ^{II}K-SiZnW$_{11}$ is 3514.74 g mol^{-1}. The synthesis of ^{II}K-SiZnW$_{11}$ produced 2.207 g (0.628 mmol) of small white crystals, making the yield 64.54 %. Wang *et al.*[61] reported this compound with the chemical formula $K_6SiZnW_{11}(H_2O)O_{39}\cdot 15H_2O$, which has a lower water content. If the sample had coordinated 15 water molecules, the molar mass would have been 3262.53 g mol^{-1} and the yield 69.52 %. Table 12 also shows that the ^{II}K-SiZnW$_{11}$ sample contains carbon, which is unexpected. However, this might possibly be caused by the fact that the synthesis uses CH_3COOK.

^{II}K precipitate

Table 13: EA results for the unknown ^{II}K precipitate.

	N [%]	C [%]	H [%]
Found	0.00	1.16	3.30
Calculated for CH_3COOK	0.00	24.48	3.08

In an attempt to characterise the white precipitate that was formed on top of some of the ^{II}K samples, some of the precipitate was attempted analysed. This was done by isolating and analysing some clear crystals that were created after ^{II}K-$SiNiW_{11}$ was removed from its solvent. To ensure that this was not just residue of CH_3COOK crystallising in the solution, the EA results for the clear crystals and the calculated values for CH_3COOK are compared in Table 13. It is clear from this comparison that CH_3COOK contains far more carbon than what was found in the unknown crystals. The EA data also shows that carbon and hydrogen only make up about 4.5 % of the compound, meaning it mostly consists of other elements available in the solution. In the case of the ^{II}K-$SiNiW_{11}$ synthesis, the chemicals that would be available are $H_4SiW_{12}O_{40}\cdot xH_2O$, $Ni(SO_4)\cdot 6H_2O$, CH_3COOH and CH_3COOK. Even though these crystals were also analysed by IR (see page 47 for the results), further or more detailed analysis would be vital to make any sort of conclusion with respect to what this compound is.

Brief overview of the EA results and yields for the potassium syntheses

Table 14: Overview of the determined chemical formula, molar mass and yield for the potassium compounds.

	Chemical formula	Molar mass [g mol^{-1}]	Yield [%]
^{I}K-$SiAlW_{11}$	$K_5SiAlW_{11}(H_2O)O_{39}\cdot 41H_2O$	3653.41	10.67
^{II}K-$SiCoW_{11}$	$K_6SiCoW_{11}(H_2O)O_{39}\cdot 82H_2O$	4463.09	54.69
^{I}K-$SiCrW_{11}$	$K_5SiCrW_{11}(H_2O)O_{39}\cdot 36H_2O$	3588.35	11.48
^{II}K-$SiCuW_{11}$	$K_6SiCuW_{11}(H_2O)O_{39}\cdot 57H_2O$	4017.32	55.46
^{I}K-$SiFeW_{11}$	$K_5SiFeW_{11}(H_2O)O_{39}\cdot 53H_2O$	3898.46	23.93
^{II}K-$SiMnW_{11}$	$K_6SiMnW_{11}(H_2O)O_{39}\cdot 27H_2O$	3468.26	59.83
^{II}K-$SiNiW_{11}$	$K_6SiNiW_{11}(H_2O)O_{39}\cdot 30H_2O$	3526.06	66.60
^{II}K-$SiZnW_{11}$	$K_6SiZnW_{11}(H_2O)O_{39}\cdot 29H_2O$	3514.74	64.54

4.2.2 Discussion of the EA results and yields for the potassium compounds

Before starting to compare the EA results for the potassium compounds, one thing must first be underlined; the final elemental analysis of all the samples in this project was performed during a time of high humidity. When it was noticed that this significantly affected the EA results for the potassium compounds, it was decided that results from an analysis done earlier in the year should be used instead as it would provide more accurate results. Unfortunately, such results were not available for the ^{I}K-SiAlW$_{11}$, ^{II}K-SiCoW$_{11}$, ^{I}K-SiCrW$_{11}$, ^{II}K-SiCuW$_{11}$ and ^{I}K-SiFeW$_{11}$ samples, as they had no previously analysed samples. This is most likely the reason why these samples are found to coordinate between 40 and 80 water molecules, while the other samples coordinate around 30. Still, even the samples with the lowest water content have coordinated more water than what is reported in the literature, with ^{II}K-SiMnW$_{11}$ being the closest to the literature with its 28 water molecules, compared to the 22 molecules reported by Zonoz *et al.*[62]

As mentioned previously, all samples were dried in a desiccator as well as air dried after synthesis, and it was assumed that this would remove most of the excess water. However, this was either not the case or the compounds coordinated water from the atmosphere after being dried. In the case of the ^{II}K-SiCuW$_{11}$ sample, it was synthesised shortly before analysis, so its high water content could indicate that it did not spend enough time in the desiccator. The ^{II}K-SiCoW$_{11}$ sample, on the other hand, which is arguably the worst offender, was synthesised months before analysis, and therefore spent more time in the desiccator without benefit. If the potassium compounds do coordinate large amounts of water from the atmosphere, it would cause some issues when calculating the yield of the syntheses. The product of each of the syntheses was weighed right after the samples were removed from the desiccator, when they contained the least water, to provide the most accurate yields. However, the samples were not analysed right after weighing. This means that if they acquired more mass, in the form of water, between weighing and analysis, the molar mass calculated using the EA results would be higher than the molar mass of the product weighed after the synthesis, leading to an overall lower yield. To determine if this was an issue, the samples could have been weighed before analysis to see if there was an increase in weight, but this was not considered while the experiments were carried out. As a consequence, it cannot be confirmed whether the high water content of the samples were caused by coordination of water from the air, or simply insufficient drying of the samples. However, to achieve more accurate results in future work with potassium Keggin

POMs it would be recommended to use a vacuum pump in combination with heating to remove any excess water from the samples.

The potassium compounds were synthesised using two different syntheses: ^{I}K which was based on Ma *et al.*[54, 55] and used for substitutions with X^{3+} metals and ^{II}K which was based on Weakley *et al.*[56] and used for substitutions using X^{2+} metals. At a very early stage of this project, the X^{2+} substitution (using Cu^{2+} and Mn^{2+}) was also attempted using a synthesis by Tourné *et al.*[63] However, because this synthesis relied on evaporation of water at room temperature, it was drastically slower than other synthesis options and was therefore abandoned. It should be noted that due to the slow evaporation, this synthesis did provide the largest crystals out of all the syntheses in this project.

When comparing the yields of the different potassium syntheses (see Table 14), there is a significant difference between ^{I}K and ^{II}K. Regardless of the high water content, the yield of the ^{II}K synthesis is relatively high at around 55-65 %, while the yield of the ^{I}K synthesis is lower at about 10-25 %. The ^{II}K synthesis is also quite a lot faster since crystals could be formed by cooling the solution to room temperature for most of the metals. For some metals such as Mn it could take some time, but by leaving the solution over night or cooling it to 5 ºC the product would crystallise. On the other hand, in the ^{I}K synthesis the crystallisation happened at 5 ºC and could take weeks to reach completion. This means that the ^{II}K synthesis both provided a better yield and required less time. An attempt was made to use $Al(NO_3)_3$ in the ^{II}K synthesis to see if it was possible to speed up the synthesis of K-$SiAlW_{11}$; however, this did not provide any crystals, only a small amount of white powder that was precipitated out over a week or so. Unfortunately, there was no opportunity to further explore this during this project, but part of the issue most likely came from not adjusting the pH to the new start material.

The issue that did arise with the ^{II}K synthesis was that it produces an unknown white precipitate. The syntheses that visibly contained this impurity were those of ^{II}K-$SiCoW_{11}$, ^{II}K-$SiMnW_{11}$ and ^{II}K-$SiNiW_{11}$, but it would be reasonable to assume that it also occurred for the ^{II}K-$SiCuW_{11}$ and ^{II}K-$SiZnW_{11}$ syntheses as well, as the synthesis was not changed for these metals. The reason why we cannot macroscopically confirm that the precipitate was in the ^{II}K-$SiCuW_{11}$ and ^{II}K-$SiZnW_{11}$ products, is that these products were pale blue and white, respectively, thereby making a white precipitate hard to see. As mentioned in some of the results, the precipitate was created on top of the product, meaning it was precipitated after the crystallisation. Theoretically,

the crystals could therefore be removed from the solution before the precipitation of the white compound. However, trying to decide when the crystallisation of the product was complete and when the precipitation of the white compound would start was nearly impossible. By plain observation of the syntheses, it seems that the precipitation rate is dependent on the crystallisation rate of the product. The compounds that crystallise slowly, such as ^{II}K-SiMnW$_{11}$, could be left in the solution for a couple of days before the white precipitate was created, while the faster crystallisations, such as that of ^{II}K-SiNiW$_{11}$ and ^{II}K-SiCoW$_{11}$, produced the white precipitate within minutes. In one instance, in an attempt to remove the white precipitate, a ^{II}K-SiCoW$_{11}$ sample was recrystallised using warm water and filtration; however, the precipitate dissolved with the compound and precipitated out again when the solution cooled.

Without extensive analysis, it is not possible to determine the composition of the white precipitate, but from the EA results there is clearly a carbon containing compound present, at least in final solution of the ^{II}K-SiNiW$_{11}$ synthesis. This could explain why all the EA results for the compounds synthesised by the ^{II}K synthesis show the presence of carbon even though they are inorganic compounds. However, the products of the ^{I}K synthesis also show the presence of carbon, as well as nitrogen, and they do not have any visible impurity present. These results for ^{I}K and ^{II}K could therefore be a consequence of carbon and nitrogen containing chemicals being used in the synthesis. If this is the case, the traces of nitrogen and carbon should be possible to remove by recrystallisation.

To summarise, due to insufficient drying, many of the potassium samples contain far more water than is expected based on the literature. When this water was acquired is uncertain, and may therefore have caused the calculated yields to be lower than they should be. Consequently, for better calculations and more accurate results, improved drying methods, such as a vacuum pump and heating, would be necessary in future work with the potassium POM compounds. Regardless, the difference in yield between the ^{I}K and ^{II}K syntheses is substantial, with ^{I}K resulting in a yield of 10-25 %, while ^{II}K gave a yield of 55-65 %. The ^{II}K synthesis was also the fastest of the two, making it the most advantageous. However, an issue with the ^{II}K synthesis, as opposed to the ^{I}K synthesis, is that it produces an unknown white precipitate. This precipitate could be the reason why all the ^{II}K EA results show presence of carbon, but it could also be caused by CH_3COOK residue. The ^{I}K products also show presence of carbon, as well as nitrogen, which might be a result of residue of the start material.

4.2.3 IR results for the potassium compounds

K-SiAlW$_{11}$

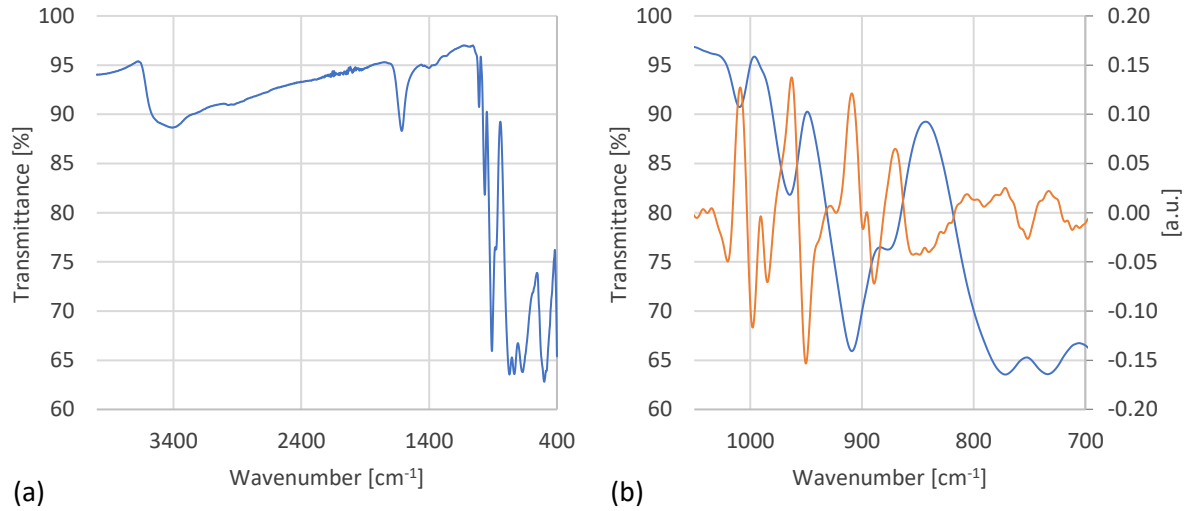

Figure 4: (a) The complete IR spectrum for ^{I}K-SiAlW$_{11}$, (b) the IR (blue) and second derivative (orange) spectra from 1050 – 700 cm^{-1} for ^{I}K-SiAlW$_{11}$.

Table 15: Overview of IR data for ^{I}K-SiAlW$_{11}$.

Wavenumber [cm^{-1}]			**Assignment**
Experimental*	**Second derivative***	**Literature[64]**	
1009.44	1008.92	1010	W=O stretch
964.63	962.90	968	Si-O stretch
909.01	909.03, 928.34	922	W-Ob-W stretch
733.83, 771.68	771.74, 732.79, 805.91, 779.47, 796.91	743	W-Oc-W stretch

*Sorted by intensity.

When compared to the peaks characteristic for Keggin POMs (see Table 1), the IR spectrum in Figure 4 matches well with what is expected in the 1050 to 700 cm^{-1} range, indicating a successful synthesis of the desired POM. According to theoretical values presented in Table 1, the peaks observed at 3407.26, 2971.09 and 1614.31 cm^{-1} in Figure 4 are caused by water in the sample.

When compared to values found in the literature (see Table 15), the values for the W=O and Si-O stretches are in good agreement, while the values for the W-Ob-W and W-Oc-W are not. In the case of the W-Ob-W stretch, the second derivative of the experimental data shows a signal at about 928 cm^{-1}, which correlates with the literature, but is not the strongest signal

assigned to this stretch. For the W-Oc-W stretch, all the experimental data differ from what is found in the literature. Even though there is no signal at about 743 cm^{-1} in the second derivative of the experimental data, there is a chance that the peaks reported in literature is caused by a combination of different second derivative signals.

Most likely, the deviations in the W-Ob-W and W-Oc-W peaks are not caused by any impurities in the sample, as the product appears homogeneous and none of the peaks can be found in the IR data for neither SiW_{11} (see Table 1) nor $Al(NO_3)_3 \cdot 9H_2O$ (see Appendix), which are the start materials for the synthesis.

K-SiCoW$_{11}$

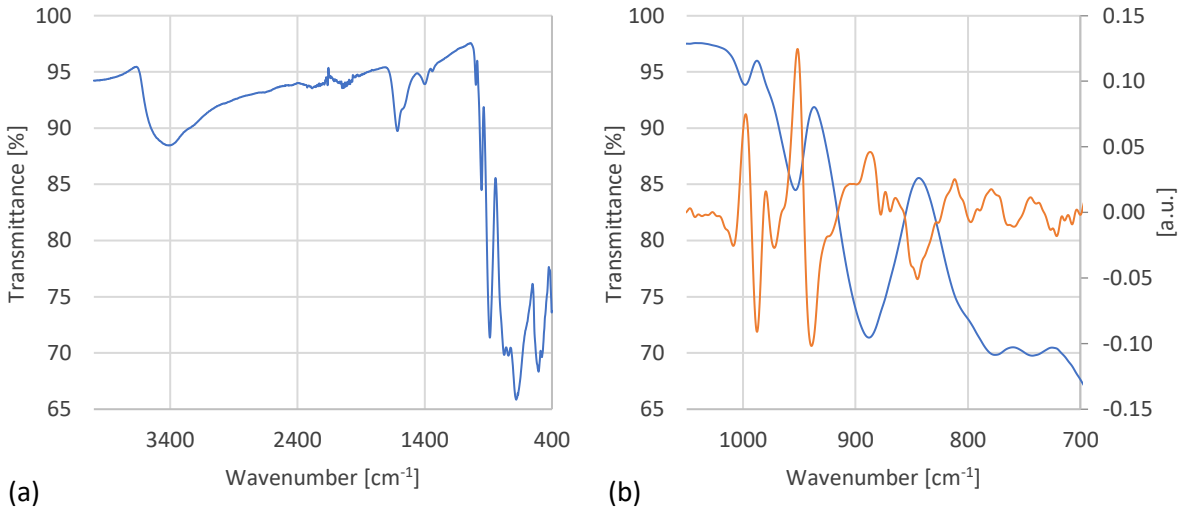

Figure 5: (a) The complete IR spectrum for ^{II}K-SiCoW$_{11}$, (b) the IR (blue) and second derivative (orange) spectra from 1050 – 700 cm^{-1} for ^{II}K-SiCoW$_{11}$.

Table 16: Overview of IR data for ^{II}K-SiCoW$_{11}$.

Wavenumber [cm^{-1}]					**Assignment**
Experimental*	**Second derivative***	**Literature[60]**	**Literature[61]**	**Literature[62]**	
997.94	997.53	1001	1001	1004	W=O stretch
953.25	951.43, 979.58	956	950	962	Si-O stretch
886.93	886.93, 873.33, 864.44	887	907	900	W-Ob-W stretch
742.72, 775.93	811.75, 779.24, 744.30, 737.05, 791.50	736	794	796, 742	W-Oc-W stretch

*Sorted by intensity.

Based on the values presented in Table 1, we can see that the IR spectrum presented in Figure 5 shows the four characteristic peaks that we expect to find in the spectra for Keggin POMs, indicating a successful synthesis. The values in Table 1 also indicate that the peaks observed at 3414.72 cm^{-1} and 1614.34 cm^{-1} in the IR spectrum for ^{II}K-SiCoW$_{11}$ (see Figure 5) are caused by the presence of water in the sample.

When experimental IR data are compared to the literature values from Duan *et al.*[60] (see Table 16) it can be observed that most of the values are in good agreement; however, the W-Oc-W value differs. Upon further research into the reported IR data for this compound, data from Wang *et al.*[61] and Zonoz *et al.*[62] were also found. The values they reported for the W=O, Si-O and W-Ob-W stretches seem to agree more or less with the values from Duan *et al.*,[60] but their values in the 800-700 cm^{-1} range vary. Zonoz *et al.*[62] report a peak at 742 cm^{-1} which correlates well with the peak observed at 742.72 cm^{-1} in the experimental spectrum, but none of the sources report a peak around 775 cm^{-1}. One interesting observation is that many of the theoretical values, though they do not correlate with the experimental values, can be found in the second derivative of the experimental data.

It is unlikely that any of the deviations from the literature are caused by impurities in the samples, as none of the deviating peaks agree with the IR spectrum for the start material, cobalt(II) acetate (see Appendix).

K-SiCrW$_{11}$

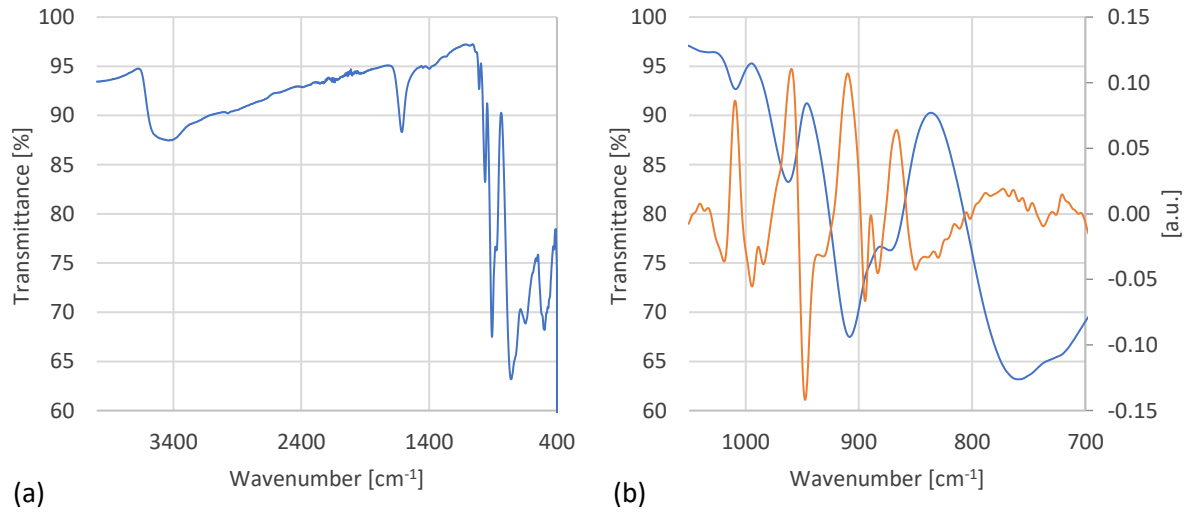

Figure 6: (a) The complete IR spectrum for ^{I}K-SiCrW$_{11}$, (b) the IR (blue) and second derivative (orange) spectra from 1050 – 700 cm^{-1} for ^{I}K-SiCrW$_{11}$.

Table 17: Overview of IR data for ^{I}K-SiCrW$_{11}$.

Wavenumber [cm^{-1}]		Assignment
Experimental	**Second derivative***	
1008.84	1009.31	W=O stretch
962.31	959.57	Si-O stretch
908.16	909.87, 866.72	W-Ob-W stretch
758.89	772.80, 763.70, 788.04, 720.53, 755.70, 746.95, 729.16, 805.41, 704.09	W-Oc-W stretch

*Sorted by intensity.

It can be assumed, based on the IR data in Table 1, that the peaks observed at 3431.53, 2974.68 and 1613.35 cm^{-1} in Figure 6 are caused by the presence of water in the compound. It was not possible to find any literature values for the K-SiCrW$_{11}$; however, compared to the values presented in Table 1, the observed peaks for ^{I}K-SiCrW$_{11}$ (see Table 17) do not present any major deviation. The fact that the compound produces an IR spectrum with the characteristic four peaks, within the same range as other samples, confirms that there has been a successful synthesis of a POM structure.

K-SiCuW$_{11}$

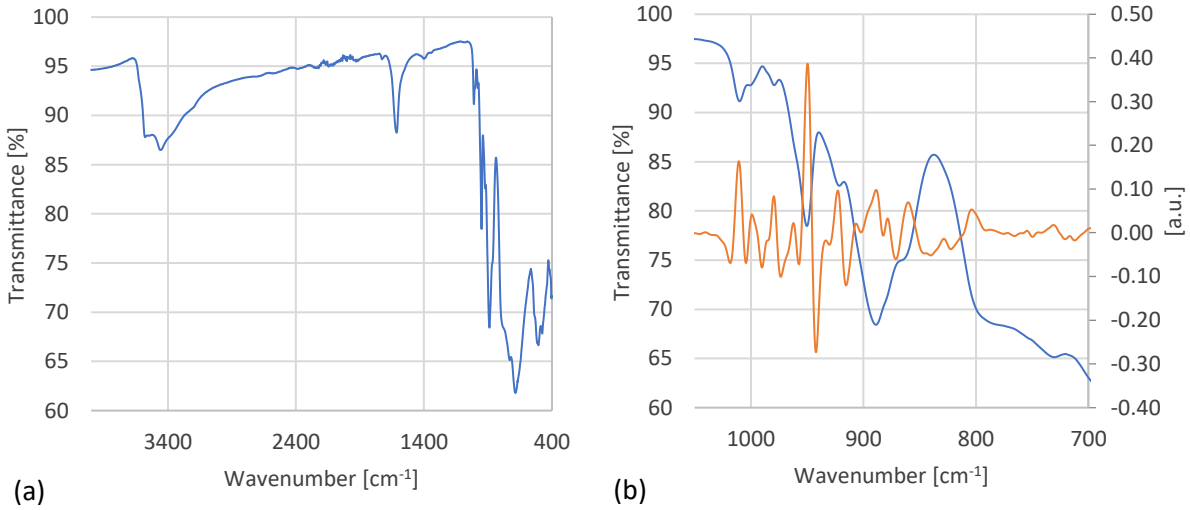

Figure 7: (a) The complete IR spectrum for ^{II}K-SiCuW$_{11}$, (b) the IR (blue) and second derivative (orange) spectra from 1050 – 700 cm^{-1} for ^{II}K-SiCuW$_{11}$.

Table 18: Overview of IR data for ^{II}K-SiCuW$_{11}$.

Wavenumber [cm^{-1}]			Assignment
Experimental	**Second derivative***	**Literature[60]**	
1010.09	1010.73, 999.01	1008	W=O stretch
950.25	949.62, 979.65, 962.21	950	Si-O stretch
888.85	888.66, 922.75, 860.17, 878.46, 906.41	886	W-Ob-W stretch
730.31	803.85, 731.00, 754.57, 787.53, 744.44, 771.51, 759.62, 716.56	736	W-Oc-W stretch

*Sorted by intensity.

According to Table 1, the peaks observed at 3577.07, 3459.95 and 1613.51 cm^{-1} in Figure 7 are caused by water in the sample. When the experimental values are compared to the literature values for K-SiCuW$_{11}$ from Duan *et al.*[60] (see Table 18), a good agreement is observed with a slight deviation of the W-Oc-W peak. When compared to the characteristic peaks in Table 1, we see that the IR spectrum has the four characteristic peaks in the 1050-700 cm^{-1} range.

One observation that needs to be commented on is that the ^{II}K-SiCuW$_{11}$ IR spectrum has more peaks in the 1050-700 cm^{-1} range than the other potassium compounds (see Figure 7 (b)). This comes across both in the normal spectrum as well as in the second derivative of the spectrum, and could indicate that some of the product has adapted a sandwich structure rather than a Keggin structure.[65]

K-SiFeW$_{11}$

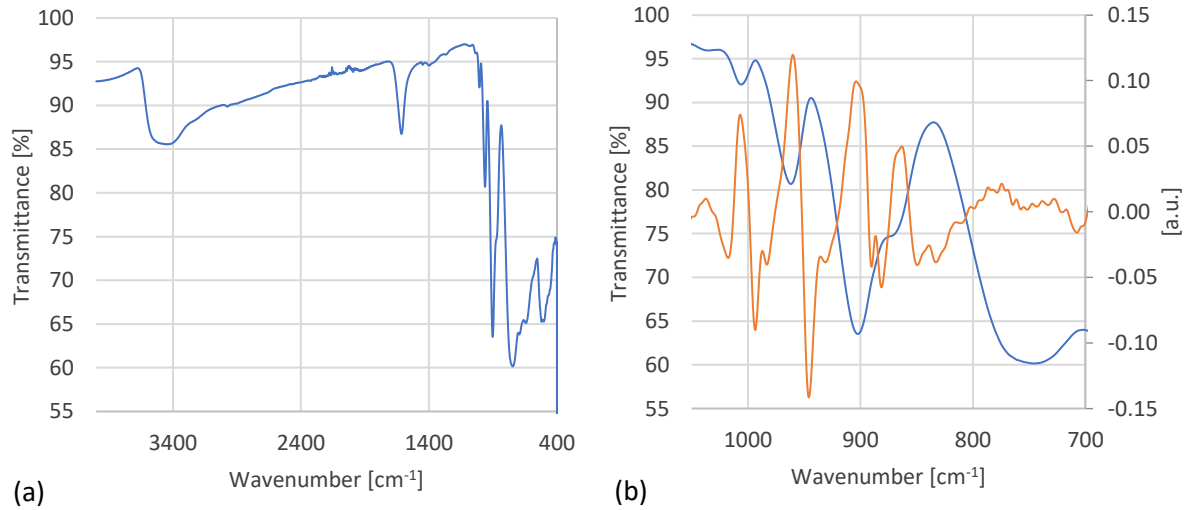

Figure 8: (a) The complete IR spectrum for ^{I}K-SiFeW$_{11}$, (b) the IR (blue) and second derivative (orange) spectra from 1050 – 700 cm^{-1} for ^{I}K-SiFeW$_{11}$.

Table 19: Overview of IR data for ^{I}K-SiFeW$_{11}$.

Wavenumber [cm^{-1}]			Assignment
Experimental	**Second derivative***	**Literature[60]**	
1005.97	1006.85	1012	W=O stretch
961.82	960.01	971	Si-O stretch
902.34	903.83, 863.12	902	W-Ob-W stretch
745.68	774.37, 786.47, 769.15, 782.28, 761.38, 727.89, 793.88, 738.22, 747.15, 801.88, 754.91, 717.06	750	W-Oc-W stretch

*Sorted by intensity.

When compared to the data in Table 1, we see that the IR spectrum for ^{I}K-SiFeW$_{11}$ in Figure 8 has all the peaks that we expect to find in the spectra of Keggin-type POMs. The peaks observed at 3451.22, 2975.00 and 1614.97 cm^{-1} are according to the data presented in Table 1, caused by the presence of water in the analysed sample. In Table 19 the experimental peaks are compared to values from Duan *et al.*[60] As can be observed, the experimental values for the W=O, Si-O and W-Oc-W stretches are a bit lower than what is found in the literature, while the values for the W-Ob-W stretch are about the same. When compared to the IR data for the start materials, SiW$_{11}$ (see Table 4) and Fe(NO$_3$)$_3$·9H$_2$O (see Appendix), it does not appear that the deviation has anything to do with there being residue of the start materials in the product. Macroscopically, the product was a different colour from the start material and appeared homogeneous, indicating that the synthesis of ^{I}K-SiFeW$_{11}$ was successful.

K-SiMnW$_{11}$

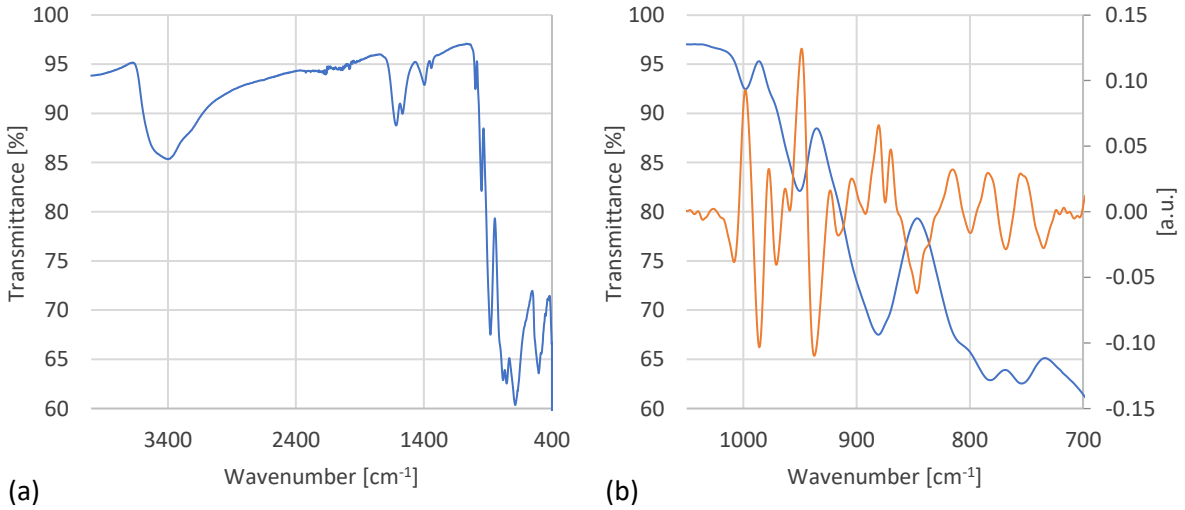

Figure 9: (a) The complete IR spectrum for ^{II}K-SiMnW$_{11}$, (b) the IR (blue) and second derivative (orange) spectra from 1050 – 700 cm^{-1} for ^{II}K-SiMnW$_{11}$.

Table 20: Overview of IR data for ^{II}K-SiMnW$_{11}$.

Wavenumber [cm^{-1}]				Assignment
Experimental*	**Second derivative***	**Literature[60]**	**Literature[62]**	
998.01	998.15	999	1000	W=O stretch
950.18	948.49, 977.45, 963.01	951	960	Si-O stretch
880.72	880.44, 869.80, 904.22, 923.24	885	898	W-Ob-W stretch
754.22, 781.93	815.18, 783.92, 755.18, 732.69	765	794, 759	W-Oc-W stretch

*Sorted by intensity.

When compared to the characteristic IR peak presented in Table 1, we see that the IR spectrum in Figure 9 has the peaks we expect to find for POM structures in the 1050-700 cm^{-1} range, indicating a successful synthesis. The IR spectrum for ^{II}K-SiMnW$_{11}$ (Figure 9) also has two peaks, one at 3399.65 cm^{-1} and one at 1617.28 cm^{-1}, that according to Table 1 are caused by the presence of water in the sample. Compared to the data found from Duan *et al.*[60] the experimental IR data for ^{II}K-SiMnW$_{11}$ is very similar, with the exception of the W-Oc-W stretch peak (see Table 20). Compared to the theoretical values, the peak with the highest intensity is the one that is most similar. This peak is also very similar to a peak found in the IR spectrum for manganese(II) acetate (see Appendix), which is one of the start materials in this synthesis. When comparing the IR spectrum of the crude sample with a recrystallised sample (see Figure 10), the intensity of this peak seems to decrease when the sample is recrystallised from water. As manganese(II) acetate is soluble in water, it would not be possible to remove by recrystallisation from water, meaning this peak most likely is not caused by traces of manganese(II) acetate in the analysed sample. As mentioned previously there was a white impurity in some of the potassium products, ^{II}K-SiMnW$_{11}$ included; however, this impurity dissolves with the product during recrystallisation and reappears when the solution cools back to room temperature.

When doing further research it was found that Zonoz *et al.*[62] also provided IR data for ^{II}K-SiMnW$_{11}$. When comparing the data from Zonoz *et al.*[62] with the experimental data reported in Table 20, it can be seen that the peaks for the W=O are similar; however, the values from Zonoz *et al.*[62] for both the Si-O and W-Ob-W stretches are higher than the experimental values reported herein and the values from Duan *et al.*[60] listed in Table 20. The experimental values in the 800-700 cm^{-1} range have some similarities to the values reported by Zonoz *et al.*,[62] but not with the values from Duan *et al.*,[60] showing that there is varying data reported in the literature.

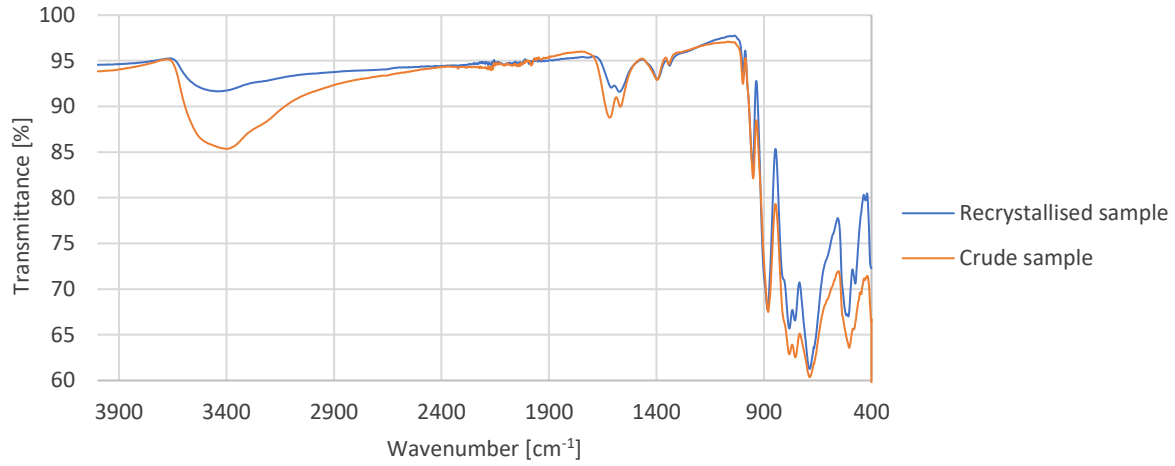

Figure 10: Comparison of the IR spectra for a recrystallised and a crude ^{II}K-SiMnW$_{11}$ sample.

K-SiNiW$_{11}$

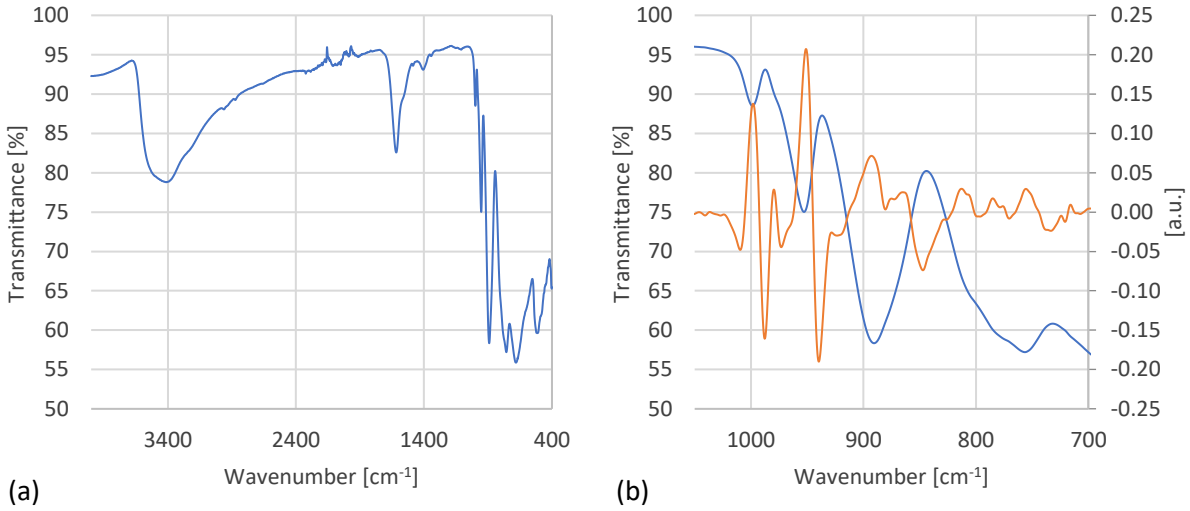

Figure 11: (a) The complete IR spectrum for ^{II}K-SiNiW$_{11}$, (b) the IR (blue) and second derivative (orange) spectra from 1050 – 700 cm^{-1} for ^{II}K-SiNiW$_{11}$.

Table 21: Overview of IR data for ^{II}K-SiNiW$_{11}$.

Wavenumber [cm^{-1}]					**Assignment**
Experimental	**Second derivative***	**Literature[61]**	**Literature[62]**	**Literature[66]**	
998.55	998.05	1003	1000	-	W=O stretch
952.78	951.01, 979.57	960	960	953	Si-O stretch
890.52	892.79, 865.05, 875.04	904	898	908	W-Ob-W stretch
756.47	755.56, 812.75, 785.02, 776.09	794	798	790	W-Oc-W stretch

*Sorted by intensity.

When comparing the values observed in the IR spectrum for ^{II}K-SiNiW$_{11}$ (see Figure 11) with the values presented in Table 1, we see that the IR spectrum contains all four peaks that are considered characteristic for the Keggin POM structure, indicating that the correct compound has been successfully obtained. From the data in Table 1, it can also be assumed that the peaks observed at 3409.39 cm^{-1} and 1616.64 cm^{-1} are caused by the presence of water in the sample.

Compared to the IR data from Wang *et al.*,[61] the experimental IR values are consistently lower. This is unexpected, with the peak assigned to the W=O stretch being the closest to the literature values. To provide further comparison of the experimental data, two other sets of IR data from the literature are presented in Table 21. The first set of values is from Zonoz *et al.*[62] and the second set is from Jiang *et al.*[66] When comparing with these two sets of data, the experimental value for the W=O stretch is in good agreement with the data from Zonoz *et al.*[62] and the peak assigned to the Si-O stretch is similar to the data from Jiang *et al.*,[66] while the rest of the data points fall slightly or significantly lower than the literature data. This goes to show that, even though the experimental data is not necessarily in good agreement with the literature data, different sets of literature data may also disagree with each other.

The only value that significantly deviates from all the literature data, is the one assigned to the W-Oc-W stretch. This peak cannot be found in the spectrum for nickel(II) sulphate which is the start material for this synthesis (see Appendix), and is therefore, probably not caused by nickel(II) sulphate residue in the product. As has been seen from previous IR spectra, the W-Oc-W peak is composed of many different second derivative signals. Even though there is no data point around 800-790 cm^{-1} in the second derivative of the experimental data, there is a chance that the peaks reported in literature could be caused by a combination of different second derivative signals.

K-SiZnW$_{11}$

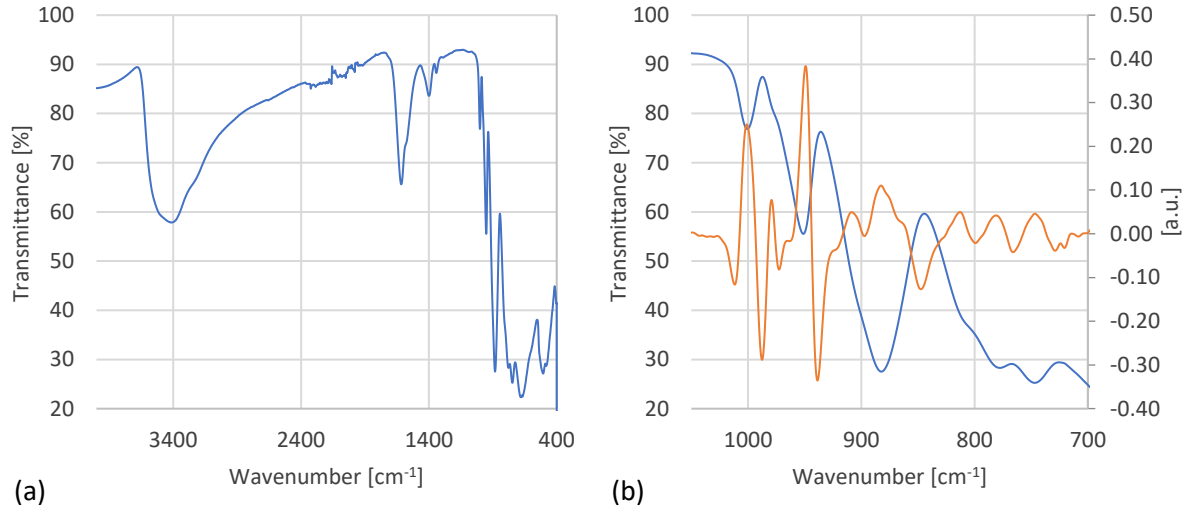

Figure 12: (a) The complete IR spectrum for ^{II}K-SiZnW$_{11}$, (b) the IR (blue) and second derivative (orange) spectra from 1050 – 700 cm^{-1} for ^{II}K-SiZnW$_{11}$.

Table 22: Overview of IR data for ^{II}K-SiZnW$_{11}$.

Wavenumber [cm^{-1}]			**Assignment**
Experimental*	**Second derivative***	**Literature[61]**	
1000.64	1001.12	-	W=O stretch
951.17	949.14, 979.25	953	Si-O stretch
882.28	882.55, 908.48	880	W-Ob-W stretch
746.82, 777.56	812.84, 746.65, 781.05	743	W-Oc-W stretch

*Sorted by intensity.

According to the data presented in Table 1, the IR spectrum for the ^{II}K-SiZnW$_{11}$ compound (see Figure 12) contains all the four characteristic peaks for a Keggin POM compound. We can also see that the peaks observed at 3417.11 cm^{-1} and 1615.75 cm^{-1} in Figure 12, are caused by water in the sample.

When researching the theoretical values Wang *et al.*[61] was the only source found that reported IR data for ^{II}K-SiZnW$_{11}$ (see Table 22). However, they do not provide a value around 1000 cm^{-1}, but from comparison with the other synthesised potassium compounds we are confident that the peak at 1000.64 cm^{-1} can be assigned to the W=O stretch. When comparing the peaks assigned to the Si-O, W-Ob-W and W-Oc-W stretches with what is reported by Wang *et al.*[61] we can see that they are similar, indicating that the correct compound has been obtained.

^{II}K impurity

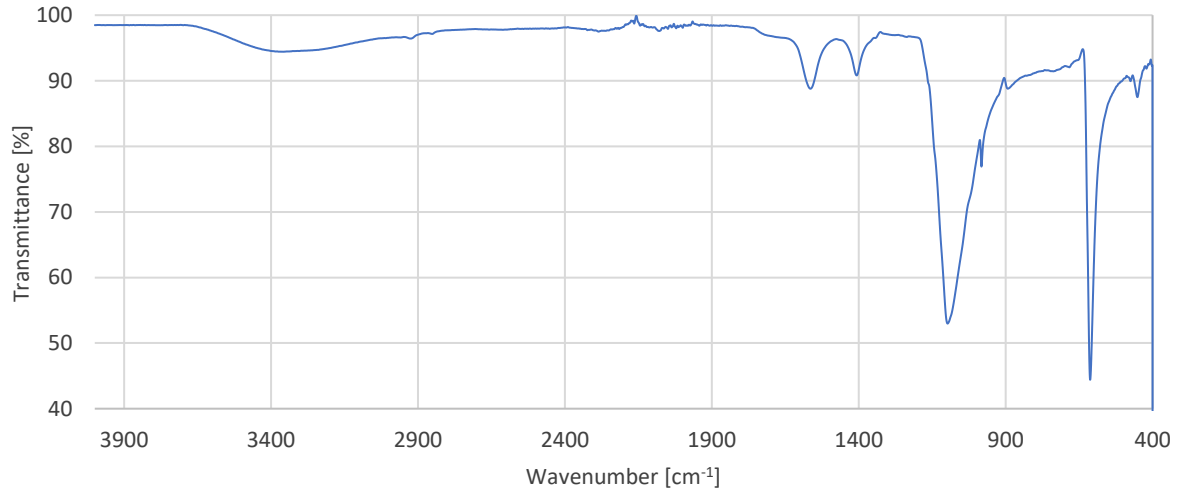

Figure 13: The complete IR spectrum for the unknown ^{II}K precipitate.

When comparing the IR data in Figure 13 with the characteristic POM peaks described in Table 1, we see that the IR data for this compound does not contain the peaks we would expect for a Keggin POM compound. This means that the clear crystals that were isolated from the ^{II}K-$SiNiW_{11}$ solution, could be the precipitate seen on top of the product. It also means that the precipitate is neither SiW_{11} nor $H_4SiW_{12}O_{40}\cdot xH_2O$ residue that has crystallised in the solution.

Table 23: Overview of IR data for the unknown ^{II}K precipitate.

Wavenumber [cm^{-1}]
3357.30 (w, br)
1564.13 (w, sh)
1407.00 (w, sh)
1097.49 (s, sh)
982.15 (m, sh)
612.25 (s, sh)
451.47 (w, sh)

The EA results for the clear crystals found in the ^{II}K-$SiNiW_{11}$ solution, show that they contain carbon. This could indicate that these crystals are some form of organic compound. As it is not possible to determine the structure of a compound from its IR spectrum, the IR data in Table 23 will not be thoroughly interpreted. However, what is interesting about this IR data is that the peak at 982.15 cm^{-1} is the only peak that falls within the 1050-700 cm^{-1} range, which is the area of interest for the POM compounds. This means that, if this indeed is the white precipitate found in some of the samples, it does not greatly impact the IR spectra for the POM compounds within this range.

Overview of all IR spectra for the potassium compounds

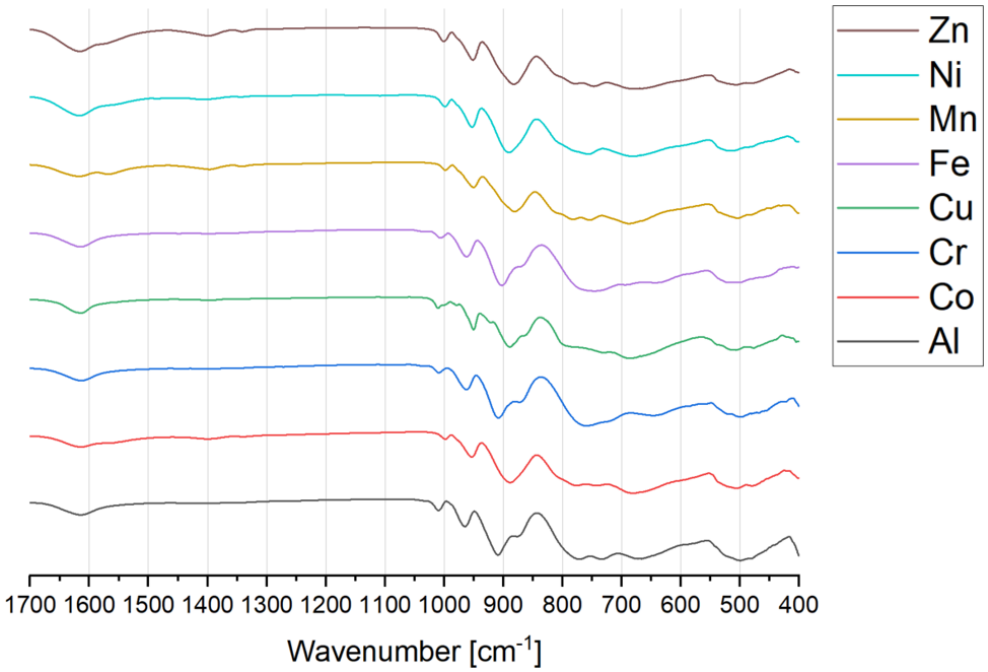

Figure 14: Overview of normalised IR spectra for the potassium compounds.

When we compare all the IR spectra for the potassium compounds (see Figure 14), two features of interest appear. Firstly, it is clear that all the IR spectra have the four peaks in the 1050-700 cm^{-1} range that are characteristic for the monosubstituted Keggin structure. Secondly, we see a clear shift in the peak positions depending on the metal introduced into the Keggin structure. When looking at the peak around 1000 cm^{-1} it is shifted to the highest wavenumber for Cu (1010.09 cm^{-1}), followed by Al (1009.44 cm^{-1}), Cr (1008.84 cm^{-1}), Fe (1005.97 cm^{-1}), Zn (1000.64 cm^{-1}), Ni (988.55 cm^{-1}), Mn (998.01 cm^{-1}) and Co (997.94 cm^{-1}). Further analysis and discussion of what might cause this will be given later, in Section 4.5.

4.2.4 Discussion of the IR results for the potassium compounds

When viewing the IR spectra for all the different samples together, they all have at least one peak between 3600 and 3350 cm^{-1}, and one peak around 1616 cm^{-1}. According to Table 1 these peaks show that there is water in the samples, which reinforces the interpretation of the EA results, discussed in Section 4.2.2. When looking at all the spectra in Figure 14, we see that they all have the same general shape, with three very distinct peaks in the 1050-850 cm^{-1} range and one less clear peak between 850-700 cm^{-1}. These peaks also correlate with what is considered characteristic for monosubstituted Keggin structures (see Table 1), which strongly suggests that the syntheses were successful.

When the IR data for the different samples were compared to their respective literature values, they are mostly in agreement with what was expected, though with some observed deviations. There are a couple of factors that could explain these deviations. Firstly, particularly in the case of the compounds with the consistently lower results, the deviations could simply be caused by the IR data being recorded by different people, with different instruments and in different work environments. Secondly, we know from the second derivative of the experimental data, that the peaks assigned to the W-Ob-W and W-Oc-W stretches consist of multiple second derivative signals. Small deviations in these peaks could therefore be caused by varying intensity in the second derivative signals. Based on the IR data presented for what might be the observed white precipitate on some of the products (see Figure 13), we can tell that this impurity most likely did not cause the deviations in the range 1050 to 700 cm^{-1}.

When comparing the ^{II}K-SiCoW$_{11}$ and ^{II}K-SiNiW$_{11}$ compounds with literature data, there were multiple sources to compare with. Here, it was very clear that, though the experimental data was not in good agreement with one data set, it could be in agreement with another. This shows that the data reported in literature varies. It should therefore not be put too much weight on whether or not the experimental data is exactly the same as the literature data, but rather focus on the fact that all the samples from potassium syntheses had an IR spectrum that is characteristic for a monosubstituted Keggin POM.

All of this is to say that, even though some of the experimental IR values are not in good agreement with values from the literature, we can still say with a high degree of certainty that the syntheses were successful. In most of the samples there was a clear colour change from start material to product, with the only exceptions being the ^{I}K-SiAlW$_{11}$ and ^{II}K-SiZnW$_{11}$ samples, whose start materials and products are all white. However, regardless of the colour, all the IR spectra for the samples changed from the start materials to the products, showing that there had been a definite change in their structure. All the IR spectra contained the characteristic peaks associated with a Keggin-type POM structure, which strongly indicates a successful synthesis of the desired POM compounds.

To summarise the IR results for the potassium compounds, there are some important points to emphasise. Firstly, all the IR spectra for the potassium compounds had peaks indicating the presence of water in the samples. This is in agreement with what was found in the interpretation

of the EA results, discussed in Section 4.2.2. Secondly, in the situations where it was possible to find multiple pieces of literature that provided IR data for the compounds in question, it was clear that what is reported in literature can vary noticeably. This means that very detailed comparisons with data from the literature, though it can provide useful insight, should not be weighted too heavily when trying to confirm if a synthesis was successful or not. Finally, all of the potassium samples analysed in this project had IR spectra with very similar characteristics, both compared to each other and compared to known Keggin POM IR spectra (see Table 1). They all have the three very distinct peaks in the 1050-850 cm^{-1} range and one less clear peak between 850-700 cm^{-1}, as can be seen in Figure 14, which strongly suggests a successful synthesis of potassium POM compounds.

4.2.5 Brief comparison of the potassium syntheses based on the discussed results

Both the EA and IR results for the potassium POM compounds suggests that the syntheses were successful. All the IR spectra showed that the compounds had an IR spectrum with the correct characteristics, and that they were mostly in good agreement with what was previously available in literature. The IR analysis also showed no distinction based on whether compounds were synthesised with ^{I}K or ^{II}K.

The main difference between the ^{I}K and ^{II}K syntheses was in terms of the yield. Due to the issue of the potassium samples containing a lot of water, the calculated molar mass for the compounds could be higher than they should be, leading to lower calculated yields. However, based on the yield calculations, ^{II}K is the superior synthesis, though it does have the issue of producing an impurity which ^{I}K does not.

4.3 Synthesis and analysis of the TBA compounds

4.3.1 EA results and yields for the TBA compounds

TBA-$SiAlW_{11}$

TBA-$SiAlW_{11}$ was only attempted synthesised using one of the TBA syntheses: ^{III}TBA.

Table 24: EA results for TBA-$SiAlW_{11}$.

	N [%]	C [%]	H [%]
Found for ^{III}TBA-$SiAlW_{11}$	1.41	19.17	3.89
Calculated for $(N(C_4H_9)_4)_3K_2SiAlW_{11}(H_2O)O_{39}$	1.19	16.36	3.15
Calculated for $(N(C_4H_9)_4)_4KSiAlW_{11}(H_2O)O_{39}$	1.50	20.62	3.95

Based on the EA results in Table 24, the nitrogen, carbon and hydrogen values for the ^{III}TBA product are all lower than the calculated values for $(N(C_4H_9)_4)_4KSiAlW_{11}(H_2O)O_{39}$, though they are not so low as to represent $(N(C_4H_9)_4)_3K_2SiAlW_{11}(H_2O)O_{39}$. This indicates that the ^{III}TBA synthesis successfully replaced four of the five potassium atoms with TBA molecules. As the hydrogen value for ^{III}TBA-$SiAlW_{11}$ is already lower than the calculated values, there does not seem to be any non-coordinated water to this sample at the time of the analysis. With the chemical formula $(N(C_4H_9)_4)_4KSiAlW_{11}(H_2O)O_{39}$, the molar mass of the compound is 3728.25 g mol^{-1} and the yield of the synthesis is 83.08 %. The synthesis produced a white powder with no visible impurities.

TBA-$SiCoW_{11}$

TBA-$SiCoW_{11}$ was attempted synthesised using two of the different TBA syntheses: ^{II}TBA and ^{III}TBA.

Table 25: EA results for TBA-$SiCoW_{11}$.

	N [%]	C [%]	H [%]
Found for ^{II}TBA-$SiCoW_{11}$	1.48	20.71	4.32
Found for ^{III}TBA-$SiCoW_{11}$	1.66	22.81	3.80
Calculated for $(N(C_4H_9)_4)_4K_2SiCoW_{11}(H_2O)O_{39}$	1.47	20.23	3.87
Calculated for $(N(C_4H_9)_4)_5KSiCoW_{11}(H_2O)O_{39}$	1.75	24.01	4.58

When comparing the EA results for the two different TBA syntheses (see Table 25), it can be observed that there are some differences between the results. The nitrogen and carbon values

for the ^{III}TBA product are higher, while the hydrogen value is lower than what is seen for the ^{II}TBA product. Still, they have both been assigned to $(N(C_4H_9)_4)_4K_2SiCoW_{11}(H_2O)O_{39}$. The reason is that even though ^{III}TBA-$SiCoW_{11}$ has higher nitrogen and carbon values than what is expected for $(N(C_4H_9)_4)_4K_2SiCoW_{11}(H_2O)O_{39}$, they are not so high as to equal the values of $(N(C_4H_9)_4)_5KSiCoW_{11}(H_2O)O_{39}$. In the case of ^{II}TBA-$SiCoW_{11}$, the hydrogen value is the only one that is higher than what is calculated for $(N(C_4H_9)_4)_4K_2SiCoW_{11}(H_2O)O_{39}$. This could mean that the sample contains some non-coordinated water molecules; however, to reach a hydrogen value of 4.32 % the compound would have to coordinate 14 water molecules, which seems unlikely for a compound that is not soluble in water. There is also the issue that higher water content leads to lower calculated nitrogen and carbon values.

With the chemical formula $(N(C_4H_9)_4)_4K_2SiCoW_{11}(H_2O)O_{39}$, the molar mass of the compounds are 3799.30 g mol^{-1}. Both syntheses produced homogeneous pale pink powders, and the yields of the ^{II}TBA and ^{III}TBA syntheses were 24.73 % and 87.06 %, respectively. With such a difference in yield, it is safe to say that for the synthesis of TBA-$SiCoW_{11}$ the ^{III}TBA synthesis is the most effective.

TBA-$SiCrW_{11}$

TBA-$SiCrW_{11}$ was only attempted synthesised using one of the TBA syntheses: ^{III}TBA.

Table 26: EA results for TBA-$SiCrW_{11}$.

	N [%]	**C [%]**	**H [%]**
Found for ^{III}TBA-$SiCrW_{11}$	1.78	23.93	4.18
Calculated for $(N(C_4H_9)_4)_5SiCrW_{11}(H_2O)O_{39}$	1.77	24.28	4.64

When looking at the EA results presented in Table 26, we can see that the EA data for the ^{III}TBA-$SiCrW_{11}$ sample corresponds well with the calculated values for $(N(C_4H_9)_4)_5SiCrW_{11}(H_2O)O_{39}$. These results indicate, firstly, that all five of the potassium atoms were replaced with TBA molecules, and secondly, that there is no non-coordinated water molecules in this sample. With a chemical formula $(N(C_4H_9)_4)_5SiCrW_{11}(H_2O)O_{39}$, the molar mass of the compound is 3956.62 g mol^{-1}, making the yield of the synthesis 81.07 %. The product of the synthesis was a pale green powder that appeared to be homogeneous.

TBA-$SiCuW_{11}$

$TBA\text{-}SiCuW_{11}$ was attempted synthesised using two of the different TBA syntheses; ^{I}TBA and ^{III}TBA.

Table 27: EA results for $TBA\text{-}SiCuW_{11}$.

	N [%]	C [%]	H [%]
Found for ^{I}TBA-$SiCuW_{11}$	1.51	20.99	3.96
Found for ^{III}TBA-$SiCuW_{11}$	1.67	23.02	4.25
Calculated for $(N(C_4H_9)_4)_4K_2SiCuW_{11}(H_2O)O_{39}$	1.47	20.21	3.87
Calculated for $(N(C_4H_9)_4)_5KSiCuW_{11}(H_2O)O_{39}$	1.75	23.98	4.58

If we start by looking at the EA results for the ^{I}TBA-$SiCuW_{11}$ synthesis in Table 27, we see that they are very similar to the calculated values for $(N(C_4H_9)_4)_4K_2SiCuW_{11}(H_2O)O_{39}$. This indicates that the ^{I}TBA synthesis replaced four of the six potassium atoms with TBA molecules. Most likely there is no non-coordinated water in this sample as that would lower the calculated nitrogen and carbon values, which are already slightly lower than the experimental results. With the chemical formula $(N(C_4H_9)_4)_4K_2SiCuW_{11}(H_2O)O_{39}$ the molar mass of the compound is 3803.91 g mol^{-1} and the yield of the ^{I}TBA synthesis is 28.81 %.

When looking at the ^{III}TBA-$SiCuW_{11}$ results in Table 27, the values are in better agreement with those calculated for $(N(C_4H_9)_4)_5KSiCuW_{11}(H_2O)O_{39}$ than those for $(N(C_4H_9)_4)_4K_2SiCuW_{11}(H_2O)O_{39}$. This could indicate that when synthesising $TBA\text{-}SiCuW_{11}$, ^{III}TBA replaces one more potassium atom than ^{I}TBA does. With a chemical formula $(N(C_4H_9)_4)_5KSiCuW_{11}(H_2O)O_{39}$ the molar mass of this compound is 4007.27 g mol^{-1} and the yield of the ^{III}TBA synthesis is 86.90 %. Both syntheses produced a pale blue powder that appeared homogeneous. All this considered, it seems that for the synthesis of $TBA\text{-}SiCuW_{11}$, the ^{III}TBA synthesis produced better results than the ^{I}TBA synthesis, as it both replaced more of the potassium atoms and gave a significantly higher yield.

TBA-$SiFeW_{11}$

$TBA\text{-}SiFeW_{11}$ was only attempted synthesised using one of the TBA synthesis: ^{III}TBA.

Table 28: EA results for TBA-$SiFeW_{11}$.

	N [%]	C [%]	H [%]
Found for ^{III}TBA-$SiFeW_{11}$	1.84	24.46	4.42
Calculated for $(N(C_4H_9)_4)_5SiFeW_{11}(H_2O)O_{39}$	1.77	24.26	4.63

When comparing the EA results presented in Table 28, with the calculated results for $(N(C_4H_9)_4)_5SiFeW_{11}(H_2O)O_{39}$ a good agreement is observed, though the experimental results are a bit higher for the nitrogen and carbon values. The hydrogen value, however, is lower for the experimental values than for the calculated ones, indicating that there is no non-coordinated water in the analysed sample. The chemical formula $(N(C_4H_9)_4)_5SiFeW_{11}(H_2O)O_{39}$ gives the molar mass of 3960.47 g mol^{-1} and shows that the ^{III}TBA synthesis replaced all the potassium atoms. The synthesis produced a pale yellow powder that appeared to be homogeneous and gave a yield of 92.41 %.

TBA-$SiMnW_{11}$

TBA-$SiMnW_{11}$ was attempted synthesised using two of the different TBA syntheses: ^{I}TBA and ^{III}TBA.

Table 29: EA results for TBA-$SiMnW_{11}$.

	N [%]	C [%]	H [%]
Found for ^{I}TBA-$SiMnW_{11}$	1.56	21.34	3.92
Found for ^{III}TBA-$SiMnW_{11}$	1.73	23.63	4.15
Calculated for $(N(C_4H_9)_4)_4K_2SiMnW_{11}(H_2O)O_{39}$	1.48	20.25	3.88
Calculated for $(N(C_4H_9)_4)_5KSiMnW_{11}(H_2O)O_{39}$	1.75	24.03	4.59

As can be seen from the EA results presented in Table 29, the nitrogen, carbon and hydrogen values of ^{III}TBA-$SiMnW_{11}$ are notably higher than those of ^{I}TBA-$SiMnW_{11}$. If we start by looking at the values for ^{I}TBA-$SiMnW_{11}$, we see that they correlate well with the calculated values for $(N(C_4H_9)_4)_4K_2SiMnW_{11}(H_2O)O_{39}$, though all the values are slightly higher than the calculated ones. This indicates that the ^{I}TBA synthesis replaced four out of six potassium atoms with TBA molecules. With a chemical formula $(N(C_4H_9)_4)_4K_2SiMnW_{11}(H_2O)O_{39}$ the product of the ^{I}TBA synthesis has a molar mass of 3795.30 g mol^{-1} and the yield of the synthesis is 2.95 %.

When we look at the EA results for the ^{III}TBA synthesis, however, the values are closer to what is calculated for $(N(C_4H_9)_4)_5KSiMnW_{11}(H_2O)O_{39}$ than $(N(C_4H_9)_4)_4K_2SiMnW_{11}(H_2O)O_{39}$. This shows that most likely the ^{III}TBA synthesis substitutes more potassium atoms than the ^{I}TBA synthesis. With the chemical formula $(N(C_4H_9)_4)_5KSiMnW_{11}(H_2O)O_{39}$ the molar mass of the compound is 3998.67 g mol^{-1}, making the yield of the synthesis 85.84 %. Both syntheses produced pale orange powders that appeared to be homogeneous. With such a drastic difference in yield, ^{III}TBA is clearly the most favourable of the two syntheses.

TBA-$SiNiW_{11}$

TBA-$SiNiW_{11}$ was attempted synthesised using two of the different TBA syntheses: ^{I}TBA and ^{III}TBA.

Table 30: EA results for TBA-$SiNiW_{11}$.

	N [%]	**C [%]**	**H [%]**
Found for ^{I}TBA-$SiNiW_{11}$	1.52	20.71	4.35
Found for ^{III}TBA-$SiNiW_{11}$	1.77	24.36	4.39
Calculated for $(N(C_4H_9)_4)_4K_2SiNiW_{11}(H_2O)O_{39}$	1.47	20.23	3.87
Calculated for $(N(C_4H_9)_4)_5KSiNiW_{11}(H_2O)O_{39}$	1.75	24.01	4.58

When looking at the EA results presented in Table 30, it can be observed that ^{I}TBA-$SiNiW_{11}$ has nitrogen and carbon values that are very similar to those calculated for $(N(C_4H_9)_4)_4K_2SiNiW_{11}(H_2O)O_{39}$. The experimental hydrogen value is the only one that is a bit too high compared to the calculated values. This could be an indication of non-coordinated water in the sample, but since the experimental nitrogen and carbon values already are slightly higher than the calculated ones, and adding water would only lower the calculated values more, this seems unlikely. With the chemical formula $(N(C_4H_9)_4)_4K_2SiNiW_{11}(H_2O)O_{39}$, the molar mass of the compound is 3799.06 g mol^{-1}, and the yield of the ^{I}TBA synthesis is 11.00 %.

When comparing the EA results from the ^{III}TBA synthesis with the calculated values in Table 30, they are clearly closer to the values for $(N(C_4H_9)_4)_5KSiNiW_{11}(H_2O)O_{39}$ than those for $(N(C_4H_9)_4)_4K_2SiNiW_{11}(H_2O)O_{39}$. This shows that the ^{III}TBA synthesis might have managed to substitute one more potassium atom than the ^{I}TBA synthesis. With a chemical formula $(N(C_4H_9)_4)_5KSiNiW_{11}(H_2O)O_{39}$, the molar mass of the product is 4002.42 g mol^{-1}, making the yield of the synthesis 71.39 %. Both syntheses produced pale green powders that

macroscopically were free of impurities. With the large difference in yield, and the fact that the ^{III}TBA synthesis replaced one more of the potassium atoms, it is clear that ^{III}TBA is the most beneficial of the two syntheses.

TBA-SiZnW$_{11}$

TBA-SiZnW$_{11}$ was attempted synthesised using two of the different TBA syntheses: ^{I}TBA and ^{III}TBA.

Table 31: EA results for TBA-SiZnW$_{11}$.

	N [%]	C [%]	H [%]
Found for ^{I}TBA-SiZnW$_{11}$	1.51	20.73	3.96
Found for ^{III}TBA-SiZnW$_{11}$	1.72	23.49	4.56
Calculated for (N(C$_4$H$_9$)$_4$)$_4$K$_2$SiZnW$_{11}$(H$_2$O)O$_{39}$	1.47	20.20	3.87
Calculated for (N(C$_4$H$_9$)$_4$)$_5$KSiZnW$_{11}$(H$_2$O)O$_{39}$	1.75	23.97	4.58

When we look at the EA results presented in Table 31 we see that the EA data from the product of the ^{I}TBA synthesis correspond well to the calculated data for (N(C$_4$H$_9$)$_4$)$_4$K$_2$SiZnW$_{11}$(H$_2$O)O$_{39}$. The fact that the hydrogen value for the product is higher than the calculated values could indicate that there is non-coordinated water in the sample. However, since the calculated nitrogen and carbon values are already lower than the experimental results, and would only get lower with the addition of water, this is probably not the case. With the chemical formula (N(C$_4$H$_9$)$_4$)$_4$K$_2$SiZnW$_{11}$(H$_2$O)O$_{39}$ the molar mass of the product of the ^{I}TBA synthesis is 3805.75 g mol^{-1}, making the yield of the synthesis 3.10 %.

The EA results for ^{III}TBA-SiZnW$_{11}$ are in good agreement with the calculated values for (N(C$_4$H$_9$)$_4$)$_5$KSiZnW$_{11}$(H$_2$O)O$_{39}$ (see Table 31). This suggests that the ^{III}TBA synthesis substitutes one more of the potassium atom than the ^{I}TBA synthesis. With a chemical formula (N(C$_4$H$_9$)$_4$)$_5$KSiZnW$_{11}$(H$_2$O)O$_{39}$ the molar mass of the product is 4009.12 g mol^{-1} and the yield of the synthesis is 74.27 %, making the ^{III}TBA synthesis the most favourable of the two syntheses.

Brief overview of the EA results and yields for the TBA syntheses

Table 32: Overview of the determined chemical formula, molar mass and yield for the TBA compounds.

	Chemical formula	Molar mass [g mol^{-1}]	Yield [%]
^{III}TBA-SiAlW$_{11}$	$(N(C_4H_9)_4)_4KSiAlW_{11}(H_2O)O_{39}$	3728.25	83.08
^{II}TBA-SiCoW$_{11}$	$(N(C_4H_9)_4)_4K_2SiCoW_{11}(H_2O)O_{39}$	3799.30	24.73
^{III}TBA-SiCoW$_{11}$	$(N(C_4H_9)_4)_4K_2SiCoW_{11}(H_2O)O_{39}$	3799.30	87.06
^{III}TBA-SiCrW$_{11}$	$(N(C_4H_9)_4)_5SiCrW_{11}(H_2O)O_{39}$	3956.62	81.07
^{I}TBA-SiCuW$_{11}$	$(N(C_4H_9)_4)_4K_2SiCuW_{11}(H_2O)O_{39}$	3803.91	28.81
^{III}TBA-SiCuW$_{11}$	$(N(C_4H_9)_4)_5KSiCuW_{11}(H_2O)O_{39}$	4007.27	86.90
^{III}TBA-SiFeW$_{11}$	$(N(C_4H_9)_4)_5SiFeW_{11}(H_2O)O_{39}$	3960.47	92.41
^{I}TBA-SiMnW$_{11}$	$(N(C_4H_9)_4)_4K_2SiMnW_{11}(H_2O)O_{39}$	3795.30	2.95
^{III}TBA-SiMnW$_{11}$	$(N(C_4H_9)_4)_5KSiMnW_{11}(H_2O)O_{39}$	3998.67	85.84
^{I}TBA-SiNiW$_{11}$	$(N(C_4H_9)_4)_4K_2SiNiW_{11}(H_2O)O_{39}$	3799.06	11.00
^{III}TBA-SiNiW$_{11}$	$(N(C_4H_9)_4)_5KSiNiW_{11}(H_2O)O_{39}$	4002.42	71.39
^{I}TBA-SiZnW$_{11}$	$(N(C_4H_9)_4)_4K_2SiZnW_{11}(H_2O)O_{39}$	3805.75	3.10
^{III}TBA-SiZnW$_{11}$	$(N(C_4H_9)_4)_5KSiZnW_{11}(H_2O)O_{39}$	4009.12	74.27

4.3.2 Discussion of the EA results and yields for the TBA compounds

For the TBA compounds there were three different types of syntheses attempted. The first one, ^{I}TBA, was based on the paper by Balula *et al.*[28] This synthesis was used for substituting potassium atoms in already synthesised potassium POM compounds, and was used to synthesise ^{I}TBA-SiCuW$_{11}$, ^{I}TBA-SiMnW$_{11}$, ^{I}TBA-SiNiW$_{11}$ and ^{I}TBA-SiZnW$_{11}$. Based on the EA results for all these compounds, the ^{I}TBA synthesis substituted four out of six of the potassium atoms, which was sufficient as it made the POMs soluble in organic solvents. The yield for the ^{I}TBA varied notably for the different inserted metals, ranging from about 3 % to 29 % (see Table 32). This variation in the yield is most likely due to the fact that the product was difficult to isolate, making it difficult to stay consistent. After the evaporation of DCM, when dissolving the product in acetonitrile and precipitating it out with water, it was difficult to tell when the precipitation was complete, and when filtering the solution, more often than not, a lot of the product was not caught by the filter paper. This led to the precipitation and filtration being done multiple times for the same solution, and macroscopically determining whether or not more product was being precipitated or if the precipitate in the solution simply had not been removed in the previous filtrations. When the end of a synthesis is roughly decided, it is only natural that it would lead to some variation in the yield. As the ^{I}TBA

syntheses had no parallels, this could strongly impact the reported yields. Another reason for the variation in yield could also simply be that the synthesis prefers some metal compounds over others. If more parallels had been carried out it would have been possible to get a more accurate estimate of the yield; however, rather than spend time on that, finding a way of synthesising the TBA POMs without using highly toxic chemicals, such as DCM, was prioritised.

The second synthesis attempted was ^{II}TBA, which was based on a $TBA_4Mo_8O_{26}$ synthesis found in Ginsberg.[48] This synthesis was only used to synthesise TBA-$SiCoW_{11}$, as a potentially better option was found closely after. Not only did this synthesis remove the need for DCM, it was also a lot simpler to perform than the ^{I}TBA synthesis, though the issue of filtering the TBA compounds continued for all the three TBA syntheses. According to the EA results for ^{II}TBA-$SiCoW_{11}$, it seems like this synthesis successfully replaced four out of six potassium atoms, same as in ^{I}TBA. Regarding the yield, it was at the higher end of what was achieved with the ^{I}TBA synthesis, giving a yield of 24.85 % for the synthesis of TBA-$SiCoW_{11}$ (see Table 32).

The final TBA synthesis that was attempted was ^{III}TBA. This was based on a TBA-$SiAlW_{11}$ synthesis from Kato *et al*,[26] and used for all eight metals in this project. Like the ^{II}TBA synthesis, it did not require any DCM, and was a relatively simple synthesis to perform. The only downside of this synthesis is that it lasts for three days, but it might be possible to shorten this significantly, which could be interesting to attempt in future work. However, three days needed for the synthesis, did not really impact the speed at which the TBA compounds were made, as the ^{III}TBA synthesis did not require a previously synthesised potassium compound, unlike the other TBA syntheses. This also means that the ^{III}TBA synthesis was not impacted by the lower yield and impurities from the potassium syntheses. The yield of the ^{III}TBA synthesis was also significantly higher, ranging from about 72 to 93 % (see Table 32).

According to the EA results, ^{III}TBA also seems to replace more potassium atoms with TBA molecules than ^{I}TBA. In the case of ^{III}TBA-$SiCuW_{11}$, ^{III}TBA-$SiMnW_{11}$, ^{III}TBA-$SiNiW_{11}$ and ^{III}TBA-$SiZnW_{11}$ the synthesis gave products with five TBA molecules out of the six possible ones, while with TBA-$SiCoW_{11}$ there was little difference between the ^{II}TBA and ^{III}TBA products. It should be noted, however, that the amount of TBA molecules bound to the POM anions is not that important, as long as the compound is soluble in organic solvents. Due to the success of the ^{III}TBA synthesis, ^{III}TBA-$SiAlW_{11}$, ^{III}TBA-$SiCrW_{11}$ and ^{III}TBA-$SiFeW_{11}$ were not

synthesised using any other synthesis. Their yields were good, and according to the EA results their synthesis seemed to have gone well.

To summarise, out of the three TBA syntheses that were attempted in this project, ^{III}TBA was clearly the most beneficial. Despite requiring some time to carry out, it provided by far the best yields, and also seems to give products containing more TBA molecules than ^{I}TBA and ^{II}TBA did. To further improve on this synthesis in the future, it would be interesting to see if the amount of time could be decreased. To make the process more efficient it would also be recommended to find a faster and more thorough way of removing the product from the mother liquor.

4.3.3 TG results for some of the TBA compounds

Four samples were analysed using thermogravimetry. These samples were ^{II}TBA-$SiCoW_{11}$, ^{III}TBA-$SiCrW_{11}$, ^{I}TBA-$SiCuW_{11}$ and ^{I}TBA-$SiNiW_{11}$.

TBA-$SiCoW_{11}$

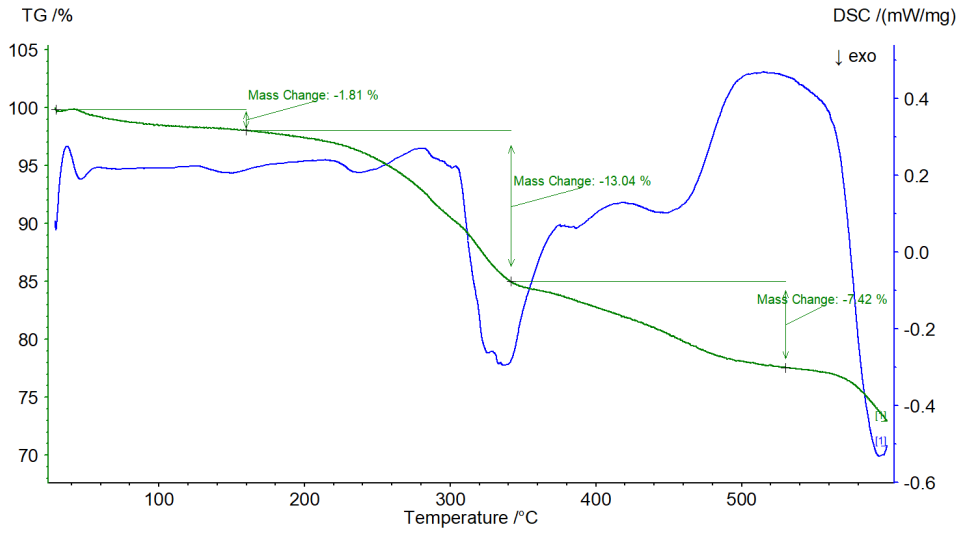

Figure 15: TG results for ^{II}TBA-$SiCoW_{11}$.

Figure 15 shows three different changes in mass when the ^{II}TBA-$SiCoW_{11}$ sample was heated from 30 to 600 °C. The first loss of mass, of 1.81 %, can be accounted for by solvent, most likely water, in the sample.[67] We assume that all organic cations would be removed in the temperature range from 250 to 600 °C. Based on Figure 15, this means that the TBA cations should make up 20.46 % of the total mass of the compound.

TBA-SiCrW$_{11}$

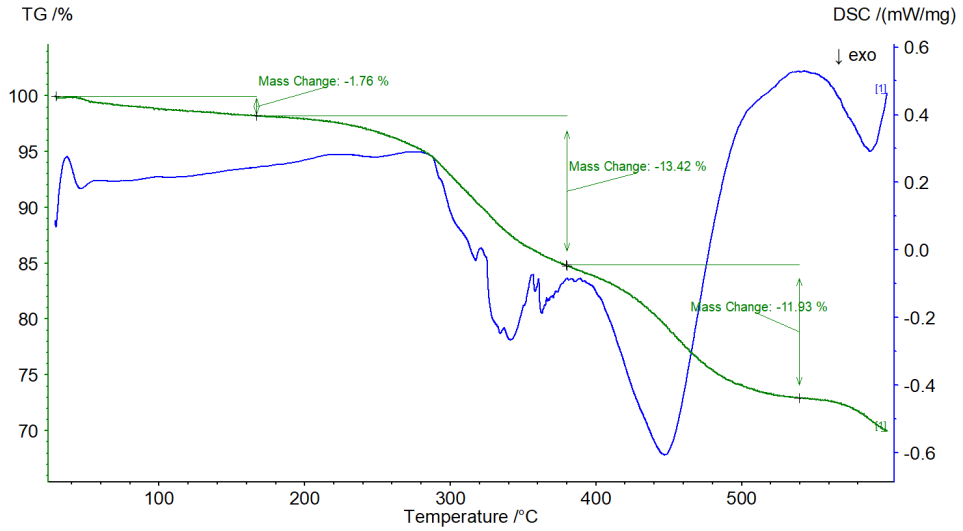

Figure 16: TG results for ^{III}TBA-SiCrW$_{11}$.

From Figure 16, we see that ^{III}TBA-SiCrW$_{11}$ loses 1.76 % of its mass when heated to about 165 °C. Most likely this can be accounted for by solvent in the sample.[67] During the following heating, from 165 to 520 °C, we see that there are two more changes in the mass, making up 25.35 %. As all organic compounds should be removed in this temperature range, we can therefore assume that the TBA cations make up those 25.35 %.

TBA-SiCuW$_{11}$

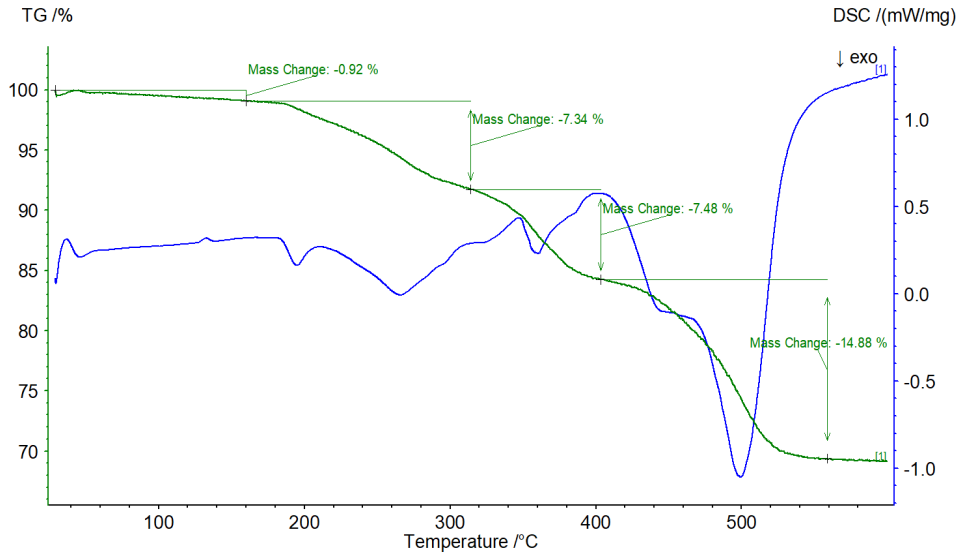

Figure 17: TG results for ^{I}TBA-SiCuW$_{11}$.

From Figure 17 we see that, unlike the other TG analysed compounds, ^{I}TBA-SiCuW$_{11}$ goes through four mass changes, when heated from 30 to 600 °C. Firstly, the sample loses 0.92 % of its mass, which presumably can be accounted for by solvent in the sample.[67] The following three changes make up 29.70 % and are probably caused by the loss of TBA cations.

TBA-SiNiW$_{11}$

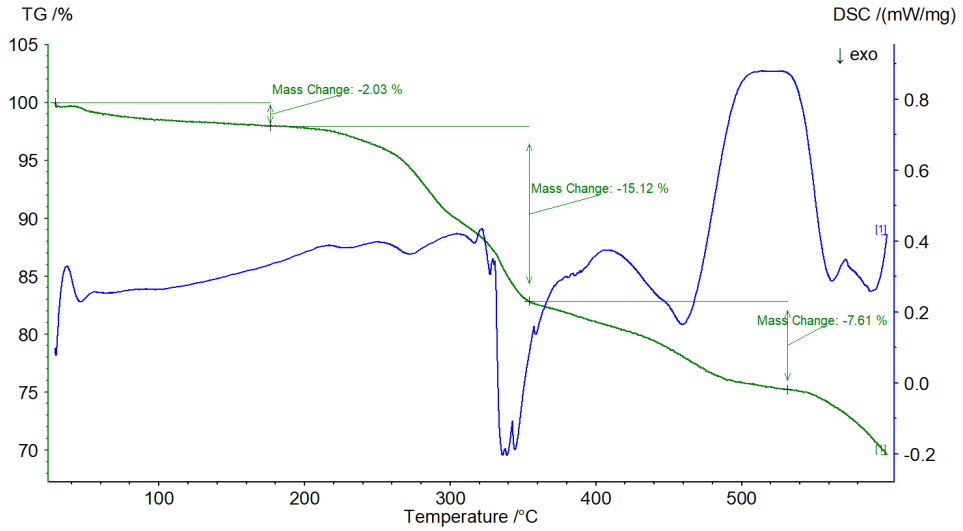

Figure 18: TG results for ^{I}TBA-SiNiW$_{11}$.

According to Figure 18, the first loss of mass below 180 °C accounts for 2.03 % of the original mass of ^{I}TBA-SiNiW$_{11}$. This weight loss, probably makes up the solvent, mainly water, in the sample.[67] The following mass changes make up 22.73 % of the mass of the compound, and can probably be accounted for by the TBA cations bound to the POM.

4.3.4 Discussion of the TG results for some of the TBA compounds

From the TG results presented, it seems that all the analysed samples contain some amount of solvent. Based on the correlating EA results for these samples, we know that there is a water molecule directly coordinated to the TBA POMs, but this would not make up 1-2 % of the molar mass. It is therefore possible that the samples acquired water from the atmosphere, as they were left out in air for some time before analysis. The TG results also show that the loss of water happened all the way up to 180 °C in some cases. As the boiling point of water is 100 °C, this seems high; however, it has been reported that removal of physically absorbed water and crystal water from TBA POM samples requires higher temperatures.[67]

Initially, it was hoped that the TG analysis could provide information about how many TBA molecules were bound to the different POM anions. However, due to the temperature program that was selected none of the samples were burned to completion, as can be seen from Figure 15 to Figure 18. As the combustion was not complete it is difficult to draw any definite conclusions about the composition of cations. With the information we do get from the TG results, we see that the compounds lose between 20 and 30 % of their mass in the 180 to 550 °C interval. Taking the incomplete combustion into consideration, this is in agreement with the EA results, which show that the TBA cations would make up about 25 to 30 % of the molar mass of these compounds.

4.3.5 IR results for the TBA compounds

TBA-$SiAlW_{11}$

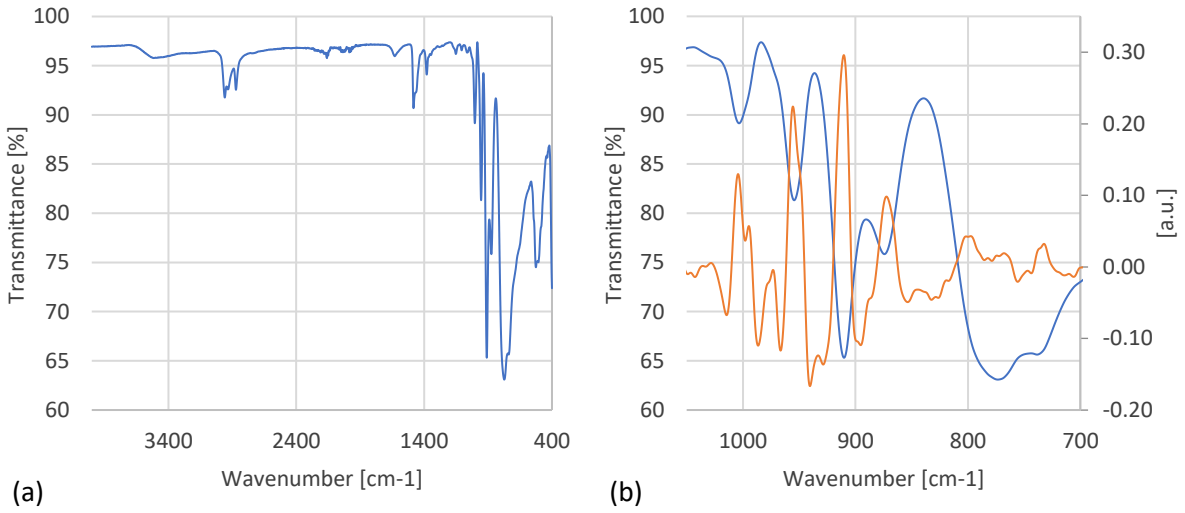

Figure 19: (a) The complete IR spectrum for TBA-$SiAlW_{11}$, (b) the IR (blue) and second derivative (orange) spectra from 1050 – 700 cm^{-1} for TBA-$SiAlW_{11}$.

Table 33: Overview of IR data for TBA-$SiAlW_{11}$.

Wavenumber [cm^{-1}]			**Assignment**
Experimental*	**Second derivative***	**Literature[26]**	
1003.41	1004.30, 994.74	1006	W=O stretch
954.43	955.55	960	Si-O stretch
910.10	910.31, 872.38	916	W-Ob-W stretch
773.41, 738.52	801.63, 797.50, 732.35, 774.19, 767.89, 782.25	799, 740	W-Oc-W stretch

*Sorted by intensity.

If we compare the IR spectrum in Figure 19 with the characteristic peaks described in Table 1, we see that the spectrum contains all the four peaks we expect to see for a Keggin-type POM structure. When compared to the IR data presented in Table 2, it is clear that the peaks observed at 2959.59, 2933.98, 2872.12, 1482.99, 1379.69 and 1151.79 cm^{-1} in Figure 19 can be attributed to the TBA cations bound to the POM. The peak at 1630.09 cm^{-1} differ from what is expected for the TBA cation, but can be found in the IR spectra for both the SiW_{11} (see Figure 3) and $Al(NO_3)_3 \cdot 9H_2O$ (see Appendix). This could mean that there is a slight impurity of these start materials in the analysed sample, or could be caused by a vibration in the POM that is simply not mentioned in the literature as it is outside the range of interest. When comparing the experimental data with data from the literature (see Table 33), it shows that the experimental data is consistently lower than the data reported by Kato *et al.*[26] The only experimental peak that deviates significantly from the literature data, is the one assigned to the W-Oc-W stretch. In the literature this peak is reported at 799 cm^{-1}, and when looking at Figure 19, we see a second derivative signal at 797.50 cm^{-1}. This signal has the second highest intensity, but it does not come through in the final spectrum. This is probably due to multiple lower intensity peaks in the same range covering the signal.

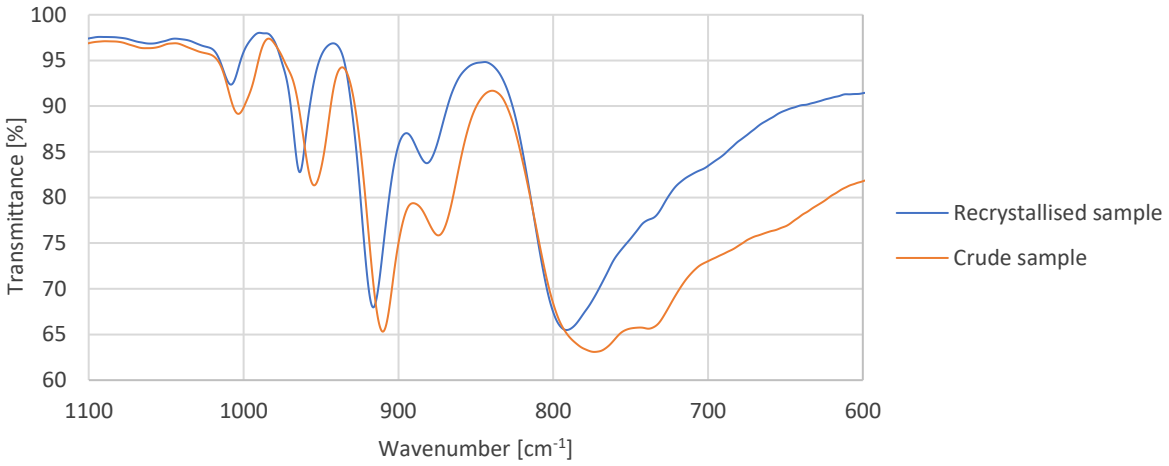

Figure 20: Comparison of the IR spectra for a recrystallised and a crude TBA-$SiAlW_{11}$ sample.

When comparing the IR results for crude TBA-$SiAlW_{11}$ products with those of recrystallised ones (see Figure 20), it can be observed that the recrystallisation causes a shift in the peaks, to the point that some of them actually are higher than the literature values in Table 33. This indicates a structural change, most likely due to the coordination of solvent molecules. However, the IR spectrum keeps its characteristic shape, confirming that we have the targeted monosubstituted Keggin structure.

TBA-SiCoW$_{11}$

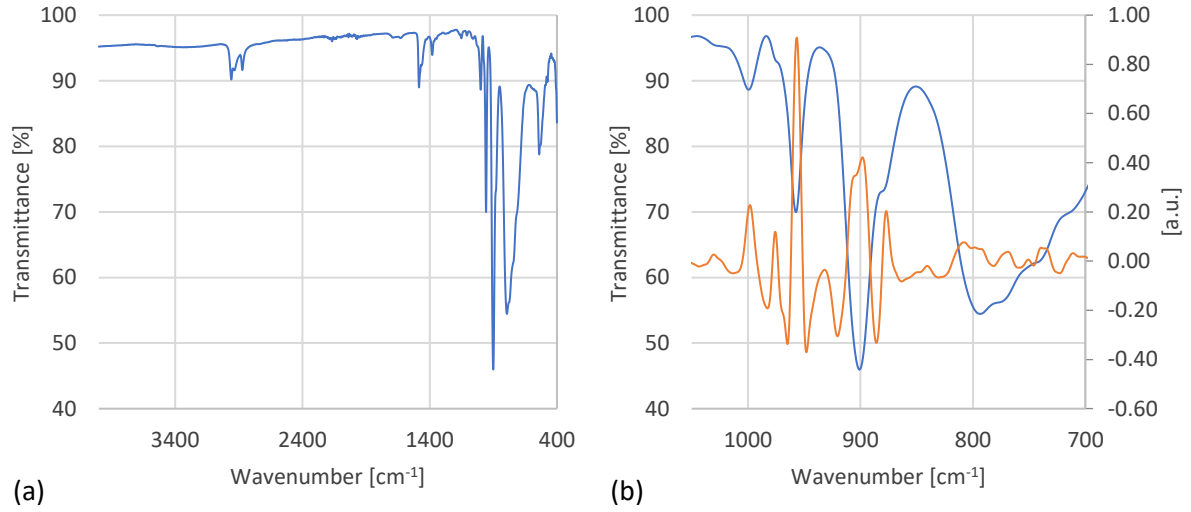

Figure 21: (a) The complete IR spectrum for TBA-SiCoW$_{11}$, (b) the IR (blue) and second derivative (orange) spectra from 1050 – 700 cm^{-1} for TBA-SiCoW$_{11}$.

Table 34: Overview of IR data for TBA-SiCoW$_{11}$.

Wavenumber [cm^{-1}]			**Assignment**
Experimental*	**Second derivative***	**Literature[28]**	
998.89	998.21	1001	W=O stretch
956.70	956.61, 975.67	959	Si-O stretch
899.88	898.12, 877.02	907	W-Ob-W stretch
791.43, 776.69	807.97, 798.40, 792.97, 739.22, 735.87, 768.91, 750.79	792	W-Oc-W stretch

*Sorted by intensity.

When comparing the characteristic IR data for POMs (see Table 1) with the IR spectrum for TBA-SiCoW$_{11}$ (see Figure 21), we see that the IR spectrum contains all the peaks we would expect to find for a Keggin-type POM structure, indicating that the target compound was successfully obtained. According to the IR value presented in Table 2, the peaks observed at 2959.35, 2872.46, 1484.32 and 1380.14 cm^{-1} in Figure 21 are caused by the TBA cations bound to the POM. When compared, it can be seen that the experimental data and the data from the literature more or less correlate (see Table 34). The only signal that notably deviates from the literature data, is the signal assigned to the W-Ob-W stretch. Since the TBA-SiCoW$_{11}$ compounds were made using two different syntheses, had the same IR spectra and appeared homogeneous, it is unlikely that residue of the start materials would have caused the deviation

of this peak. The IR data for the TBA-$SiCoW_{11}$ also did not notable change when the sample was recrystallised, as can be observed in Figure 22.

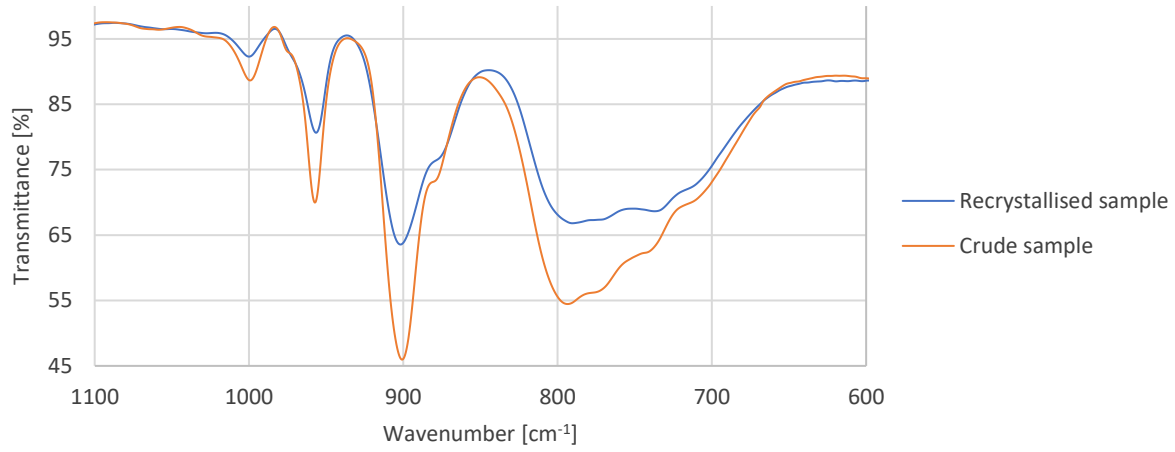

Figure 22: Comparison of the IR spectra for a recrystallised and a crude TBA-$SiCoW_{11}$ sample.

TBA-$SiCrW_{11}$

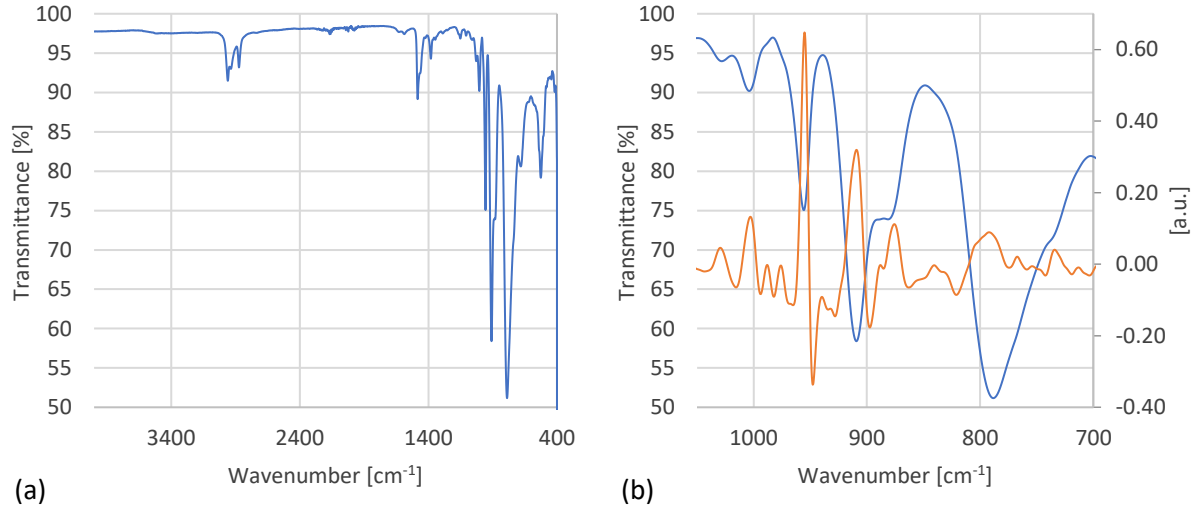

Figure 23: (a) The complete IR spectrum for TBA-$SiCrW_{11}$, (b) the IR (blue) and second derivative (orange) spectra from 1050 – 700 cm^{-1} for TBA-$SiCrW_{11}$.

Table 35: Overview of IR data for TBA-$SiCrW_{11}$.

Wavenumber [cm^{-1}]		**Assignment**
Experimental	**Second derivative***	
1003.89	1002.83	W=O stretch
955.71	955.03	Si-O stretch
909.26	909.14, 875.72	W-Ob-W stretch
788.36	792.08, 734.21, 767.24	W-Oc-W stretch

*Sorted by intensity.

When compared to the data presented in Table 2, the peaks at 2960.00, 2936.02, 2873.15, 1483.64 and 1380.79 cm^{-1} in the IR spectrum (see Figure 23) can be assumed to be caused by the TBA cations bound to the POM.

It was not possible to find IR data for the TBA-$SiCrW_{11}$ compound in the literature, but when compared to the data in Table 1, we see that the IR spectrum for TBA-$SiCrW_{11}$ contains the peaks that are characteristic for the monosubstituted Keggin IR spectra, indicating that the desired compound was obtained. When compared to the IR data for SiW_{11} in Table 4, which is a start material in this synthesis, it can be observed that the peaks assigned to the Si-O and W-Oc-W stretches are very similar to each other. This does not necessarily mean that there is residue of SiW_{11} in the product. As the TBA-$SiCrW_{11}$ product appears to be homogeneous, it is more likely that the similarities are caused by the fact that the two compounds have many of the same bonds.

When comparing the IR spectra for crude and recrystallised TBA-$SiCrW_{11}$ samples (see Figure 24), it can be seen that the peaks assigned to the W=O, Si-O and W-Ob-W stretches shift to slightly higher values, while the peak assigned to the W-Oc-W shifts to a slightly lower value when the sample is recrystallised. This indicates a small change in the structure, probably caused by the coordination of solvent. The characteristic peaks observed in the spectrum show that it is still the desired monosubstituted Keggin structure.

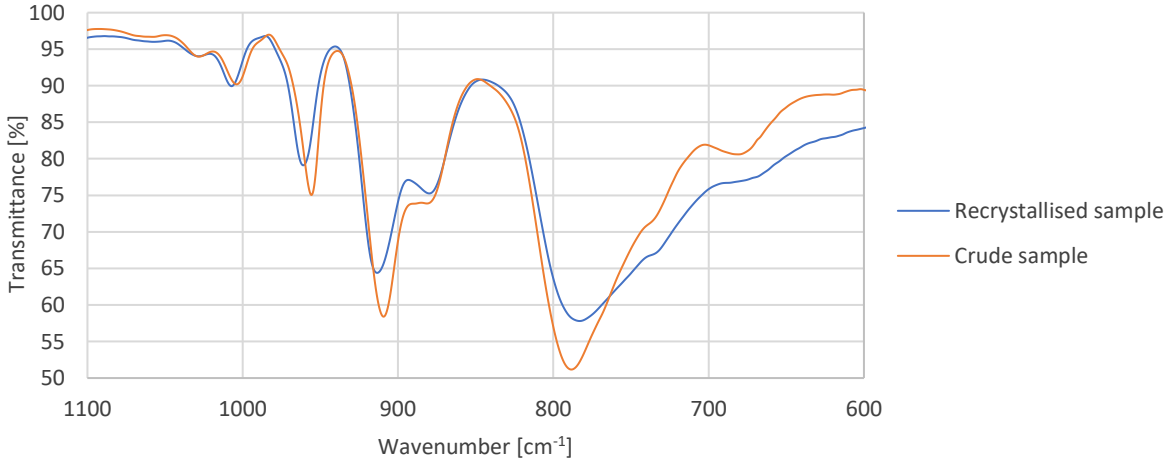

Figure 24: Comparison of the IR spectra for a recrystallised and a crude TBA-$SiCrW_{11}$ sample.

TBA-SiCuW$_{11}$

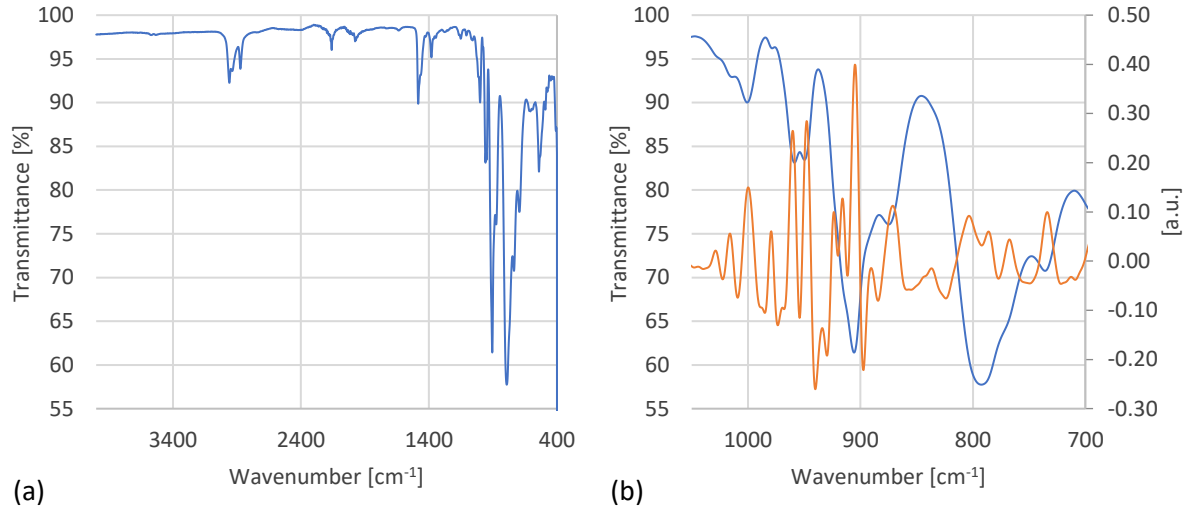

Figure 25: (a) The complete IR spectrum for TBA-SiCuW$_{11}$, (b) the IR (blue) and second derivative (orange) spectra from 1050 – 700 cm^{-1} for TBA-SiCuW$_{11}$.

Table 36: Overview of IR data for TBA-SiCuW$_{11}$.

Wavenumber [cm^{-1}]			**Assignment**
Experimental*	**Second derivative***	**Literature[28]**	
1000.65	999.73, 1016.00	1001	W=O stretch
958.59, 949.69	947.72, 960.00, 979.16	959	Si-O stretch
905.62	904.76, 915.89, 871.23, 923.57	907	W-Ob-W stretch
792.47, 735.84	803.42, 733.91, 786.12, 767.49, 691.71	792, 740	W-Oc-W stretch

*Sorted by intensity.

When comparing with the data presented in Table 1, we see that the IR spectrum for TBA-SiCuW$_{11}$ (see Figure 25) contains all the characteristic peaks we expect to find in the spectra for Keggin-type POM structures, indicating that the synthesis was successful. According to the IR spectrum for TBA-SiCuW$_{11}$ (see Figure 25), there are peaks at 2959.40, 2873.17, 1484.06 and 1380.83 cm^{-1}. When compared to the theoretical values presented in Table 2, it can be assumed that these peaks are caused by the TBA cations bound to the POM structure.

When the IR results for TBA-SiCuW$_{11}$ are compared to the IR data found in the literature (see Table 36), it can be observed that they are in good agreement. The only place there is a slight deviation is for the signal with the lowest intensity assigned to the W-Oc-W. However, the deviation here is not large enough to be significant. As TBA-SiCuW$_{11}$ was synthesised using

two different syntheses, both producing samples with the same IR spectrum, it is safe to assume that the different start materials used did not affect the IR spectrum of this compound.

When comparing the IR spectra of a crude sample and a recrystallised sample (see Figure 26), it can be seen that some of the signals change. Firstly, we can see that the second peak assigned to the Si-O stretch, disappears when the compound is recrystallised. Secondly, we can also see that there is a slight shift in the position of the peak assigned to the W-Ob-W stretch. This indicates a structural change, probably caused by the coordination of solvent. The characteristic peaks observed in the spectrum show that it is still the target monosubstituted Keggin structure.

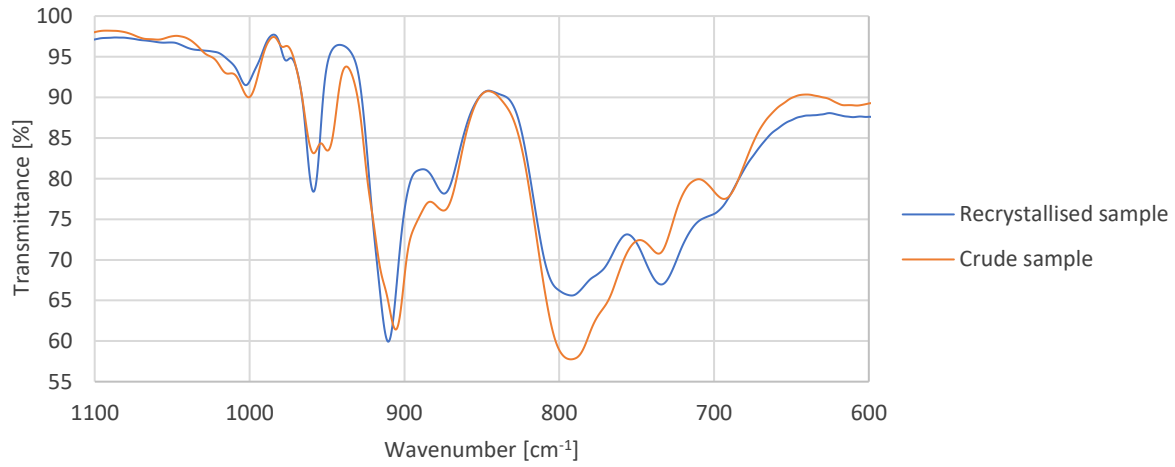

Figure 26: Comparison of the IR spectra for a recrystallised and a crude TBA-$SiCuW_{11}$ sample.

Finally, similar to what was observed for the K-$SiCuW_{11}$ samples, both the IR spectrum and the second derivative of the IR spectrum for the TBA-$SiCuW_{11}$ sample show a lot more peaks than the spectra for any of the other TBA compounds. This could possibly be caused by the creation of the sandwich structure for the POM.[65]

TBA-SiFeW$_{11}$

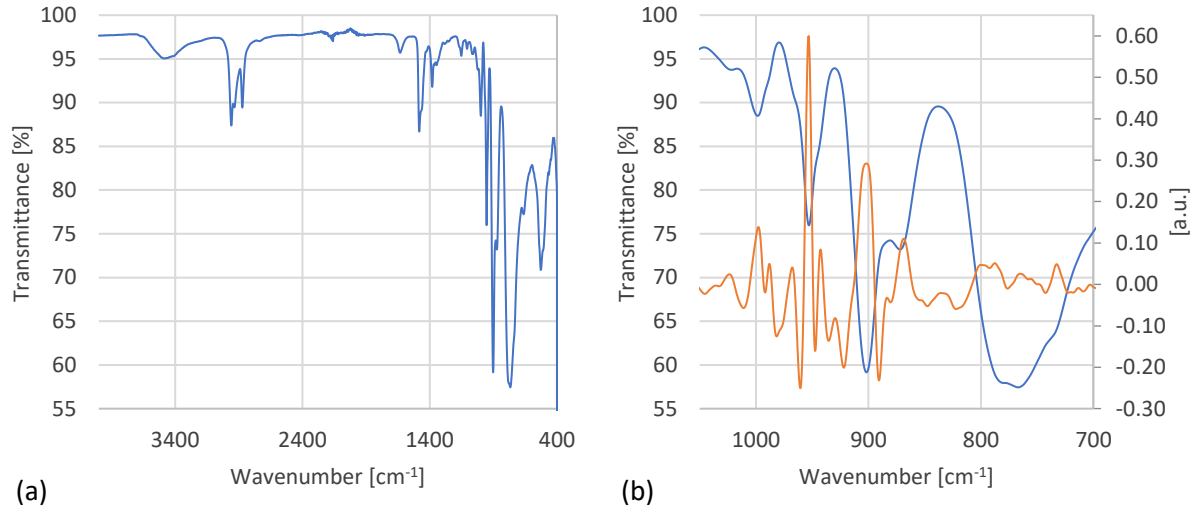

Figure 27: (a) The complete IR spectrum for TBA-SiFeW$_{11}$, (b) the IR (blue) and second derivative (orange) spectra from 1050 – 700 cm^{-1} for TBA-SiFeW$_{11}$.

Table 37: Overview of IR data for TBA-SiFeW$_{11}$.

Wavenumber [cm^{-1}]			**Assignment**
Experimental*	**Second derivative***	**Literature[28]**	
998.44	997.76, 988.01	1005	W=O stretch
952.90	953.21, 942.57, 967.70	960	Si-O stretch
901.74	901.71, 868.66	913	W-Ob-W stretch
779.52 766.85	787.65, 732.64, 799.94, 764.89, 755.67, 748.80	796, 740	W-Oc-W stretch

*Sorted by intensity.

If we compare the peaks found in the IR spectrum in Figure 27 with the characteristic peaks described in Table 1, we see that all the four characteristic peaks can be found in the IR spectrum for the TBA-SiFeW$_{11}$ compound, indicating a successful synthesis. Figure 27 shows peaks at 2958.93, 2934.69, 2872.50, 1482.38, 1380.31 and 1345.68 cm^{-1}, which according to the values presented in Table 2 can be attributed to the TBA cations bound to the POM structure. The IR spectrum also has a peak at 3485.43 cm^{-1}, which could indicate that there is some water in this sample according to the value presented in Table 1. As the compound is not water-soluble, it is not expected to coordinate much water, but since it was synthesised from an aqueous solution, it is not surprising that there could be water in the sample. The IR spectrum also shows a peak at 1632.57 cm^{-1}, which is not explained by either TBA or water. Most likely this peak can be explained by a bond vibration in the compound, which has not been mentioned in the literature as it is outside the area of interest.

When compared to data from the literature (see Table 37), it can be observed that all experimental data are lower. This cannot be explained by looking at the IR spectra for $Fe(NO_3)_3 \cdot 9H_2O$ (see Appendix) or SiW_{11} (see Figure 3), and is therefore probably not caused by any impurity in the sample. As we have seen for some of the other TBA compounds, there can be change in the IR spectrum when the compound is recrystallised; however, the TBA-$SiFeW_{11}$ compound was not recrystallised, and therefore, any changes that would occur are unknown.

TBA-$SiMnW_{11}$

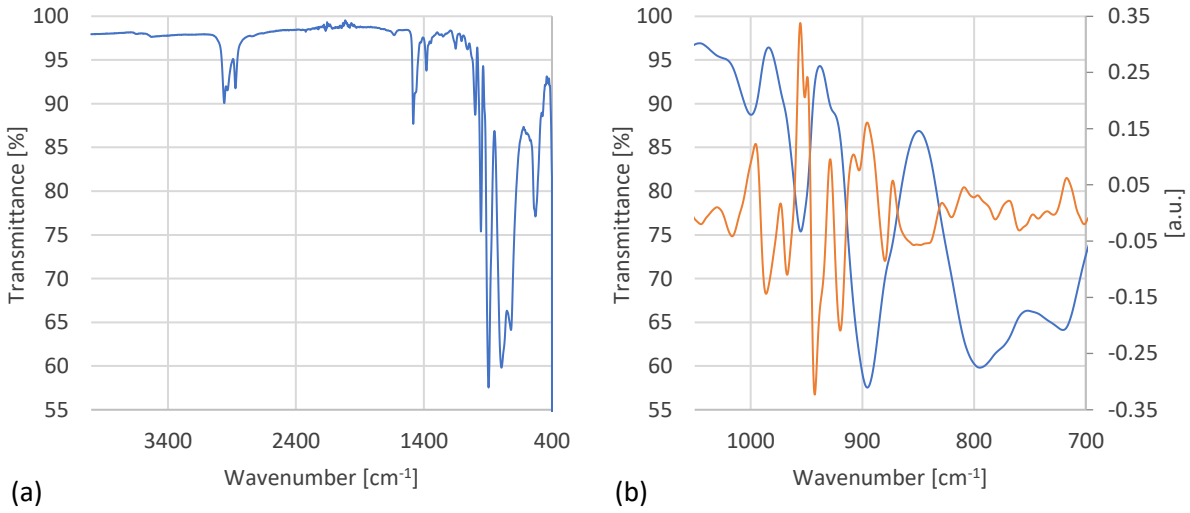

Figure 28: (a) The complete IR spectrum for TBA-$SiMnW_{11}$, (b) the IR (blue) and second derivative (orange) spectra from 1050 – 700 cm^{-1} for TBA-$SiMnW_{11}$.

Table 38: Overview of IR data for TBA-$SiMnW_{11}$.

Wavenumber [cm^{-1}]			**Assignment**
Experimental*	**Second derivative***	**Literature[28]**	
999.47	995.47	1004	W=O stretch
955.07	955.44, 949.13, 973.16	960	Si-O stretch
895.44	895.61, 907.84, 928.70, 872.67	915, 894, 875	W-Ob-W stretch
794.82, 720.36	808.84, 717.00, 796.76, 768.59, 828.56, 734.55	793	W-Oc-W stretch

*Sorted by intensity.

When comparing with the characteristic peaks for Keggin-type POMs found in Table 1, we can see that the IR spectrum for TBA-$SiMnW_{11}$ (see Figure 28) contains all the peaks we expect to find for the compound, indicating that the target compound was successfully produced.

According to the values presented in Table 2, the peaks observed at 2960.37, 2872.78, 1483.64, 1380.69 and 1152.65 cm^{-1} in Figure 28, are caused by the TBA cations bound to the POM.

When compared to IR data from the literature (see Table 38), it can be seen that the peaks assigned to the W=O and Si-O stretches are a bit lower than what is reported by Balula *et al.*[28] The experimental peak assigned to the W-Ob-W stretch can be found among the values from the literature; however, Balula *et al.*[28] report a couple more peaks in this range than can be observed in the experimental spectrum in Figure 28. Even though these values are not in the experimental spectrum, they can be found in the second derivative, meaning that the peaks are present in the experimental data as well, but that their intensity in not high enough to come through in the final spectrum.

The peak assigned to the W-Oc-W stretch can also be found in the literature data. Here Balula *et al.*[28] do not provide any data below 793 cm^{-1} so it is not possible to know if they also found a peak around 720 cm^{-1}. However, a similar peak can be found in the literature data for SiW_{11}. As this compound was synthesised using two different syntheses, where only one uses SiW_{11} as a start material, it is unlikely that the peak at 720 cm^{-1} shows an impurity. Rather, it could be caused by a bond found in both SiW_{11} and TBA-$SiMnW_{11}$. There was not recorded any IR spectrum for a recrystallised sample of TBA-$SiMnW_{11}$ and thus it is not possible to comment on whether recrystallisation would have affected the IR data.

TBA-$SiNiW_{11}$

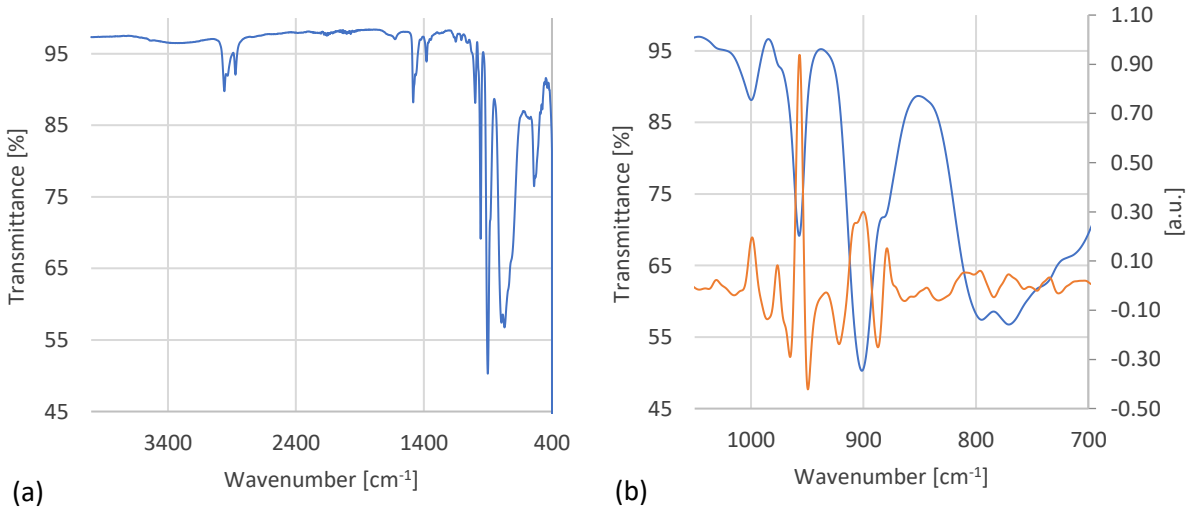

Figure 29: (a) The complete IR spectrum for TBA-$SiNiW_{11}$, (b) the IR (blue) and second derivative (orange) spectra from 1050 – 700 cm^{-1} for TBA-$SiNiW_{11}$.

Table 39: Overview of IR data for TBA-$SiNiW_{11}$.

Wavenumber [cm^{-1}]			Assignment
Experimental*	**Second derivative***	**Literature[28]**	
999.68	998.91	1001	W=O stretch
957.08	956.77, 976.42	958	Si-O stretch
901.32	906.69, 900.09, 879.06	907	W-Ob-W stretch
770.73, 794.84	796.29, 809.80, 770.86, 734.70	807, 721	W-Oc-W stretch

*Sorted by intensity.

If the IR spectrum for TBA-$SiNiW_{11}$ is compared to the characteristic peak described in Table 1, we can see that the IR spectrum contains all the peaks that would be expected for a Keggin-type POM. When compared to the data presented in Table 2, the peaks seen at 2959.40, 2934.59, 2872.86, 1484.28 and 1380.11 cm^{-1} in Figure 29 can be assumed to be caused by the TBA cations bound to the POM anion.

Compared to the IR data from Balula *et al.*[28] (see Table 39), the experimental values for the W=O and Si-O stretches are similar to what is found in the literature. In the case of the W-Ob-W stretch the values differ; however, it can be seen that a signal similar to the one found in the literature is in the second derivative of the experimental IR spectrum. This is also the case for the 807 cm^{-1} peak from the literature assigned to the W-Oc-W stretch. Why these peaks are in the second derivative spectrum, but not in the normal spectrum, could be due to their intensity. Considering the other peaks assigned to the W-Oc-W stretch, there are differences between the literature and the experimental values. The experimental peaks that are not found in the literature data could be in the second derivative of the literature data, but since this is not provided, it is not possible to say for certain. Since all the synthesised TBA-$SiNiW_{11}$ samples have the same IR spectra, even when made with different syntheses, it is unlikely that any deviation is caused by the presence of start material in the product. Either way, the characteristic peaks observed in the spectrum and the fact that the product appears homogeneous indicates that the synthesis of a monosubstituted Keggin structure was successful.

When comparing the IR spectra of crude and recrystallised TBA-$SiNiW_{11}$ samples (see Figure 30), it can be observed that some of the values shift lower when the sample is recrystallised. However, this shift is so small that it should not be of any concern.

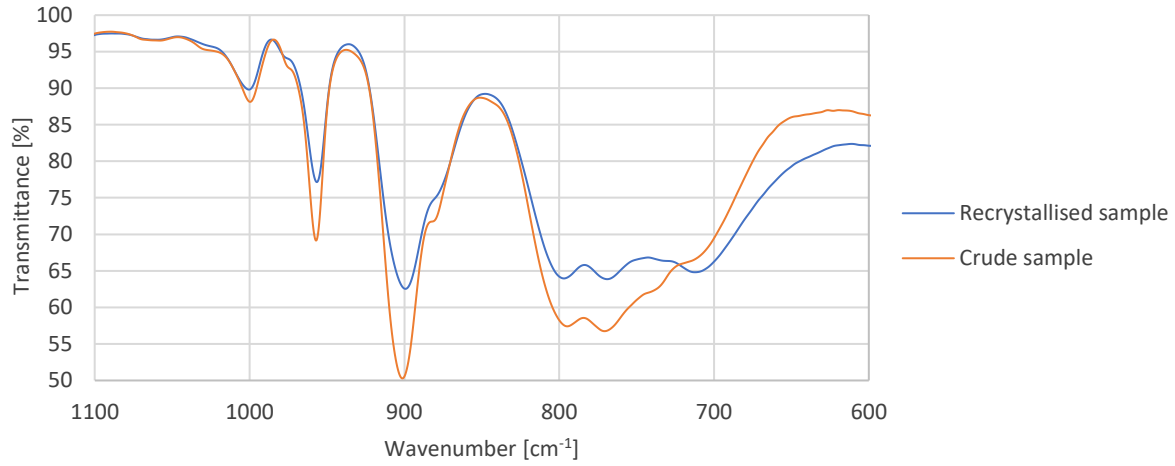

Figure 30: Comparison of the IR spectra for a recrystallised and a crude TBA-SiNiW$_{11}$ sample.

TBA-SiZnW$_{11}$

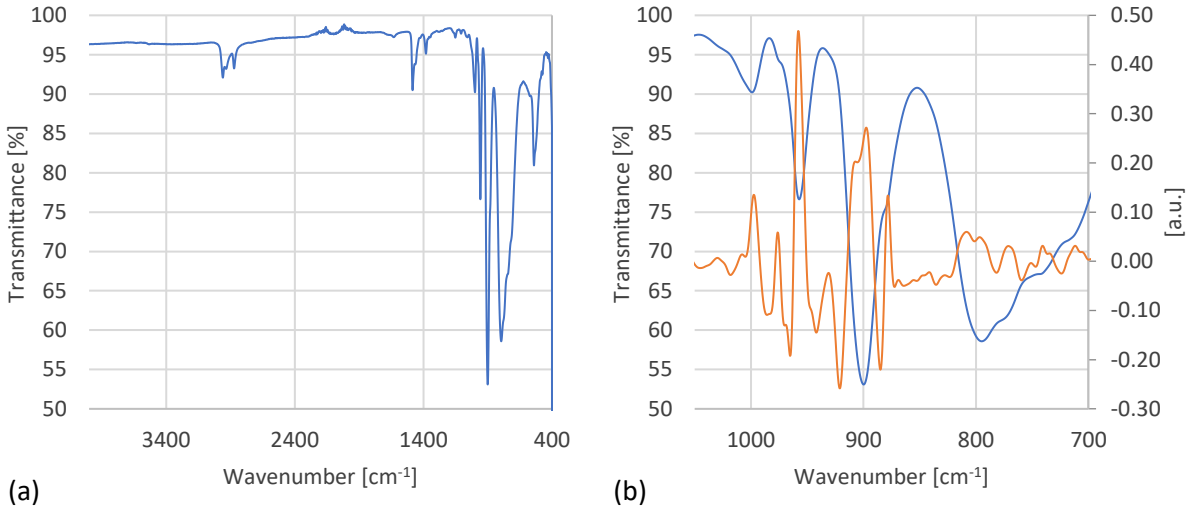

Figure 31: (a) The complete IR spectrum for TBA-SiZnW$_{11}$, (b) the IR (blue) and second derivative (orange) spectra from 1050 – 700 cm^{-1} for TBA-SiZnW$_{11}$.

Table 40: Overview of IR data for TBA-SiZnW$_{11}$.

Wavenumber [cm^{-1}]		**Assignment**
Experimental	**Second derivative***	
999.00	997.36, 1007.83	W=O stretch
957.12	957.80, 976.13	Si-O stretch
899.76	897.46, 907.16, 878.22	W-Ob-W stretch
794.84	808.35, 796.67, 771.15, 740.68, 734.65	W-Oc-W stretch

*Sorted by intensity.

When comparing the peaks in the 1050 to 700 cm^{-1} range in the IR spectrum for TBA-$SiZnW_{11}$ (see Table 40) with the characteristic peaks described in Table 1, we can observe that the IR spectrum contains all the peaks that are expected for a Keggin-type POM structure. The TBA-$SiZnW_{11}$ IR spectrum also has some peaks at 2959.74, 2933.87, 2872.25, 1484.23 and 1380.23 cm^{-1} (see Figure 31), which according to the data in Table 2 are caused by the TBA cations bound to the POM. It was not possible to find any literature IR data for TBA-$SiZnW_{11}$, but since the spectrum contains the characteristic peaks, we can assume that the synthesis of a POM structure was successful. As all IR spectra for the TBA-$SiZnW_{11}$ are the same despite using different syntheses, it can also be assumed that residue of start material did not affect the recorded IR data.

Overview of all IR spectra for the TBA compounds

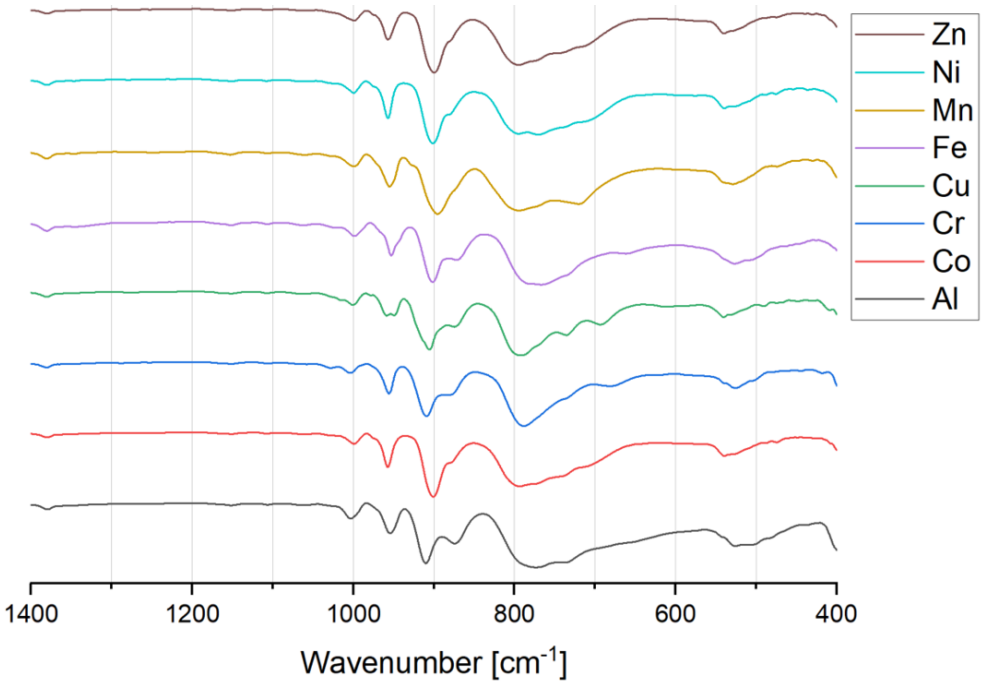

Figure 32: Overview of normalised IR spectra for the TBA compounds.

When we look at all the IR spectra for the TBA POM compounds collectively (see Figure 32), we see that there is displacement in the peaks in the 1050-700 cm^{-1} range. As the only difference between the compounds is the inserted metals, it is natural to assume that this displacement is caused by the metals inserted into the POM structure. The displacement here is significantly less than for the potassium compounds, suggesting that the cation also plays a crucial role in the peak positions. When looking at the peaks around 1000 cm^{-1} we see that it has the highest wavenumber for Cr (1003.89 cm^{-1}), followed by Al (1003.41 cm^{-1}), Cu (1000.65 cm^{-1}), Ni

(999.68 cm^{-1}), Mn (999.47cm^{-1}), Zn (999.00 cm^{-1}), Co (998.89 cm^{-1}) and Fe (998.44 cm^{-1}). Further analysis and discussion of what might cause this will be given later, in Section 4.5.

4.3.6 Discussion of the IR results for the TBA compounds

If we look at all the IR spectra for the TBA compounds, we see that they all contain peaks in the 2990-2850 cm^{-1}, 1480-1430 cm^{-1} and 1395-1340 cm^{-1} ranges. Based on the information provided in Table 2, we know that this indicates that TBA cations were successfully bound to the monosubstituted Keggin structures. We can also see that all the TBA IR spectra contain the four characteristic peaks that we expect to find for Keggin-type POMs (see Table 1). This indicates that the syntheses of Keggin-type POMs with TBA cations have been successful.

When the experimental data was compared to data previously published, there were a few different outcomes. There are various reasons why there may be deviations from the literature. In the case of the compounds with consistently lower values, it might simply be caused by the IR spectra being recorded under different conditions and on different instruments. For the compounds that only differ in one or two peaks, it could be due to difference in intensity of the second derivative signals. In some cases, though data from literature did not correlate with the experimental spectra, they could be found in the second derivative of the same spectra. This shows that the compound most likely contains the bond to cause the vibration, but that the intensity of the IR signal is not strong enough or gets covered by other signals.

As discussed previously for the IR results of the potassium POM compounds, the IR data reported in the literature can be fairly varying. With the TBA compounds in question, it was not possible to find more than one source in the literature, and in the case of TBA-$SiCrW_{11}$ and TBA-$SiZnW_{11}$ it was not possible to find any. This makes it difficult to evaluate whether deviations between experimental and literature data are caused by normal variations in the spectra or actual problems with the samples. However, despite some deviation from the literature, all the compounds have the spectrum expected for TBA containing POM structures, meaning the syntheses most likely produced the desired products.

In some of the IR results there is a comparison between the spectra for crude and recrystallised samples, but due to time constraints, not all samples were recrystallised. From those that were recrystallised, we can see that the IR spectra for TBA-$SiCoW_{11}$ and TBA-$SiNiW_{11}$ were not

significantly affected by the recrystallisation. In the case of TBA-$SiCuW_{11}$, one peak was removed and one moved slightly. As can be observed from the IR spectrum for TBA-$SiCuW_{11}$ (see Figure 25) there are more peaks in this spectrum than for any of the other TBA compounds. This could mean that there is trace of the TBA-$SiCuW_{11}$ sandwich structure in the sample, and the removal of a peak in the spectrum could therefore indicate that there has become less of the sandwich structure in the sample.[65] The only two samples that showed significant change between the IR spectra for the crude and recrystallised samples were the TBA-$SiAlW_{11}$ and TBA-$SiCrW_{11}$ samples. In both these cases most of the peaks were displaced to higher values, which could indicate a slight change in the structure of the compounds most likely caused by the coordination of solvent. Either way, the IR spectra kept their shape and characteristic peaks, indicating that they retained the structure of a monosubstituted Keggin-type POM.

To summarise, the IR spectra for the TBA compounds contained all the peaks signifying a Keggin-type POM, as well as the peaks showing the presence of TBA cations. Therefore, even though some of the IR spectra are not identical to their counter parts in literature, the IR data strongly indicates that the syntheses of Keggin-type POMs with TBA cations were successful.

4.3.7 Brief comparison of the TBA syntheses based on the discussed results

To summarise, based on the EA and IR results for the TBA Keggin compounds, the syntheses of the different compounds were successful. Though some of the IR spectra deviated slightly from the literature, they all contained the peaks associated with a Keggin-type POM anion bound to TBA cations. There was also no deviation in the IR spectra for samples of the same compound synthesised using different TBA syntheses.

When comparing the EA results for compounds synthesised with multiple of the TBA syntheses, it appears that the ^{III}TBA synthesis manages to bind more TBA molecules to the POM than the ^{I}TBA synthesis. It also seems that there is no difference in the product depending on whether it was synthesised using ^{II}TBA or ^{III}TBA, but since this comparison was only made for one of the compounds it should not be considered a certainty. Normally these results would be confirmed using TG analysis, but due to the temperature program that was run, this is not possible. The amount of TBA molecules bound to the POM anions, however, is not that important, as long as the compound is soluble in organic solvents, and therefore could be used for homogeneous catalysis. As all the products were either precipitated using water or

precipitated from an aqueous solution, we know that they have bound enough TBA molecules to be insoluble in water.

Finally, out of the three TBA POM syntheses that were attempted in this project, the ^{III}TBA synthesis produced by far the best yield. This synthesis is also not very work intensive and does not require any highly toxic chemicals, though it does take unnecessarily long to perform. Finally, the synthesis also does not require pre-synthesised potassium Keggin compounds, which eliminates any consequential errors from that. This is all to say that, out of the three TBA POM syntheses, ^{III}TBA is the most beneficial one, with regard to yield and health, safety and environment (HSE).

4.4 Results and discussion of the SXRD analysis

4.4.1 SXRD Results

Due to time constraints, only three samples were analysed using single crystal X-ray diffraction. These samples were K-SiMnW$_{11}$, ^{II}K-SiCuW$_{11}$ and ^{I}TBA-SiCuW$_{11}$, and their results are presented in Table 41. The K-SiMnW$_{11}$ sample that was analysed was actually synthesised using a synthesis from Tourné *et al.*,[63] which as mentioned previously, produced good crystals that were suitable for full SXRD analysis. For this project, only pre-experimental unit cell data were collected for comparison with known crystal structure data available in the literature.

Table 41: Reduced cell SXRD results for K-SiCuW$_{11}$, TBA-SiCuW$_{11}$ and K-SiMnW$_{11}$.

	a [Å]	**b [Å]**	**c [Å]**	***α* [º]**	***β* [º]**	***γ* [º]**	**Volume [Å^3]**
K-SiMnW$_{11}$	14.20	14.20	12.46	90.00	90.00	90.00	2510.48
^{II}K-SiCuW$_{11}$	13.17	13.83	14.72	88.89	75.62	70.04	2434.56
^{I}TBA-SiCuW$_{11}$	15.18	15.20	15.19	109.45	109.43	109.52	2700.00

Table 42: Reduced cell SXRD data from the literature.

Chemical formula	**a [Å]**	**b [Å]**	**c [Å]**	***α* [º]**	***β* [º]**	***γ* [º]**	**Volume [Å^3]**
$K_6SiNiW_{11}(H_2O)O_{39}\cdot 14\ H_2O$[a]	14.09	14.09	12.46	90.00	90.00	90.00	2471.79
$(N(C_4H_9))_4SiW_{12}O_{40}$[b]	15.22	15.22	15.22	109.47	109.47	109.47	2714.75
$(N(C_4H_9))_4H_2SiPtW_{11}O_{40}$[b]	15.30	15.30	15.30	109.47	109.47	109.47	2758.08

a: data from publication by Allmen *et al.*,[68] b: data from publication by Klonowski *et al.*[69]

4.4.2 Discussion of the SXRD results

By comparing the SXRD results obtained in this project (see Table 41) with SXRD data found for similar POM compounds in the literature (see Table 42), we can see whether or not the structures of the synthesised compounds are similar to those reported in the literature. From the values presented in Table 42, we see that there is very little difference between the SXRD data reported for $(N(C_4H_9))_4SiW_{12}O_{40}$ and $(N(C_4H_9))_4H_2SiPtW_{11}O_{40}$. This indicates that the different metals inserted into the initial silicon tungsten POM structure, do not cause a large enough change in the structure of the POM to significantly affect the SXRD results.

Starting with the potassium compounds, we see that the K-$SiMnW_{11}$ compound is in good agreement with the published values from Allmen *et al*,[68] and the similarities between the recorded and literature data reinforce that the synthesis of K-$SiMnW_{11}$ was successful in producing the desired structure. On the other hand, when comparing the experimental data for the ^{II}K-$SiCuW_{11}$ compound with the literature, we see that there is a difference between the values. This difference might be an indication that the ^{II}K-$SiCuW_{11}$ compound has obtained a sandwich structure,[65] rather than a standard Keggin structure; however, as these SXRD data are not complete data sets, it is difficult to confirm this.

Finally, we look at the ^{I}TBA-$SiCuW_{11}$ compound, which very much correlates to the literature values reported by Klonowski *et al*,[69] indicating a successful synthesis. It is interesting to note that even though the IR spectra for both K-$SiCuW_{11}$ and TBA-$SiCuW_{11}$ showed a surprising number of peaks compared to the other compounds in this project, they showed different degrees of success in the SXRD analysis.

4.5 Comparison of IR results using MLR regression

As mentioned earlier, when the IR spectra for the potassium and TBA salts were compared, a displacement of the four peaks assigned to the W=O, Si-O, W-Ob-W and W-Oc-W stretches was discovered. Since the only difference between the anions was their inserted metal ions, it was assumed that this displacement was caused by properties specific to these metal ions. In an attempt to understand which properties affected the displacement most strongly, the data was analysed using MLR.

To achieve the most accurate comparison, the wavenumbers of the second derivative signals with the highest intensity were used (overview of the IR data can be found in the Appendix). The chemical properties that were considered in the comparison were the atomic mass, atomic radii and electronegativity of the metal ions and the bond dissociation energy of their metal-oxygen bonds (their numerical values can be found in the Appendix). These properties were chosen because variation within them would affect either the bond strength or mass of a POM, which would lead to different vibrational frequencies and therefore wavenumbers (see Formula 8). On the next pages the MLR results for the potassium and TBA compounds will be presented followed by a discussion of the results.

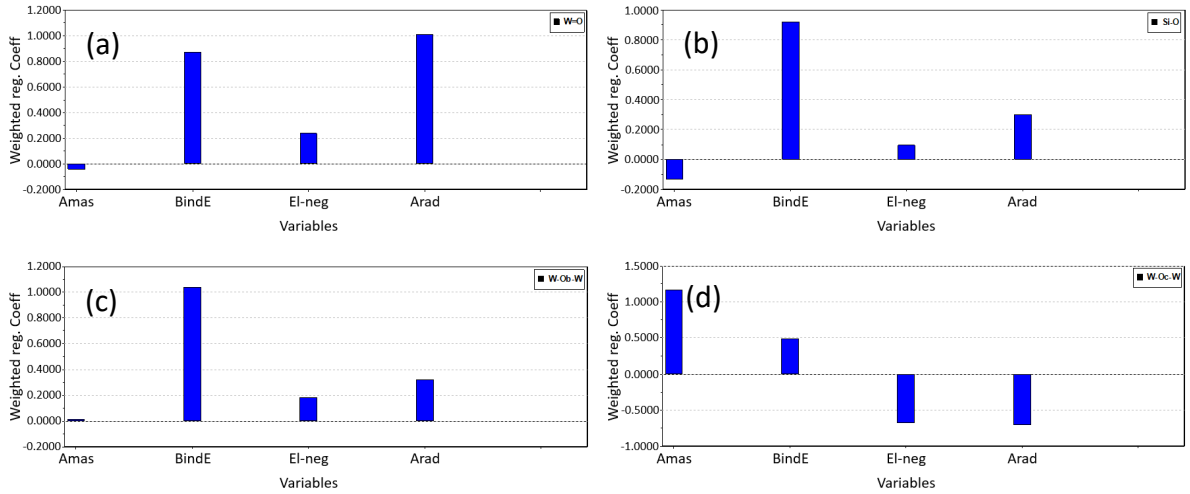

Figure 33: Weighted regression coefficients for the peak positions of the (a) W=O, (b) Si-O, (c) W-Ob-W and (d) W-Oc-W stretches for all the potassium compounds (where Amas = atomic mass, BindE = bond dissociation energy, El-neg = electronegativity and Arad = atomic radii).

The bar charts in Figure 33 show how the peak positions for the W=O, Si-O, W-Ob-W and W-Oc-W stretches for all the potassium compounds correlate with the atomic mass, bond dissociation energy, electronegativity and atomic radii. According to the figure, the W=O peak position positively correlates with the atomic radii, the bond dissociation energy and to some extent the electronegativity. The Si-O and W-Ob-W peak positions both have a strong positive correlation to bond dissociation energy and weaker positive correlations to the atomic radii and electronegativity. Additionally, the Si-O peak position also has a weak negative correlation to the atomic mass. Finally, the W-Oc-W peak position has a strong positive correlation to the atomic mass, as well as weaker negative correlations to the electronegativity and atomic radii. The W-Oc-W peak position also has a weak positive correlation to the bond dissociation energy.

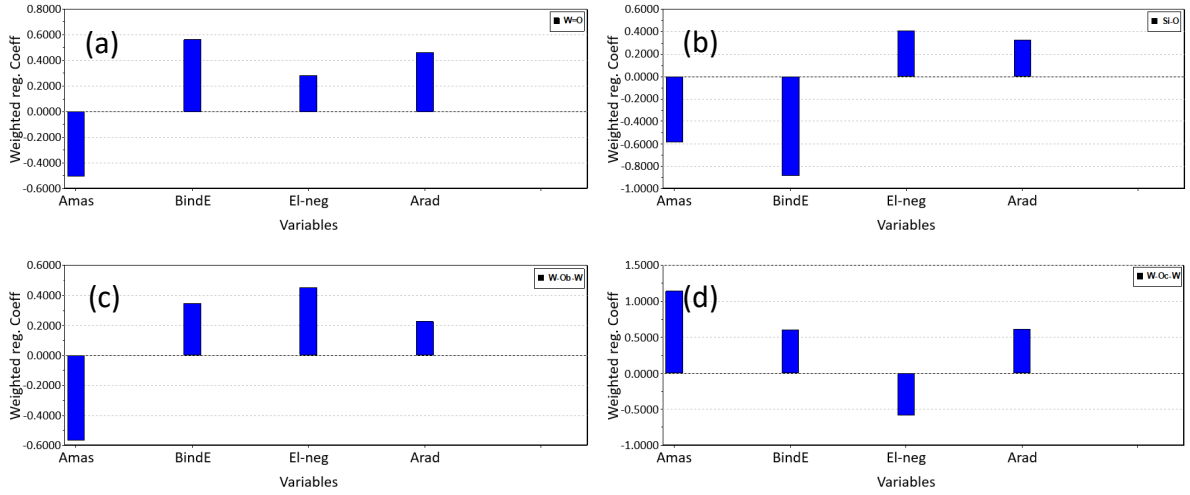

Figure 34: Weighted regression coefficients for the peak positions of the (a) W=O, (b) Si-O, (c) W-Ob-W and (d) W-Oc-W stretches for all the TBA compounds (where Amas = atomic mass, BindE = bond dissociation energy, El-neg = electronegativity and Arad = atomic radii).

The bar charts in Figure 34 show how the peak positions for the W=O, Si-O, W-Ob-W and W-Oc-W stretches for all the TBA compounds correlate with the atomic mass, bond dissociation energy, electronegativity and atomic radii. According to the figure, the W=O and W-Ob-W peak positions for the TBA compounds positively correlate with the bond dissociation energy, atomic radii and the electronegativity, while they negatively correlate with the atomic mass. The Si-O peak position negatively correlates with the bond dissociation energy and atomic mass, while it has weaker positive correlations with the electronegativity and atomic radii. Finally, the W-Oc-W peak position correlates positively with the atomic mass and to a lesser extent the bond dissociation energy and atomic radii. The W-Oc-W peak position also negatively correlates to the electronegativity.

If we compare the correlations found for the potassium compounds with those found for the TBA compounds, we can see that they have mostly the same correlations with some notable differences. This indicates that the cation bound to the POM anion also has an effect on the peak position of the W=O, Si-O, W-Ob-W and W-Oc-W stretches. When looking at the coefficient of determination (see Appendix), we also see that generally the potassium models have a better fit between predicted and measured variables, showing that the observed peak positions for the potassium compounds are more accurately predicted by the set of chosen chemical properties than the peak positions for the TBA compounds. Since the cations are the only difference between the two sets of compounds, this shows that there are properties specific

to the cations, e.g. their size, which more significantly affect the peak positions of the TBA compounds.

To illustrate why it is necessary to consider multiple variables when looking for correlations between the peaks, we can compare the order of the peak positions to the chemical properties. According to the MLR results, the W=O peak position for the potassium compounds correlates with the atomic radii and dissociation energy. In order of decreasing atomic radii the metal ions are Cu > Zn > Al = Cr = Mn > Fe > Co > Ni. If we compare this with the order of the W=O peak positions observed in Figure 14, we see that the orders is mostly the same, except for Ni and Zn, which have the lowest and second highest atomic radii, but fall just below the middle for the W=O peak positions. If we then compare the peak positions with the order of metal-oxygen bond dissociation energy for the metals (Al > Cr > Fe > Co > Ni > Mn > Cu > Zn), we can again observe that the orders are mostly the same, with the exception of Co, Cu and Zn. From these comparisons, we can see that neither of these chemical properties can perfectly describe the displacements observed in the spectra. We therefore see the necessity of considering multiple variables when looking for correlations between the peak positions.

The MLR analyses show that there are significant correlations between the peak positions of the potassium and TBA compounds and the atomic mass, bond dissociation energy, electronegativity and atomic radii of the inserted metals. The analyses also show deviations in the results for the potassium and TBA compounds, which strongly indicate that the cation has a significant effect on the IR peak positions, particularly for the TBA compounds. Further MLR analyses for these compounds should therefore include comparisons with chemical properties relating to the cations.

5 Conclusions and Outlook

During this project the potassium and TBA salts for $[SiXW_{11}O_{39}]^{n-}$, where X = Al^{3+}, Co^{2+}, Cr^{3+}, Cu^{2+}, Fe^{3+}, Mn^{2+}, Ni^{2+} and Zn^{2+}, were synthesised, due to their potentially beneficial catalytic properties. One of the aims of this project was to find syntheses that are time efficient, do not use highly toxic reagents and give high yields, since this is required for any successful catalyst.

In the case of the potassium compounds, two different syntheses were attempted; ^{I}K and ^{II}K. Neither of these syntheses required any highly toxic chemicals, but the ^{II}K synthesis was significantly less time consuming and produced notably higher yield, making this synthesis the most beneficial of the two. One issue with the ^{II}K synthesis, as opposed to the ^{I}K synthesis, was that it produced an unknown white precipitate, which needs to be removed if the products were to be used as catalysts. It would therefore be of interest in future work, to investigate the properties of this precipitate and find a way to either prevent or remove it. Since the ^{II}K synthesis was more efficient, future work could also benefit from adapting this synthesis to the $K_5SiAlW_{11}(H_2O)O_{39}$, $K_5SiCrW_{11}(H_2O)O_{39}$ and $K_5SiFeW_{11}(H_2O)O_{39}$ compounds. As can be concluded from the EA results, one necessary measure for any further work with the potassium compounds, is obtaining proper equipment for drying and safely storing the samples.

The TBA compounds were considered most promising for catalysis, but the syntheses reported in the literature were varying and typically with low yields. Hence, the TBA syntheses were the most interesting to improve. The ^{I}TBA synthesis was the first one attempted, but it was quite time consuming, did not produce a high yield and required the use of DCM as solvent. Secondly, the ^{II}TBA synthesis was chosen. This synthesis did not require the use of DCM, took notably less time with a somewhat improved yield. However, the yield was still low, and consequently the ^{III}TBA synthesis was attempted. This synthesis resulted in a significantly higher yield than the previous two, and is therefore concluded to be the most beneficial out of the three attempted syntheses. The ^{III}TBA synthesis also did not require pre-synthesised potassium compounds, which is beneficial considering the low yield and impurities of the potassium syntheses. Overall the ^{III}TBA synthesis was a bit time consuming, but in future work it might be possible to shorten the time spent on the reaction.

During this project the analysis of the synthesised compounds was mainly focused on IR. This was because the IR data reported in the literature were limited and hugely varying and therefore

unreliable for comparisons across sources. Using MLR, correlations between displacements in the IR data for the potassium and TBA compounds with respect to the atomic mass, bond dissociation energy, electronegativity and atomic radii of the inserted metals, were found. The MLR analysis also showed that properties relating to the cations were of importance and should therefore be accounted for in future analyses.

Other analytical methods were also used, such as TG and SXRD, but due to time constraints and generally limited access to instruments at the time, more extensive analysis was not possible. In future work it would therefore be of interest to analyse the synthesised compounds further. This includes TG analysis of all the compounds, using a larger temperature range than used in this project, complete structure determination of all the compounds using SXRD and both NMR (nuclear magnetic resonance) and MS (mass spectrometry) analysis of the compounds.

6 References

1. Hamilton, L. A., et al. 2019. Plastic & Climate: The Hidden Costs of a Plastic Planet. Center for International Environmental Law.
2. Chen, F., et al. 2012. Mechanism of the Cycloaddition of Carbon Dioxide and Epoxides Catalyzed by Cobalt-Substituted 12-Tungstenphosphate. *Chemistry – A European Journal,* 18**,** 9870-9876.
3. Huo, Z., et al. 2014. Synthesis of Cyclic Carbonates from Carbon Dioxide and Epoxides Catalyzed by a Keggin-Type Polyoxometalate-Supported Rhenium Carbonyl Derivate in Ionic Liquid. *ChemCatChem,* 6**,** 3096-3100.
4. Aresta, M., et al. 2014. Catalysis for the Valorization of Exhaust Carbon: from CO2 to Chemicals, Materials, and Fuels. Technological Use of CO2. *Chemical Reviews,* 114**,** 1709-1742.
5. Arakawa, H., et al. 2001. Catalysis Research of Relevance to Carbon Management: Progress, Challenges, and Opportunities. *Chemical Reviews,* 101**,** 953-996.
6. Wang, S.-S. & Yang, G.-Y. 2015. Recent Advances in Polyoxometalate-Catalyzed Reactions. *Chemical Reviews,* 115**,** 4893-4962.
7. Katsoulis, D. E. 1998. A Survey of Applications of Polyoxometalates. *Chem. Rev.,* 98**,** 359-387.
8. Firouzabadi, H. & Jafari, A. A. 2005. Heteropoly acids, their salts and polyoxometalates as heterogenous, efficient and eco-friendly catalysts in organic reactions: Some recent advances. *Journal of the Iranian Chemical Society,* 2**,** 85-114.
9. Song, Y. F. & Tsunashima, R. 2012. Recent advances on polyoxometalate-based molecular and composite materials. *Chem. Soc. Rev.,* 41**,** 7384-402.
10. Ammam, M. 2013. Polyoxometalates: formation, structures, principal properties, main deposition methods and application in sensing. *Journal of Materials Chemistry A,* 1**,** 6291-6312.
11. Hutin, M., et al. 2011. Controlling the Molecular Assembly of Polyoxometalates from the Nano to the Micron Scale: Molecules to Materials. *Israel Journal of Chemistry,* 51**,** 205-214.
12. Pope, M. T. 1983. *Heteropoly and Isopoly Oxometalates,* Berlin, Springer-Verlag.
13. Baker, L. C. W. & Glick, D. C. 1998. Present General Status of Understanding of Heteropoly Electrolytes and a Tracing of Some Major Highlights in the History of Their Elucidation. *Chemical Reviews,* 98**,** 3-50.
14. Putaj, P. & Lefebvre, F. 2011. Polyoxometalates containing late transition and noble metal atoms. *Coordination Chemistry Reviews,* 255**,** 1642-1685.
15. Müller, A., et al. 2002. Inorganic Chemistry Goes Protein Size: A Mo368 Nano-Hedgehog Initiating Nanochemistry by Symmetry Breaking. *Angewandte Chemie International Edition,* 41**,** 1162-1167.
16. Mcallister, J., et al. 2018. *Polyoxometalate-Based Assemblies and Functional Materials,* Springer International Publishing.
17. Hutin, M., et al. 2013. Polyoxometalates: Synthesis and Structure – From Building Blocks to Emergent Materials. *Comprehensive Inorganic Chemistry II.*
18. Pauling, L. 1929. The Molecular Structure of the Tungstosilicate and Related Compounds. *Journal of the American Chemical Society,* 51**,** 2868-2880.
19. Keggin, J. F. 1933. Structure of the Molecule of 12-Phosphotungstic Acid. *Nature,* 131**,** 908.
20. Keggin, J. F. 1933. Structure of the Crystals of 12-Phosphotungstic Acid. *Nature,* 132**,** 351.

21. Keggin, J. F. 1934. The Structure and Formula of 12-Phosphotungstic Acid. *Proc. R. Soc.,* 144**,** 75-100.
22. Aparicio-Anglès, X., et al. 2012. Polyoxometalates adsorbed on metallic surfaces: immediate reduction of [SiW12O40]4− on Ag(100). *Chemical Science,* 3**,** 2020-2027.
23. Müller, A., et al. 1998. Polyoxometalates: Very Large Clusterss - Nanoscale Magnets. *Chem. Rev.,* 98**,** 239-271.
24. Nisar, A., et al. 2010. Assembling Polyoxometalate Clusters into Advanced Nanoarchitectures. *Chemistry of Materials,* 22**,** 3511-3518.
25. Li, Y., et al. 2014. Recent progress in metal-functionalized germanotungstates: from structures to properties. *RSC Adv.,* 4**,** 50679 –50692.
26. Kato, C. N., et al. 2016. Organozirconium Complex with Keggin-Type Mono-Aluminum-Substituted Silicotungstate: Synthesis, Molecular Structure, and Catalytic Performance for Meerwein–Ponndorf–Verley Reduction. *Catalysis Letters,* 146**,** 2119-2128.
27. Bassil, B. S., et al. 2007. The Tungstogermanate [Ce20Ge10W100O376(OH)4(H2O)30]56−: A Polyoxometalate Containing 20 Cerium(III) Atoms. *Angewandte Chemie International Edition,* 46**,** 6192-6195.
28. Balula, Maria s., et al. 2004. Electrochemical Behaviour of First Row Transition Metal Substituted Polyoxotungstates: A Comparative Study in Acetonitrile. *European Journal of Inorganic Chemistry,* 2004**,** 619-628.
29. Boglio, C., et al. 2006. Lanthanide Complexes of the Monovacant Dawson Polyoxotungstate [α1-P2W17O61]10− as Selective and Recoverable Lewis Acid Catalysts. *Angewandte Chemie International Edition,* 45**,** 3324-3327.
30. Kikukawa, Y., et al. 2008. Synthesis and Catalysis of Di- and Tetranuclear Metal Sandwich-Type Silicotungstates [(γ-SiW10O36)2M2(μ-OH)2]10− and [(γ-SiW10O36)2M4(μ4-O)(μ-OH)6]8− (M = Zr or Hf). *Journal of the American Chemical Society,* 130**,** 5472-5478.
31. Kikukawa, Y., et al. 2008. Synthesis of a Dialuminum-Substituted Silicotungstate and the Diastereoselective Cyclization of Citronellal Derivatives. *Journal of the American Chemical Society,* 130**,** 15872-15878.
32. Chang, R. & Goldsby, K. 2014. *General Chemistry: The Essential Concepts,* New York, McGraw-Hill.
33. Long, D.-L., et al. 2010. Polyoxometalates: Building Blocks for Functional Nanoscale Systems. *Angewandte Chemie International Edition,* 49**,** 1736-1758.
34. Sakakura, T., et al. 2007. Transformation of Carbon Dioxide. *Chemical Reviews,* 107**,** 2365-2387.
35. Paddock, R. L. & Nguyen, S. T. 2001. Chemical CO2 Fixation: Cr(III) Salen Complexes as Highly Efficient Catalysts for the Coupling of CO2 and Epoxides. *Journal of the American Chemical Society,* 123**,** 11498-11499.
36. Li, F., et al. 2003. A novel and effective Ni complex catalyst system for the coupling reactions of carbon dioxide and epoxides. *Chemical Communications***,** 2042-2043.
37. Szczepankiewicz, S. H., et al. 1998. Interaction of Carbon Dioxide with Transition-Metal-Substituted Heteropolyanions in Nonpolar Solvents. Spectroscopic Evidence for Complex Formation. *Inorganic Chemistry,* 37**,** 4344-4352.
38. North, M., et al. 2010. Synthesis of cyclic carbonates from epoxides and CO2. *Green Chemistry,* 12**,** 1514-1539.
39. Chen, S., et al. 2015. A multi-component polyoxometalate and its catalytic performance for CO2 cycloaddition reactions. *Dalton Transactions,* 44**,** 10152-10155.
40. Sankar, M., et al. 2004. Effective catalytic system of zinc-substituted polyoxometalate for cycloaddition of CO2 to epoxides. *Applied Catalysis A: General,* 276**,** 217-222.

41. Chen, F., et al. 2010. Transition-Metal-Substituted Keggin-Type Germanotungstates for Catalytic Conversion of Carbon Dioxide to Cyclic Carbonate. *Catalysis Letters,* 139**,** 38-41.
42. Yasuda, H., et al. 2005. Efficient synthesis of cyclic carbonate from carbon dioxide catalyzed by polyoxometalate: the remarkable effects of metal substitution. *Journal of Catalysis,* 233**,** 119-122.
43. Housecroft, C. E. & Sharpe, A. G. 2012. *Inorganic Chemistry,* Harlow, Pearson Education Limited.
44. Harris, D. C. & Lucy, C. A. 2016. *Quantitative Chemical Analysis,* New York, W. H. Freeman and Company.
45. Mohrig, J. R., et al. 2014. *Laboratory Techniques in Organic Chemistry,* New York, W. H. Freeman and Company.
46. Atkins, P. & Paula, J. D. 2017. *Elements of Physical Chemistry,* Oxford, Oxford University Press.
47. Jolly, W. L. 1970. *The Synthesis and Characterization of Inorganic Compounds,* Englewood Cliffs, N.J., Prentice-Hall, inc.
48. Ginsberg, A. P. 1990. *Inorganic Syntheses,* New York, Wiley.
49. Moore, D., et al. 2017. *Introduction to the Practice of Statistics,* New York, W. H. Freeman and Company.
50. Yan, X. & Su, X. G. 2009. *Linear Regression Analysis,* New Jersey, World Scientific.
51. Ermrich, M. & Opper, D. 2013. *XRD for the analyst: Getting acquainted with the principles,* Almelo, PANalytical.
52. Atkins, P. & Paula, J. D. 2014. *Atkins' Physical Chemistry,* Oxford, Oxford University Press.
53. Haines, P. J. 1995. Thermogravimetry. *In:* HAINES, P. J. (ed.) *Thermal Methods of Analysis: Principles, Applications and Problems.* Dordrecht: Springer Netherlands.
54. Ma, R., et al. 1997. Synthesis, Characterization and Catalytic Performance of Positional Isomers of Al-germanium-substituted Tungstosilicane Heteropoly Complexes. *J. Inorg. Chem.,* 12**,** 278-280.
55. Ma, R., et al. 2011. Synthesis and Thermal decomposition reaction kinetics of α-SiW11Al and tetrabutylammonium charge-tranfer complex. *Huaxue Shiji (Chemical Reagent),* 33**,** 307-310; 372.
56. Weakley, T. J. R. & Malik, S. A. 1967. Heteropolyanions containing two different heteroatoms—I. *Journal of Inorganic and Nuclear Chemistry,* 29**,** 2935-2944.
57. Nakamoto, K. 2009. *Infrared and Raman spectra of inorganic and coordination compounds : Pt. A : Theory and applications in inorganic chemistry,* New York, Wiley.
58. Walrafen, G. E. 1964. Raman Spectral Studies of Water Structure. *The Journal of Chemical Physics,* 40**,** 3249-3256.
59. Bamoharram, F. F. 2009. Vibrational Spectra Study of the Interactions Between Keggin Heteropolyanions and Amino Acids. *Molecules,* 14**,** 3214-3221.
60. Duan, X., et al. 2018. Fabrication of Metal-Substituted Polyoxometalates for Colorimetric Detection of Dopamine and Ractopamine. *Materials (Basel, Switzerland),* 11**,** 674.
61. Wang, Z., et al. 2012. Visible-light photocatalytic H2 evolution over a series of transition metal substituted Keggin-structure heteropoly blues. *Chinese Science Bulletin,* 57**,** 2265-2268.
62. Zonoz, F. M. 2016. Electrochemistry Investigation of the Monolacunary and Their Transition Metal Substituent Keggin-Type Polyoxometalates. *Electrocatalysis,* 7**,** 215-225.

63. Tourné, C. M., et al. 1970. Triheteropolyanions containing copper(II), manganese(II), or manganese(III). *Journal of Inorganic and Nuclear Chemistry,* 32**,** 3875-3890.
64. Liu, X., et al. 2012. Photocatalytic hydrogen evolution under visible light irradiation by the polyoxometalate α-[AlSiW11(H2O)O39]5− -Eosin Y system. *International Journal of Hydrogen Energy,* 37**,** 12150-12157.
65. Sadakane, M., et al. 2007. Dimerization of mono-ruthenium substituted α-Keggin-type tungstosilicate [α-SiW11O39RuIII(H2O)]5− to μ-oxo-bridged dimer in aqueous solution: synthesis, structure, and redox studies. *Dalton Transactions***,** 2833-2838.
66. Jiang, Y., et al. 2015. A detailed study on the working mechanism of a heteropoly acid modified TiO2 photoanode for efficient dye-sensitized solar cells. *Physical Chemistry Chemical Physics,* 17**,** 6778-6785.
67. Degirmenci, L., et al. 2010. ETBE synthesis over silicotungstic acid and tungstophosphoric acid catalysts calcined at different temperatures. *Fuel Processing Technology,* 91**,** 737-742.
68. Von Allmen, K., et al. 2015. Nickel-Containing Keggin-Type Polyoxometalates as Hydrogen Evolution Catalysts: Photochemical Structure–Activity Relationships. *ChemPlusChem,* 80**,** 1389-1398.
69. Klonowski, P., et al. 2014. Synthesis and Characterization of the Platinum-Substituted Keggin Anion α-H2SiPtW11O404–. *Inorganic Chemistry,* 53**,** 13239-13246.
70. Lide, D. R. 2010. *CRC Handbook of Chemistry and Physics*, CRC Press.

7 Appendix

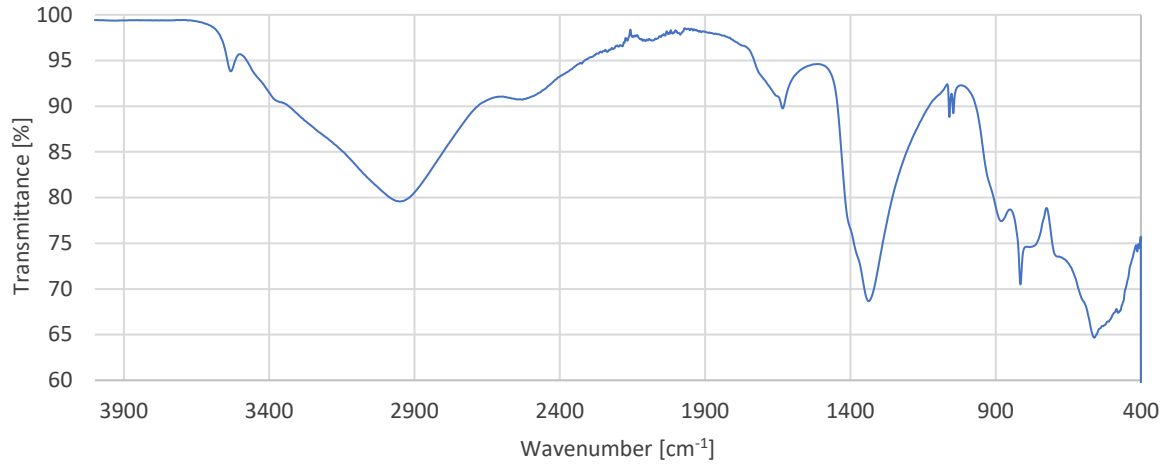

Figure 35: IR spectrum for aluminium nitrate nonahydrate ($Al(NO_3)_3 \cdot 9H_2O$).

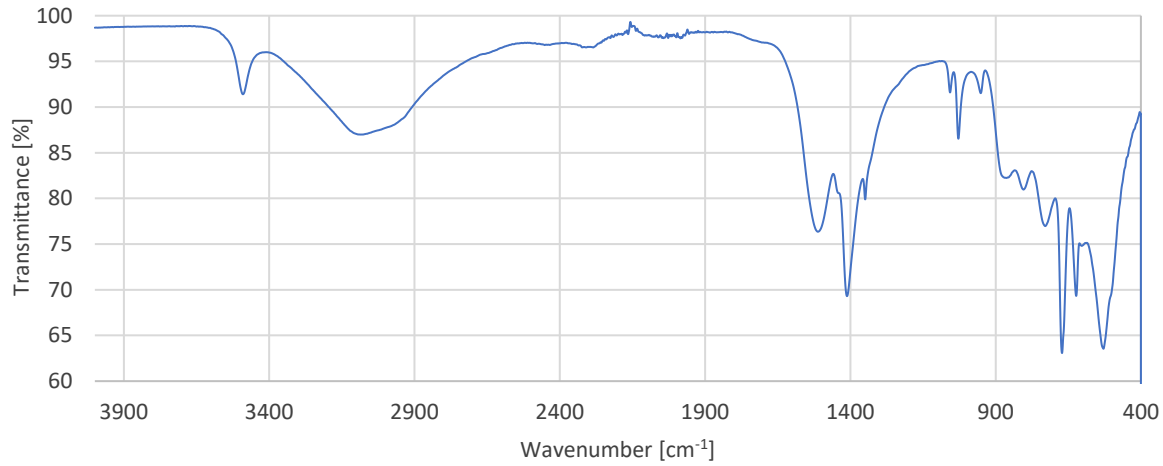

Figure 36: IR spectrum for cobalt(II) acetate tetrahydrate ($Co(CH_3COO)_2 \cdot 4H_2O$).

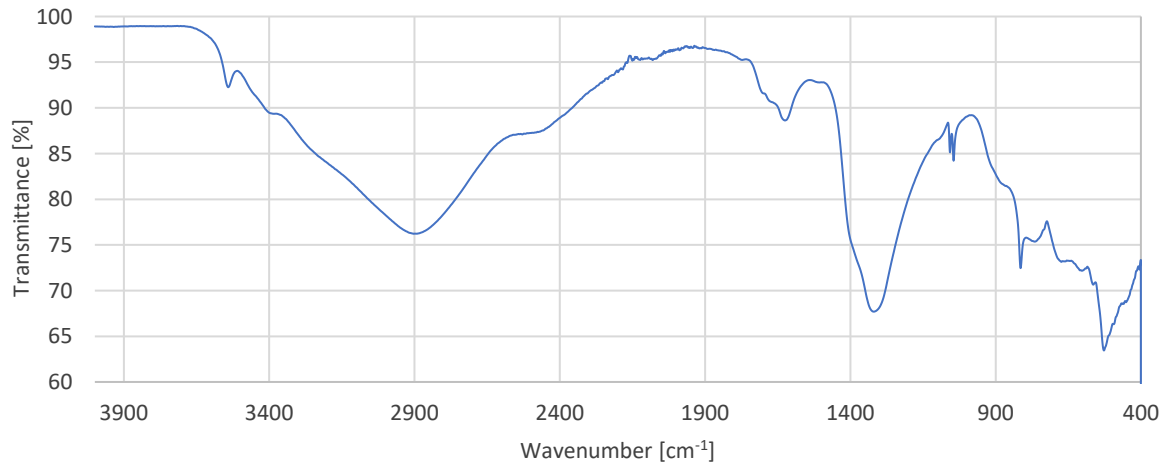

Figure 37: IR spectrum for chromium(III) nitrate nonahydrate ($Cr(NO_3)_3 \cdot 9H_2O$).

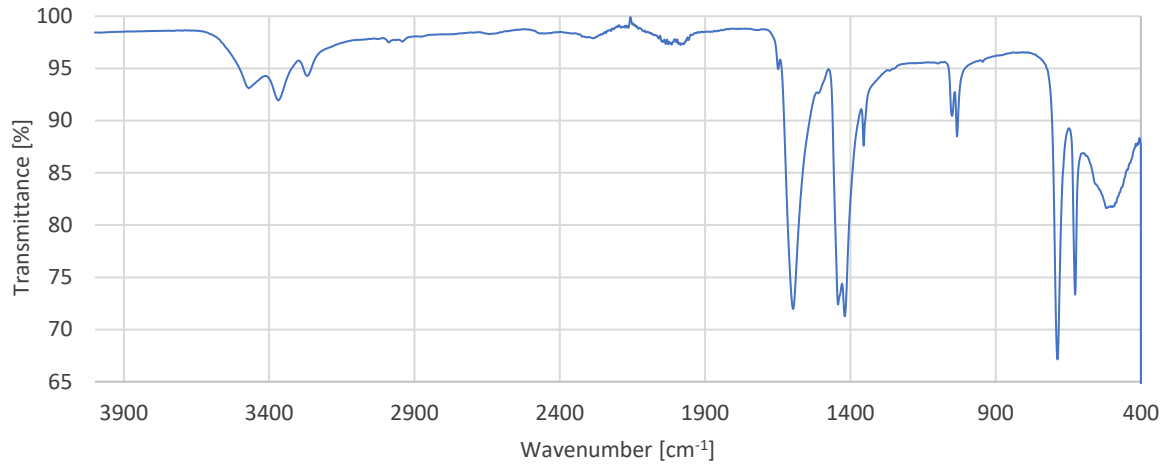

Figure 38: IR spectrum for copper(II) acetate monohydrate ($Cu(CH_3COO)_2 \cdot H_2O$).

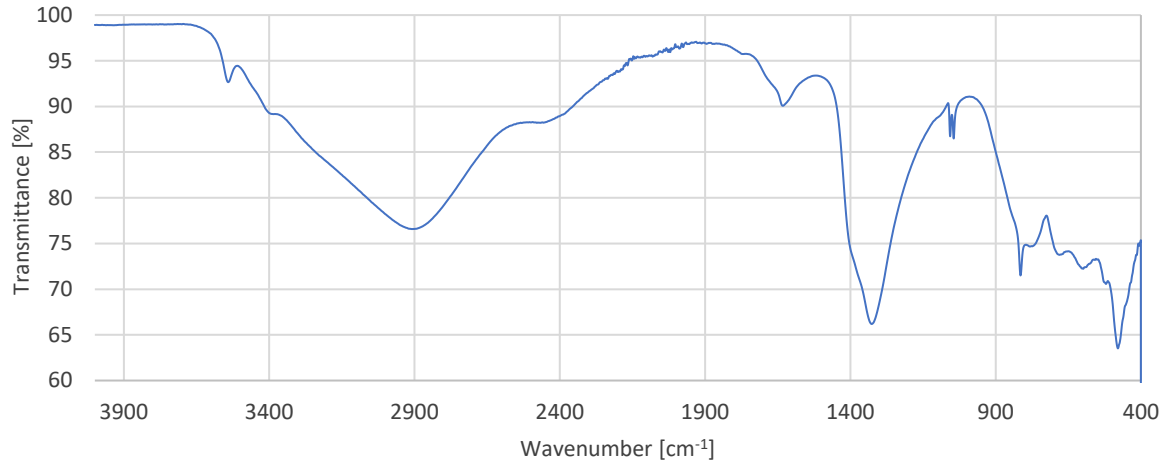

Figure 39: IR spectrum for iron(III) nitrate nonahydrate ($Fe(NO_3)_3 \cdot 9H_2O$).

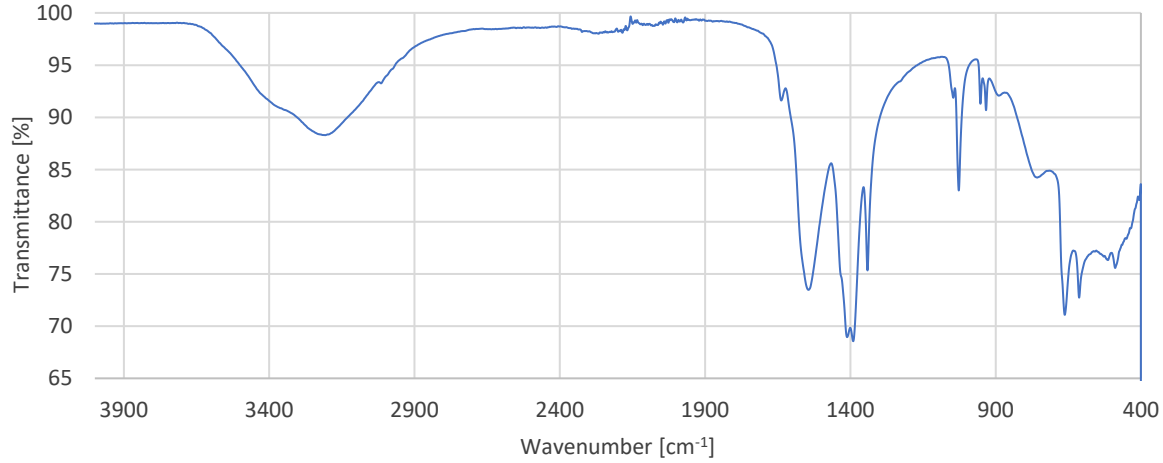

Figure 40: IR spectrum for manganese(II) acetate tetrahydrate ($Mn(CH_3COO)_2 \cdot 4H_2O$).

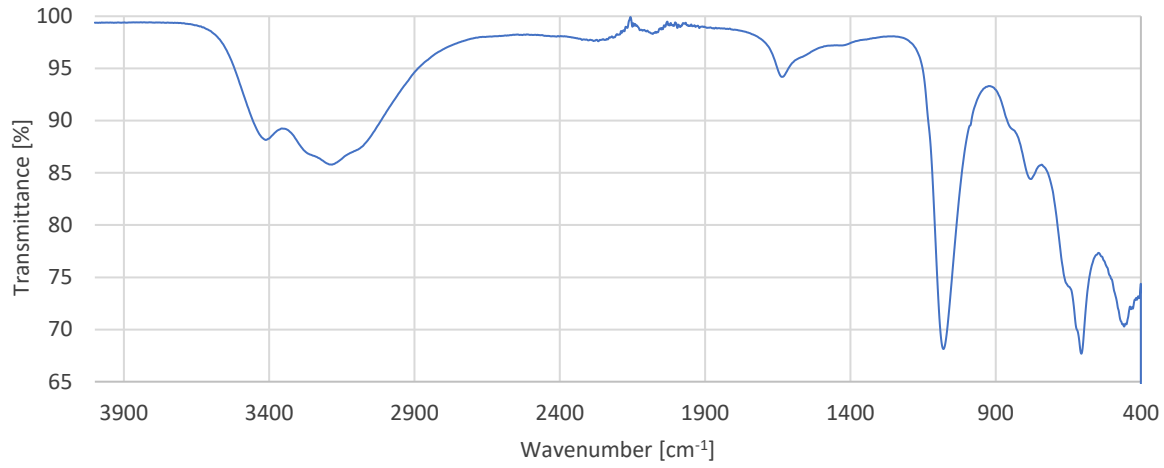

Figure 41: IR spectrum for nickel(II) sulphate hexahydrate ($Ni(SO_4)\cdot 6H_2O$).

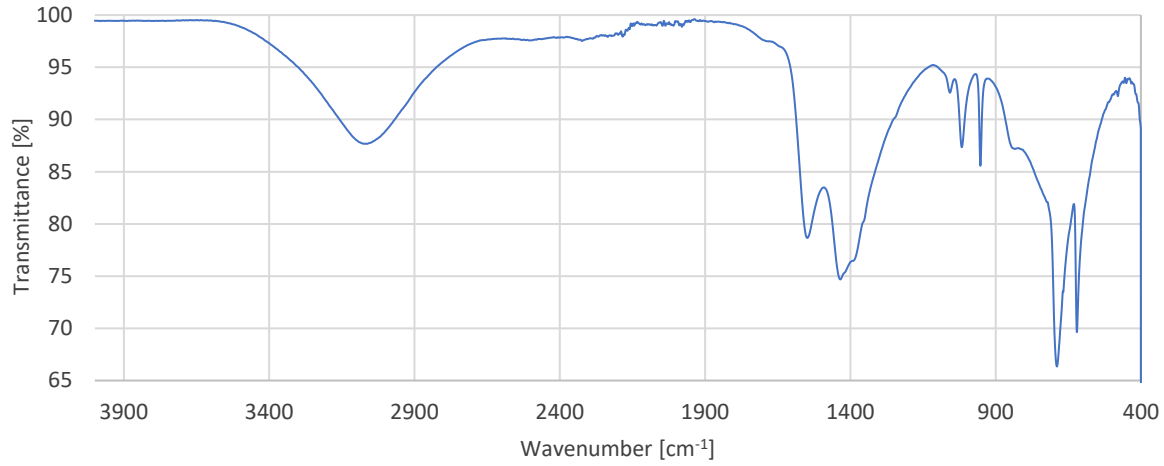

Figure 42: IR spectrum for zinc acetate dihydrate ($Zn(CH_3COO)_2\cdot 2H_2O$).

Table 43: Wavenumbers used for the comparison of IR data by MLR regression.

Compound	Wavenumber [cm^{-1}]			
	W=O stretch	**Si-O stretch**	**W-Ob-W stretch**	**W-Oc-W stretch**
K-SiAlW$_{11}$	1008.92	962.90	909.03	733.83
K-SiCoW$_{11}$	997.53	951.43	886.93	742.72
K-SiCrW$_{11}$	1009.31	959.57	909.87	758.89
K-SiCuW$_{11}$	1010.73	949.62	888.66	730.31
K-SiFeW$_{11}$	1006.85	960.01	903.83	745.68
K-SiMnW$_{11}$	998.15	948.49	880.44	754.22
K-SiNiW$_{11}$	998.05	951.01	892.79	756.47
K-SiZnW$_{11}$	1001.12	949.14	882.55	746.82
TBA-SiAlW$_{11}$	1004.30	955.55	910.31	773.41
TBA-SiCoW$_{11}$	998.21	956.61	898.12	791.43
TBA-SiCrW$_{11}$	1002.83	955.03	909.14	788.36
TBA-SiCuW$_{11}$	999.73	960.00	904.76	792.47
TBA-SiFeW$_{11}$	997.76	953.21	901.71	779.52
TBA-SiMnW$_{11}$	995.47	955.44	895.61	794.82
TBA-SiNiW$_{11}$	998.91	956.77	906.69	770.73
TBA-SiZnW$_{11}$	997.36	957.80	897.46	794.84

Table 44: Overview of atomic mass, atomic radii, bond dissociation energies and electronegativity for the inserted metals.

Metal	**Atomic mass**	**Atomic radii* [r_{cov}/Å]**	**Bond dissociation energy (M-O)* [D^{o}_{298}/kJ mol^{-1}]**	**Electronegativity***
Al	26.98	1.35	501.00	1.61
Co	58.93	1.33	397.40	1.88
Cr	52.00	1.35	461.00	1.66
Cu	63.55	1.52	287.40	1.90
Fe	55.85	1.34	407.00	1.83
Mn	54.94	1.35	362.00	1.55
Ni	58.69	1.24	366.00	1.91
Zn	65.38	1.45	250.00	1.65

*Values are from CRC Handbook of Chemistry and Physics.[70]

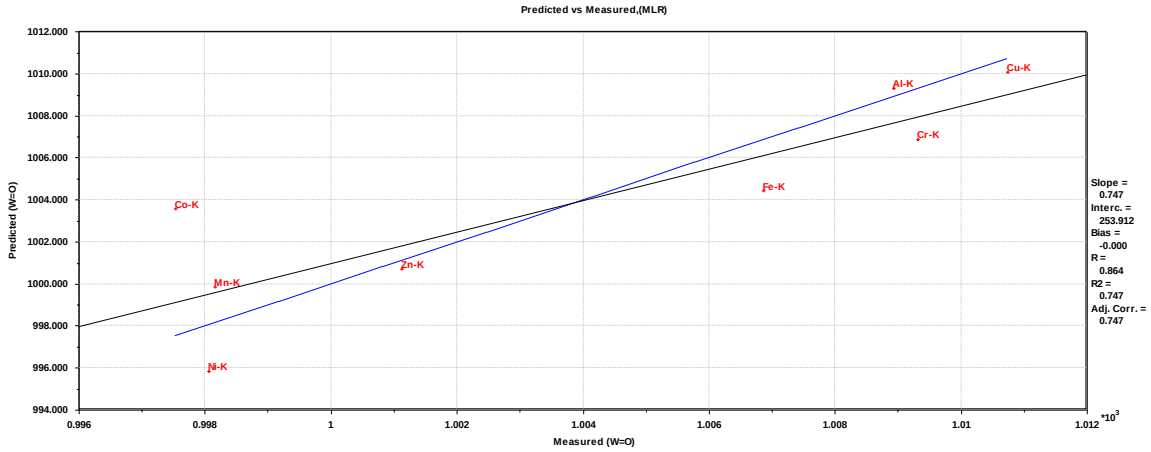

Figure 43: Plot of predicted vs measured values for the W=O stretch peak position for the potassium compounds.

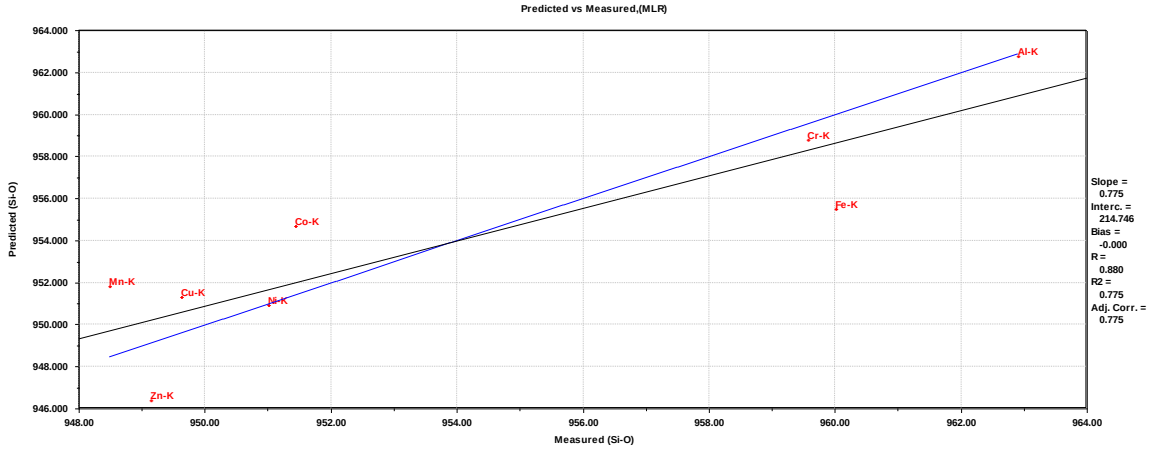

Figure 44: Plot of predicted vs measured values for the Si-O stretch peak position for the potassium compounds.

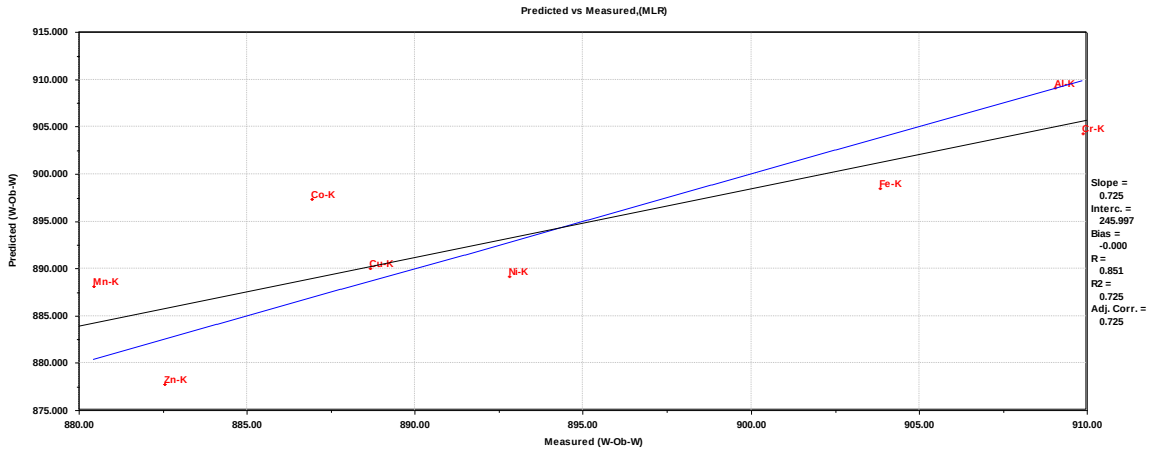

Figure 45: Plot of predicted vs measured values for the W-Ob-W stretch peak position for the potassium compounds.

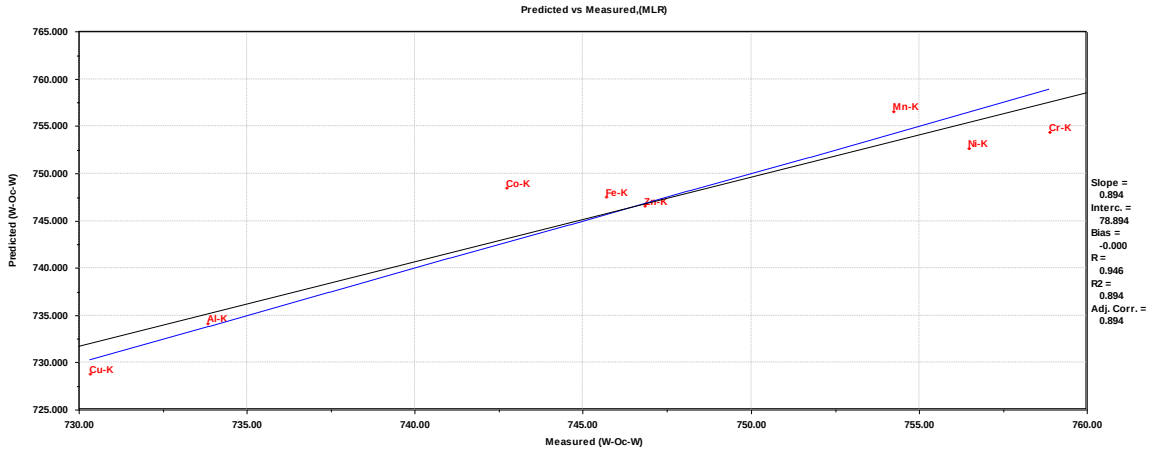

Figure 46: Plot of predicted vs measured values for the W-Oc-W stretch peak position for the potassium compounds.

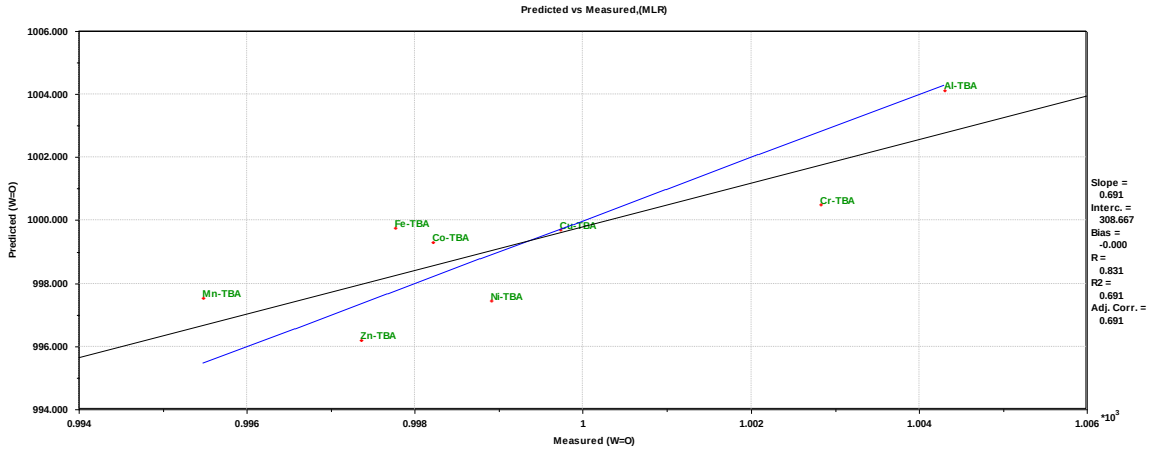

Figure 47: Plot of predicted vs measured values for the W=O stretch peak position for the TBA compounds.

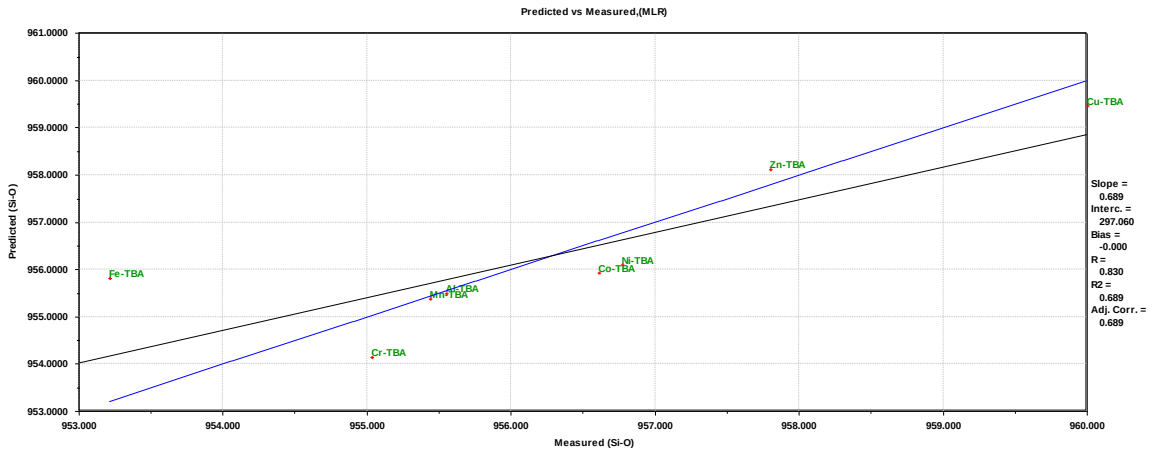

Figure 48: Plot of predicted vs measured values for the Si-O stretch peak position for the TBA compounds.

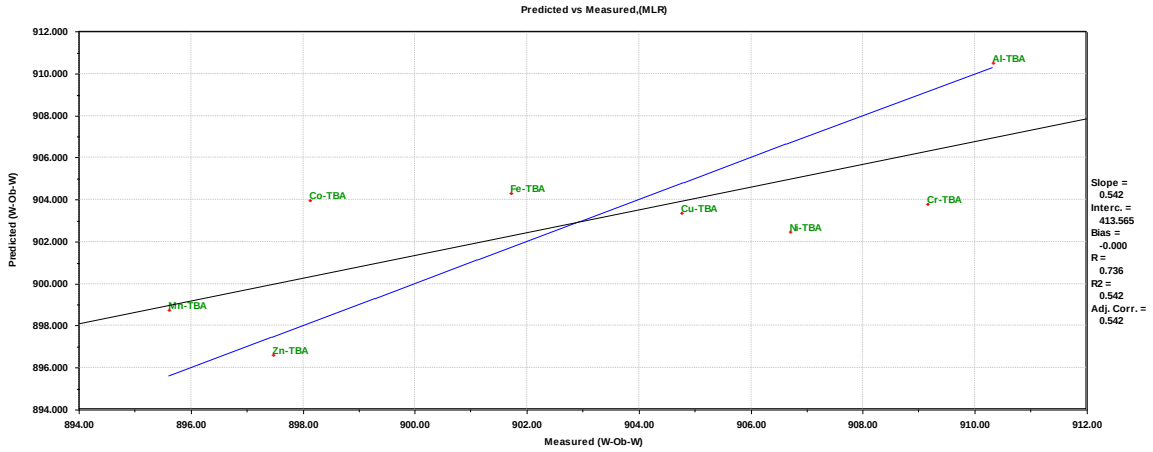

Figure 49: Plot of predicted vs measured values for the W-Ob-W stretch peak position for the TBA compounds.

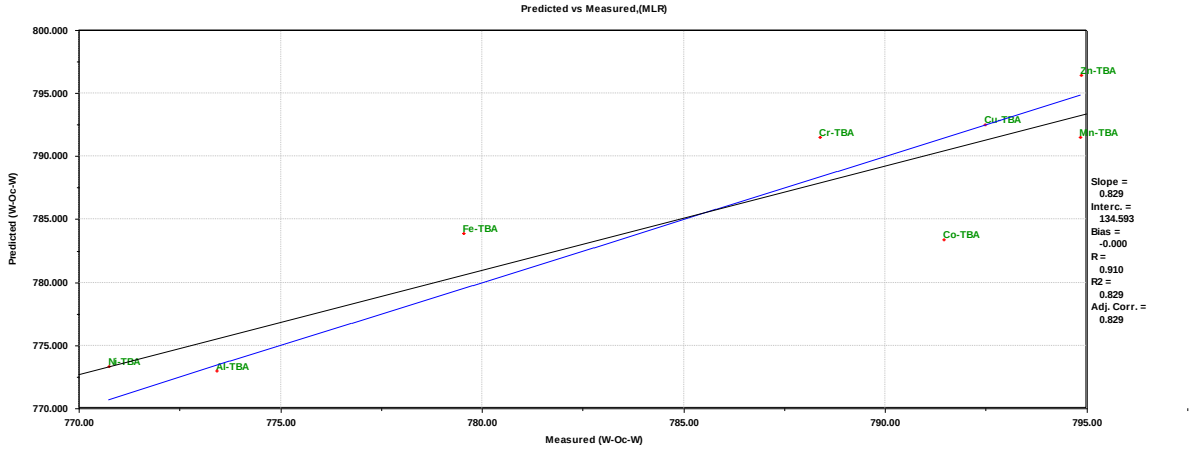

Figure 50: Plot of predicted vs measured values for the W-Oc-W stretch peak position for the TBA compounds.